# HIGHWAY RESEARCH RECORD

**Number 311**

# Pavement Slipperiness, Roughness, and Condition Evaluation

7 Reports

Subject Areas

26 Pavement Performance
51 Highway Safety

HIGHWAY RESEARCH BOARD
DIVISION OF ENGINEERING NATIONAL RESEARCH COUNCIL
NATIONAL ACADEMY OF SCIENCES—NATIONAL ACADEMY OF ENGINEERING
WASHINGTON, D.C. 1970

Standard Book Number 309-01810-2

Price: $3.00

Available from

Highway Research Board
National Academy of Sciences
2101 Constitution Avenue
Washington, D.C. 20418

## *Department of Design*

W.B. Drake, Chairman
Kentucky Department of Highways, Lexington

L. F. Spaine
Highway Research Board Staff

### PAVEMENT DIVISION

Milton E. Harr, Chairman
Purdue University, Lafayette, Indiana

### COMMITTEE ON SURFACE PROPERTIES-VEHICLE INTERACTION

(As of December 31, 1969)

David C. Mahone, Chairman
Virginia Highway Research Council, Charlottesville

M.D. Armstrong
Glenn G. Balmer
Joseph E. Bell
A. D. Brickman
W.F.R. Briscoe
John E. Burke
William C. Burnett
A.Y. Casanova, III
John H. Cox
Blaine R. Englund
E.A. Finney
William Gartner, Jr.
Ralph C.G. Haas
Douglas I. Hanson
Robert N. Janeway
B.F. McCullough
Robert B. McGough
W.E. Meyer
Paul Milliman
A.B. Moore
Desmond F. Moore
Ralph A. Moyer
F. William Petring
Bayard E. Quinn
John J. Quinn
F.A. Renninger
Rolands L. Rizenbergs
Hollis B. Rushing
Richard K. Shaffer
Elson B. Spangler
Sam Spinner
W.E. Teske
M. Lee Webster
E.A. Whitehurst
Ross G. Wilcox
Dillard D. Woodson

### COMMITTEE ON PAVEMENT CONDITION EVALUATION

(As of December 31, 1969)

Malcolm D. Graham, Chairman
New York Department of Transportation, Albany

Frederick E. Behn
W.B. Drake
Karl H. Dunn
Leroy D. Graves
Ralph C.G. Haas
W.S. Housel
W. Ronald Hudson
C.S. Hughes, III
James W. Lyon, Jr.
Alfred W. Maner
Phillip L. Melville
A.B. Moe
Frank P. Nichols, Jr.
Bayard E. Quinn
G.Y. Sebastyan
Foster A Smiley
Elson B. Spangler
Bertram D. Tallamy
W.E. Teske
Allan P. Whittemore
Eldon J. Yoder

# Foreword

This RECORD brings together seven papers describing results of research and development from a variety of interrelated projects dealing with tire-pavement interaction, surface properties, and pavement condition evaluation. It will be of interest to administrators, engineers, and others responsible for making basic decisions relating to these areas of concern.

A theoretical approach for explaining and predicting automobile hydroplaning phenomena is presented in the first paper by Daughaday and Balmer. The analytical approach is based on a mathematical model in which the water flow under the tire is divided into three distinct regions and interacts with assumed forms of tire deformation. The model is used to compute hydrodynamic pressure distributions, lift coefficients, and flow fields for both partial hydroplaning and the onset of total hydroplaning.

The paper by Schonfeld presents a method of classifying pavement surfaces according to their geometry and a means of using the classification to estimate skid resistance. Textural characteristics of surfaces are identified by stereophotography and coded for correlation with skid numbers measured with a standard skid trailer. An acceptable degree of correlation was obtained. The author outlines several useful potentials for the method.

The ability to predict the riding qualities of a pavement and the dynamic forces imparted to a pavement by a vehicle provides a basis for the establishment of a valid roughness level or spectrum for the pavement under consideration. The paper by Quinn, Engja, and Zable describes a procedure by which a modified BPR roughometer is used to measure roughness spectra. The authors conclude that the spectrum thus obtained is relatively free from arbitrary decisions required when such a spectrum is calculated from highway profile measurements obtained by a wide variety of devices. Walker and Hudson describe a profile-gathering and analysis system that provides quantitative records of a road profile at speeds up to 60 mph. The paper presents the details of a system that includes a surface dynamics profilometer subsystem and an anolog-to-digital data conversion and processing subsystem. It is demonstrated that rapid and effective data processing is essential for a usable system.

Structural performance of postwar concrete pavements in Michigan is the subject of the paper by Holbrook. The investigation reveals, among other things, that structural performance is closely associated with the percentage of soft nondurable particles in coarse aggregate and average daily commercial traffic. Using these findings, a mathematical model is developed that will predict structural performance for up to 15 years of service. Research data were obtained from pavement condition surveys and readily available construction, environment, and use information.

Phang's paper reports on 4 years of experience on the performance of 36 short experimental sections of flexible pavement constructed near Brampton, Ontario. The experiment was designed to compare the performance of five types of base material laid in four thicknesses on three thicknesses of subbase. The performance of the sections is described in terms of rutting, cracking and patching, and roughness of ride. The author presents some preliminary conclusions on the relative values of base material.

The final paper, by Lund and Hendrickson, is devoted to the development of a road-rating system to evaluate performance of aggregate-surfaced (volcanic cinder) roads. By means of a multiple linear regression program, 47 forest roads in south-central Oregon were rated and statistically correlated with maintenance, rutting, watering, speed, and traffic volume. The authors conclude that the results of the study are applicable to all types of aggregate-surfaced roads.

# Contents

# A Theoretical Analysis of Hydroplaning Phenomena

H. DAUGHADAY, Cornell Aeronautical Laboratory, Inc.; and
G. G. BALMER, U.S. Department of Transportation,
Federal Highway Administration, Bureau of Public Roads

Results obtained in a theoretical study of phenomena encountered when an automotive tire rolls or skids on a pavement covered with a water film are discussed. The analysis is based on a mathematical model in which the flow is divided into a footprint region, an inlet region forward of the footprint region where the gap between the tire and the pavement is comparatively large, and an exterior flow region. In partial hydroplaning, a thick fluid film penetrates between the tire and pavement over a portion of the footprint while "semidry contact" is assumed to exist in the remainder of the footprint. The flow through the semidry portion of the footprint is analyzed using effective film thicknesses based on pavement drainage characteristics. It is found that in some cases three-dimensional flow effects appreciably lower the lift coefficients developed by hydroplaning tires. The computed variations of the thick-film penetration distance and total friction coefficient with forward speed are given for the case of partial hydroplaning and discussed in relation to experimental results. The geometry and tire deformations of the thick-film region prove to be important parameters in studying partial hydroplaning.

•TIRE HYDROPLANING is suspected to have been responsible for a number of automobile accidents in the past and to offer a potential danger at the higher operating speeds that are being contemplated for future highways. Extensive investigations by a number of researchers have disclosed considerable information concerning hydroplaning, but most of this work has been primarily of an experimental nature. This paper presents the results of a complementary attack on the problem by a more theoretical analysis of hydroplaning phenomena. A purely theoretical approach has not been attempted, and some experimental inputs have been found essential.

## DESCRIPTION OF AN ANALYTICAL MODEL FOR HYDROPLANING

The analytical treatment was based on an idealized model that incorporates the principal physical characteristics of hydroplaning. The main features of this model are shown in Figure 1, which depicts a tire in partial hydroplaning. A moving axes system is used that translates with the wheel. In this coordinate system, the water-covered pavement appears to approach the wheel from the right with a velocity of magnitude $|U_1|$. The solutions obtained with the analytical model involved finding how water flows under tire configurations of the type shown rather than studying the equivalent problem of how water is forced from beneath a tire as it moves forward.

The region forward of the footprint region where the water on the pavement first comes into contact with the tire surface is designated the inlet region. The flow field outside the inlet and footprint regions is referred to as the exterior free-surface region because it is composed of surface water and spray, which have free surfaces. The static hydrodynamic pressures can be assumed equal to atmospheric pressure through-

Paper sponsored by Committee on Surface Properties-Vehicle Interaction.

out the external free-surface region and, in particular, at the outside boundaries of the inlet and footprint regions.

As a first approximation, the outside boundary shape of the footprint region of the tire on a wet pavement is taken to be the same as that obtained on a dry pavement under corresponding operating conditions. The footprint region of the analytical model is divided into two subregions: the thick-film region and the semidry region.

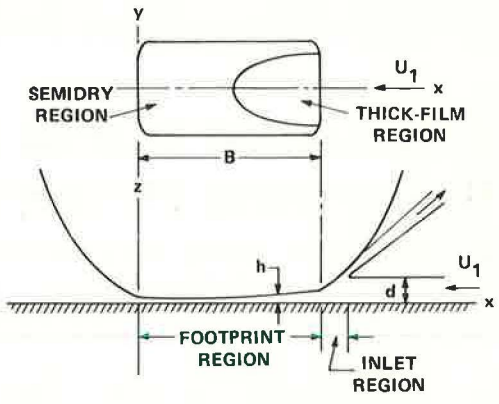


Figure 1. Schematic diagram of tire in partial hydroplaning.

Extensive work by Horne and Joyner at NASA (1) has shown clearly that, as the forward speed increases, the tire casing is deflected inward at the forward central portion of the footprint, thus permitting a relatively thick layer of water to penetrate between the tire surface and the pavement. This thick-film region enlarges as the speed increases, gradually extending further aft and toward the side edges of the footprint. In the analytical model, it is assumed that no asperities in the pavement are in contact with the tire surface within the thick-film region and, as a result, only hydrodynamic forces act on the tire tread.

Semidry regions of the footprint are defined as those in which each individual load-carrying asperity is either in dry contact with the tire surface, or the thickness of the fluid film between the load-carrying asperity and the tire surface is small compared to the depth that the asperity indents the tread surface. The hydrodynamic pressures acting in the valleys between load-carrying asperities contribute only small support to the total normal load.

Different treatments are appropriate for determining the hydrodynamic pressures in the footprint and inlet regions, but the pressures obtained for the two regions must be matched together at their mutual boundary.

The depth of water on the pavement approaching the wheel is indicated to be appreciably greater than the film thickness between the tire and pavement in the footprint region. Thus, the depth of water must be reduced in passing through the inlet region, and, at the same time, the requirement for continuity of flow must be satisfied. If smooth flow into the footprint region and around the sides of the tire is not possible, continuity is maintained by the generation of spray in the forward and side directions. Although some viscous effects are involved in the generation of spray and the production of turbulent motion in the inlet region, the pressures developed in this region are essentially due to inertia effects involved in slowing down the incoming flow.

Two different approaches were studied for treating the pressures in the inlet region. The first approach postulated a laminar inviscid flow through this region in which Bernoulli's equation could be used to determine the pressure as a function of the flow velocity. This approach should be valid for cases of hydroplaning where there is no forward spray or reverse flow from the footprint region into the inlet region. Such conditions appear to exist at speeds considerably in excess of the critical total hydroplaning speed. Solutions using this approach gave maximum hydrodynamic pressures in the inlet region of the order of 50 to 80 percent of the stagnation pressure for the incoming flow (i.e., the pressure when the fluid is brought to rest). The stagnation pressure, $\frac{1}{2} \rho U_1^2$, as given by the fluid dynamic pressure law for a wheel moving at a speed $U_1$, was also used as a reference pressure by Horne and Joyner (1).

However, partial hydroplaning is usually characterized by considerable forward spray and turbulent motion in the inlet region. Because Bernoulli's equation is not valid for these conditions, an empirical approach was used for defining the pressures in the inlet region. Experimental evidence from several cases of partial hydroplaning indicates that the ratio of the static pressure to the stagnation pressure is close to one

at the middle of the aft end of the inlet region where it adjoins the footprint region (Figs. 12 and 16b, 1; Fig. 8, 2). Therefore, in treating partial hydroplaning and the onset of total hydroplaning, a static-pressure to stagnation-pressure ratio of one was assumed to exist at the middle of the boundary between the inlet and the footprint regions. The pressure at this boundary was assumed to drop off parabolically from stagnation pressure at the centerline to atmospheric pressure at the side edges of the footprint.

This empirical treatment of the inlet region is based on cases of partial hydroplaning involving water depths on the pavement of 0.04 in. and greater. It is possible that, at extremely low water depths, smoother flow may exist in the inlet region, resulting in lower pressures as predicted by the treatment using Bernoulli's equation. The variation in hydroplaning speed with water depth reported by Gengenbach (3) might be explained by a gradual change from smooth flow to turbulent motion in the inlet region.

In the footprint region, viscous forces play a more important role than in the inlet region and have a predominant influence on the hydrodynamic pressure gradient for the case of comparatively smooth pavements. Laminar flow is assumed to exist in the footprint region because of the presence of these viscous forces.

The treatment of the hydrodynamic forces in the footprint region of the tire (6) was based on a perturbation expansion of the incompressible, steady-state Navier-Stokes equations of classical hydrodynamic theory in powers of a reduced Reynolds number. Combination of the zero-order equations obtained by this expansion resulted in Reynolds pressure equations of viscous lubrication theory. The solution of Reynolds equations gives the effect of the viscous forces in the footprint region on the hydrodynamic pressures.

A similar combination of the first-order perturbation equations obtained from the expansion gave an equation for first-order corrections to the pressures. This was of the same form as the Reynolds equation. Correction pressures that give the effect of inertia forces in the footprint region can be obtained by the solution of this equation. An alternative treatment of inertia forces is given by Eshel (4).

When the fluid film under the tire is thin, viscous forces have a greater effect than inertia forces on the hydrodynamic pressure gradients in the footprint region and little error results from computing the hydrodynamic lift load neglecting the first-order correction pressures. The results presented in this paper are limited to cases where it is permissible to neglect inertia forces in the footprint region.

It should be emphasized that inertia forces in the inlet region due to the slowing down of the flow have an important effect on the hydrodynamic pressures in all cases. These forces are still included in treating the inlet region even though inertia forces are neglected in the footprint region.

## RESULTS OBTAINED IF TIRE SURFACE IS ASSUMED TO BE PLANE IN FOOTPRINT REGION

The simplest analytical model for a tire in total hydroplaning is obtained by assuming the tire surface to be plane in the footprint region. Computations were carried out for this somewhat unrealistic configuration in order to study the importance of various parameters and the effect of three-dimensional flow. The output from the computer included automatic plotting of the pressure distribution and flow field in the footprint region as well as tabular data for the pressure and total hydrodynamic loads.

Figure 2 shows the plots obtained with a configuration having a footprint width-to-length ratio of 0.769 and a leading-edge film thickness twice that at the trailing edge. Because the pressures are measured relative to atmospheric pressure, the pressures on the side edges and trailing edge are zero. The high pressures at the leading edge of the footprint region arise from the slowing down of the fluid in the inlet region as discussed previously. It will be noted that the pressure drops off very rapidly with distance from the leading edge. This drop-off is associated with the side flow out the side edges of the footprint, which can be seen in the plot of the flow field. The curves on this plot show the direction of the average flow between the tire surface and the pavement.

A lift coefficient for a hydroplaning tire can be defined as the ratio of the average hydrodynamic pressure in the footprint region to the stagnation pressure of the incoming flow. The average ordinate in Figure 2a would be the lift coefficient for the case shown. Computations for a series of finite-aspect-ratio footprints with planar tire surfaces gave low lift coefficients because of three-dimensional flow effects. The computed lift coefficients for the planar surface configurations were approximately 20 percent of a lift coefficient derived from the empirical formula for the hydroplaning speed developed by Horne and Dreher (2). Consequently, it was concluded that the planar treatment of the tire surface was not adequate and that more realistic representations of the tire deformation in the footprint region are necessary in determining the effective water-film thickness under the tire.

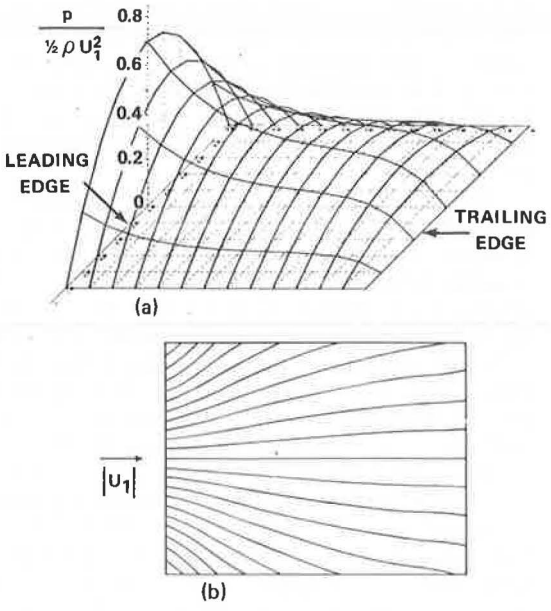


Figure 2. Skidding tire with plane surface in footprint region: (a) pressure distribution; (b) flow field in footprint region.

## EFFECTIVE FILM THICKNESSES UNDER TIRE

The effective thicknesses of the water film under a tire will be discussed for partial hydroplaning, which includes the onset of total hydroplaning as a limiting case. Passageways exist for fluid flow through the semidry region of the footprint because of the pavement texture and asperities. The resulting pavement drainage properties can be investigated experimentally as a function of surface texture and contact pressure, as described by Moore (5). The analysis of the flow in the semidry region is performed assuming an equivalent smooth pavement and an effective tire-pavement gap that will represent the measured drainage properties of actual pavements. In considering patterned tires, the effective film thicknesses under grooves running through the semidry region are primarily determined by the depth of the grooves.

The lift load is inversely proportional to the square of the minimum clearance in many lubrication problems. In analogy, the lift coefficient becomes higher in hydroplaning when the minimum clearance in the semidry region is reduced. However, a more complicated dependence on clearance is found for this case because of the near-stagnation pressures on the forward boundary of the footprint region.

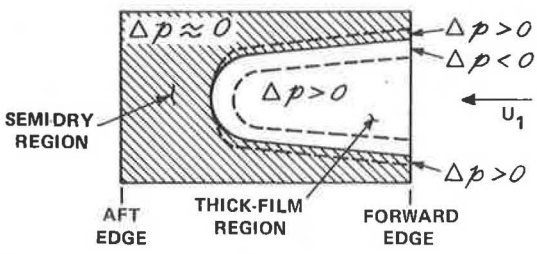


Figure 3. Changes in footprint pressure distribution in going from a dry to a wet pavement for the same forward speed and total wheel load.

The gap between the tire surface and pavement in the thick-film region depends on the tire deflections caused by hydrodynamic pressures. When analyzing a particular operating condition on a wet pavement, it is helpful to consider a corresponding dry-pavement condition for which the forward speed and total wheel load are the same. Fig-

ure 3 shows how the pressure distribution under the tire in a partial hydroplaning condition would be expected to differ from the pressure distribution for the corresponding dry-pavement condition. The thick-film region on the diagram is unshaded; the semidry region is shaded.

A thick-film region develops if the hydrodynamic pressures in the forward central portion of the footprint exceed the dry pavement pressures, thus giving positive incremental pressures. Although the incremental pressures are positive in the central portion of the thick-film region, they become negative near the side edges of the thick-film region where the hydrodynamic pressures are lower than the high dry-pavement pressures resulting from the sidewall stiffness. The combination of positive incremental pressures in the central portion of the thick-film region and negative incremental pressures near the side edges of the thick-film region tends to make the tire surface deflect up as required for the existence of such a region.

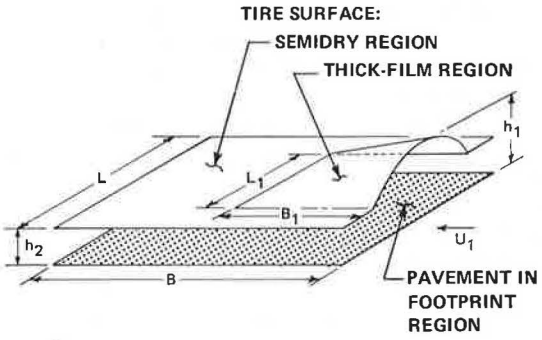


$\frac{B_1}{B} \times 100$ = THICK FILM PENETRATION (PERCENT)

$\frac{L_1}{L}$ = THICK FILM TO FOOTPRINT WIDTH RATIO

$\frac{h_1}{h_2}$ = GAP RATIO

Figure 4. Assumed form of tire surface in footprint region.

Positive incremental pressures are indicated in a narrow strip of the semidry region adjacent to the thick-film region. These "reaction" pressures would result in a curvature of the tire surface in the thick-film region tending to make it become tangent to the pavement at the boundary of the thick-film and semidry regions. For the rest of the semidry region, the incremental pressures would be expected to be small.

The total incremental load on the semidry region is seen to be positive because of the positive "reaction" pressures. Consequently, the total incremental load in the thick-film region must be negative to keep the total wheel load constant. However, as a first approximation, the total hydrodynamic load within the thick-film region of a tire in partial hydroplaning can be assumed equal to the load on the same portion of the footprint in a corresponding dry-surface operating condition, neglecting the effect of the incremental reaction loads. This assumption was made in obtaining some of the results to be discussed.

The effect of inward bulging of the tire surface on the lift coefficients in partial and total hydroplaning was studied for a series of configurations of the form shown in Figure 4. The tire-surface deformations for these smooth-tread configurations vary parabolically across the thick-film region, whereas the maximum tire-pavement gap at the centerline varies linearly from the leading edge to the maximum penetration distance of the thick-film region. The gap between the tire surface and the pavement is assumed constant in the semidry region.

## LIFT COEFFICIENTS ASSUMING NONPLANAR TIRE SURFACES IN FOOTPRINT REGION

Computations for configurations of the type shown in Figure 4 indicated, as would be expected, that the flow from the thick-film region out the side edges of the footprint is restricted by the low effective gaps in the semidry region. Consequently, the rapid drop-off of pressure with distance from the leading edge, which can be seen in Figure 2, is not obtained in this case.

A lift coefficient for the thick-film region is used for discussing partial hydroplaning, which is defined as the average hydrodynamic pressure over the thick-film region divided by the stagnation pressure of the incoming flow. This thick-film region lift co-

efficient becomes the lift coefficient for total hydroplaning when the thick-film region has extended over the entire footprint.

Lift coefficients computed for thick-film regions of the type shown in Fig-4 are shown in Figure 5 as a function of the dimensions of the thick-film region. These results are for configurations having an effective tire surface-to-pavement gap of 0.005 in. in the semidry region and a maximum gap at the forward end of the thick-film region of 0.020 in. A forward velocity of 54.0 mph was assumed in the computations.

The planform of the footprint is given in the small inset diagram in Figure 5. A footprint aspect ratio of 0.666 is assumed and a rectangular thick-film region is considered as shown previously in Figure 4. The abscissa is the ratio of the thick-film region width to the total footprint width and the ordinate is the lift coefficient for the thick-film region. Plots are shown for three values of the penetration distance of the thick-film region expressed in percent of footprint length.

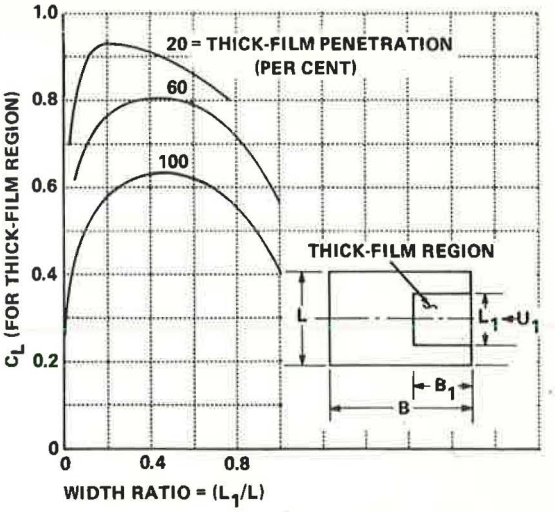


Figure 5. Lift coefficient for thick-film region: skidding tire.

For penetrations of 60 and 100 percent, the thick-film region lift coefficients peak at width ratios between 0.4 and 0.6. As the width ratio approaches 1.0, there is less restriction of the flow out the side edges of the footprint, and three-dimensional effects become more important. This explains the lower lift coefficients at a width ratio of 1.0. A lift coefficient of 0.4 for total hydroplaning is obtained at 100 percent penetration when the width ratio equals 1.0. This coefficient obtained with the assumed nonplanar configuration is appreciably higher than the lift coefficient obtained assuming a plane tire surface in the footprint region.

The lift coefficient for the thick film also becomes low where the thick-film region approaches zero width. Then the fore and aft lift distribution in the thick-film region approaches that obtained along the centerline of a configuration with a planar tire surface and a constant tire surface-to-pavement gap.

NASA photographs (1) of tires under partial and total hydroplaning conditions suggest the presence of a semidry or very thin film strip along each edge of the footprint of the order of 20 or 30 percent of the footprint width, and it is believed that the explanation of this phenomenon is associated with the lift curve shapes that have been indicated. Possibly, in these cases, sufficiently high lift coefficients would not be obtained to permit the development of a thick-film region unless the inward bulging of the tire carcass was restricted to the central portion of the footprint.

## VARIATIONS OF PENETRATION DISTANCE AND FRICTION COEFFICIENT WITH SPEED

The variations of thick-film region penetration distance and total friction force with forward speed were computed for a 6.50 by 13 smooth-tread passenger-car tire with a tire pressure of 27 psi. This configuration was selected in order to be able to compare the computed results with experimental friction data given by Horne and Joyner (1). The analysis was based on the hypothesis that the total hydrodynamic load on the thick-film region in partial hydroplaning can be assumed equal to the load on the same portion of the footprint in a corresponding dry-pavement operating condition.

The dry-pavement pressure distribution at all speeds was taken to be the same as the static bearing pressure distribution for the tire considered. Average dry-surface pressures were computed from the static bearing pressures for subregions of various widths and percentage penetrations into the footprint. It was found, in particular, that the average pressures for narrow subregions were considerably below the tire pressure of 27 psi.

The computational procedure used for finding the penetration distance involved assuming that the thick-film region occupied a particular subregion of the footprint and then looking up the average bearing pressure for this subregion on a dry pavement. The hydrodynamic loads on this subregion in partial hydroplaning were then computed for an assumed tire surface deformation shape of the form shown in Figure 4. Because the computer solution for the hydrodynamic loads was carried out in dimensionless form, it was possible to determine at what forward speed the average hydrodynamic pressure on the subregion in question would equal the corresponding dry-pavement pressure and thus be a possible partial hydroplaning condition. The growth of the thick-film region with speed was investigated by carrying out this procedure for a series of subregions.

Figure 6 shows the penetration distance obtained in this manner for several assumed configurations. The aspect ratio of the footprint was taken to be 0.666 on the basis of NASA photographs of the 6.50 by 13 tire in hydroplaning. Turbulent motion was assumed to exist in the inlet region that would result in full stagnation pressure at the center of the leading edge of the footprint region.

For a given point on the plots, the abscissa gives the skidding velocity, while the ordinate gives the thick-film penetration obtained at that velocity. The effective film thickness in the semidry region of the footprint was assumed to be 0.005 in. for all cases shown. The solid curves were obtained assuming a leading-edge gap of four times the effective gap in the semidry region, whereas the dashed curves were obtained with a gap ratio of two. Higher hydrodynamic pressures were computed for the larger gap ratio, which resulted in the more rapid penetration of the thick-film region with forward speed for this case.

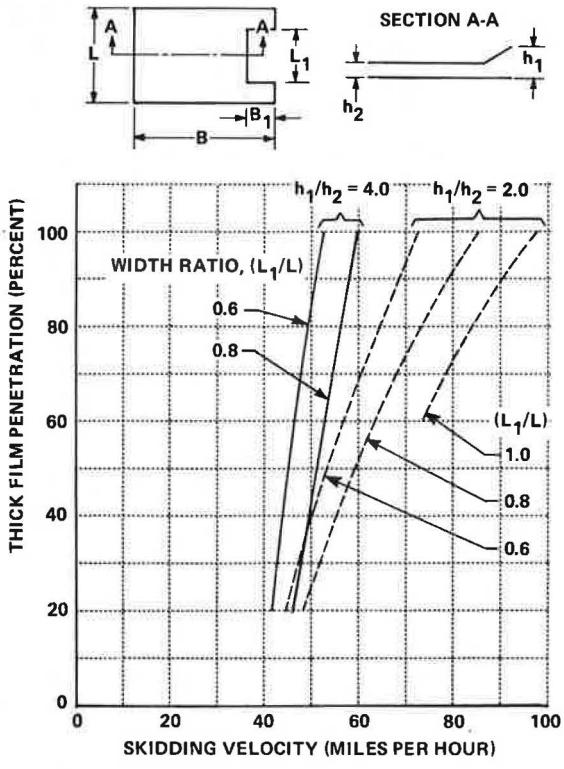


Figure 6. Effect of gap ratio ($h_1/h_2$) and width ratio ($L_1/L$) on thick-film penetration: skidding tire on textured concrete.

Curves are shown for thick-film-to-footprint-width ratios of 0.6, 0.8, and 1.0. In general, a more rapid thick-film penetration is obtained at the lower width ratios because of the lower dry-pavement pressure in the central part of the footprint and the higher thick-film region lift coefficients for these cases, as shown previously in Figure 5. However, the curves indicate that more than one combination of penetration ratio and width ratio are possible solutions at a given forward speed. It can be seen from these results that the actual tire deformation in the footprint region must be computed before a unique prediction can be made of the growth of the thick-film region.

The speed variation of the friction coefficient for a tire in partial hydroplaning was computed by making use of penetration ratio curves of the type shown in Figure 6. The viscous shear

forces acting in the thick-film region were an output from the computer solution for the flow under the tire. However, most of the friction force in partial hydroplaning arises from the contact of pavement asperity tips with the tire surface in the semidry region. An empirical approach was used for estimating the friction coefficient in the semidry region; this amounted to multiplying the portion of the wheel load carried by the semidry region by a friction coefficient for the semidry region. The friction force on the thick-film region plus the friction force on the semidry region was then divided by the total wheel load to give the average friction coefficient for the tire.

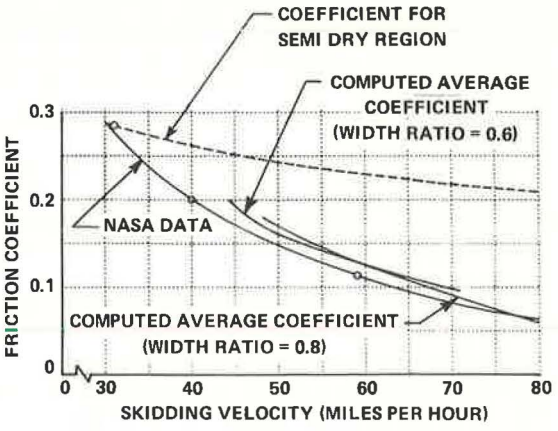


Figure 7. Friction coefficient versus forward speed: skidding tire.

Figure 7 shows plots of the variation of average friction coefficient with forward speed. The curve through the circled points is the NASA data (Fig. 22b, 1) for a 6.50 by 13 smooth-tread tire at a tire pressure of 27 psi. It was obtained in a skidding condition on a textured concrete surface.

The friction coefficient for rubber on a wet pavement varies with sliding velocity and this influences the speed variation of the total friction coefficient as well as the development of a thick-film region. It was concluded from the magnitudes of the bearing pressures on a dry pavement that a forward speed of 30 mph would have to be reached before a thick-film region would start to develop. Thus it was assumed that the total footprint was in semidry contact up to 30 mph, and the average friction coefficient at this speed was the same as the friction coefficient for the semidry region. The friction coefficient curve for the semidry region was extrapolated to speeds above 30 mph by assuming it proportional to the semidry friction curve obtained on a similar textured concrete surface with a different tire configuration. This extrapolated curve, drawn as a dotted line in Figure 7, was used in computing the average friction coefficient for the entire footprint of the 6.50 by 13 tire.

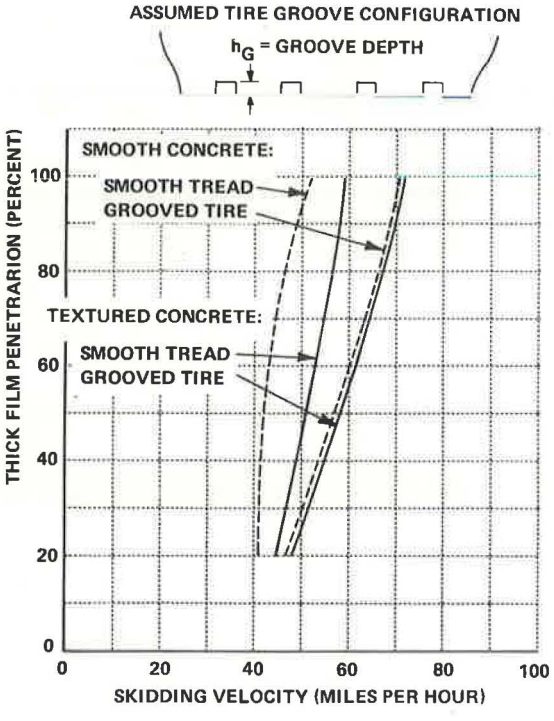


Figure 8. Effect of tire grooves on penetration distance of thick film: skidding tire.

The computed friction coefficient curves in Figure 7 were based on an effective film thickness of 0.005 in. in the semidry region and a maximum gap at the leading edge of the footprint of 2 times this magnitude. Friction coefficients computed assuming a tire-to-pavement gap ratio of 4 were found to

agree somewhat less favorably with the experimental data. Curves are shown for thick-film-to-footprint-width ratios of 0.6 and 0.8. Each of these covers a speed range in which the thick film penetrates from 20 to 100 percent of the footprint length. Again there is some overlapping of the speed ranges obtained with different assumed width ratios.

Figure 8 shows the effect of tire grooves on the penetration distance of the thick-film region. The hypothetical configuration indicated in the diagram is obtained by adding grooves to the 6.50 by 13 smooth-tread tire discussed previously. It was assumed that there was sufficient depth of water on the pavement to completely fill the tire grooves. Groove depths of 0.125 and 0.25 in. were assumed in computations for smooth and textured concrete pavements respectively.

The ratio of the widths of the thick-film region and the total footprint was assumed to be equal to 0.8, which gives a thick-film region extending between the outer edges of the two outer grooves. The tire deformations were assumed to be of the form shown in Figure 4 with a ratio of 4 for the leading-edge clearance over the clearance of the semidry region, exclusive of the tread depth.

Results computed for a textured concrete pavement with an effective clearance of 0.005 in. in the semidry region are shown as solid lines in Figure 8. The dotted curves were computed for a smooth concrete surface with an effective clearance of 0.0025 in. in the semidry region. For the textured concrete surface, the velocity for full penetration is increased from 59.0 mph for a tire without grooves to 71.5 mph for a tire with grooves. For the smooth concrete surface, the corresponding velocity increase is from 52.0 to 70.5 mph.

It is interesting to note that, when grooves are present, the curves for the textured and smooth concrete surfaces are very close together. Each of the grooves acts, essentially, as a channel that is not greatly influenced by leakage at its side edges. Thus, a nearly linear variation in pressure is found in each groove from a high value at the leading edge of the footprint to zero at the aft end. The hydrodynamic pressures over the entire thick-film region must fair through the pressures in the grooves, and the general form of the pressure distribution is established when the pressures in the grooves are given. Therefore, the pressure distribution in the thick-film region would be expected to be approximately the same for the smooth and textured surfaces.

The hydrodynamic pressures at the aft end of the footprint tend to be lower for a tire with grooves than with a smooth tire because of the linear variation of pressure in the grooves. Although these lower pressures in the aft portion of the thick-film region can delay the full penetration of the thick-film region to a somewhat higher speed, they cannot be expected to eliminate total hydroplaning except possibly at surface water depths where the grooves are not completely filled with water.

## CONCLUSIONS

It is believed that the theoretical approach discussed has considerable promise for explaining and predicting hydroplaning phenomena. A simplified analytical model has been used because of the complexity of the problem and, consequently, some experimental inputs in the solution are both necessary and desirable.

The results presented have indicated the sensitivity of the theoretical predictions to the method of analysis and the physical parameters used in the model. Three-dimensional flow effects are found to be important, and, in some cases, gross errors result if hydrodynamic forces are determined by two-dimensional flow theory.

The computed hydrodynamic pressures and flow field under the tire are sensitive to the effective film thickness between the tire and pavement. Effective clearances for the semidry region of the footprint can be found from experimentally determined pavement texture and drainage properties.

In the present study, the clearances in the thick-film region were based on assumed forms of tire deformation. Because the results were found to depend on the deformations assumed, a unique determination could not be made for the growth of the thick-film region with forward speed. However, such a solution could be obtained by coupling together the computation of the hydrodynamic pressures acting on a tire with the resulting tire deformation as determined experimentally or analytically.

Finally, it should be emphasized that even when the growth of the thick-film region with forward velocity is known, a good prediction of the speed variation of the total friction coefficient is dependent on having good empirical data for the friction coefficient between the tire and pavement in the semidry region.

## ACKNOWLEDGMENTS

The material in this paper was obtained as a part of a research project on "Mathematical Analysis of Hydroplaning Phenomena" sponsored by the U.S. Bureau of Public Roads. A considerable part of the mathematical analysis was carried out by C. Tung, the computer program was largely developed by S. Partee, and valuable advice was provided by I. C. Statler and J. P. Nenni, all of Cornell Aeronautical Laboratory, Inc.

The authors would like to express their appreciation to the following individuals for helpful discussions held during the course of the program: Walter B. Horne and Thomas J. Yager of NASA; I. R. Ehrlich, S. Tsakonas, and C. J. Henry of Stevens Institute of Technology; and Desmond F. Moore of West Virginia University.

## REFERENCES

1. Horne, W. B., and Joyner, U. T. Pneumatic Tire Hydroplaning and Some Effects on Vehicle Performance. SAE Internat. Automotive Engineering Congress, Detroit, Jan. 1965.
2. Horne, W. B., and Dreher, R. C. Phenomena of Pneumatic Tire Hydroplaning. NASA TN D-2056, Nov. 1963.
3. Gengenbach, W. The Effect of Wet Pavement on the Performance of Automobile Tires. Universität Karlsruhe, Germany, July 1967. Translated for limited distribution by Cornell Aeronautical Laboratory.
4. Eshel, A. A Study of Tires on a Wet Runway. Ampex Rept. RR 67-24, Sept. 1967.
5. Moore, D. F. A Study of Tire Surface Interaction for the Case of Rolling on a Wet Surface. Cornell Aeronautical Laboratory, Rept. YD-1969-V-2, July 1965.
6. Daughaday, H., and Tung, C. A Mathematical Analysis of Hydroplaning Phenomena. Cornell Aeronautical Laboratory, Rept. AG-2495-S-1, Jan. 1969.

# Photo-Interpretation of Skid Resistance

R. SCHONFELD, Department of Highways, Ontario

Stereophotographs are used for describing pavement surface textures in terms of seven texture parameters. A pavement surface is identified by a texture code number consisting of seven digits, one for each texture parameter. Several thousand pavements were tested with an ASTM skid trailer and stereophotographed. The pavement textures were analyzed and the resulting texture code numbers were correlated with the skid numbers of the wet pavements. The correlation study indicates that the skid numbers of all pavements with the same texture code number are practically the same as the skid numbers obtained by repeated test runs over one pavement section.

The skid number of a pavement surface can be estimated by assigning "friction weights" to each texture parameter. An acceptable degree of correlation between interpreted and measured skid resistance was obtained. The method described has several useful potentialities, in that (a) it offers an insight into the pavement texture-skid resistance relationship and makes pavement-texture design a practical possibility; (b) it can be used for skid-resistance determination in locations where skid trailers cannot be used (curves and intersections); (c) it can give less affluent municipal authorities a means of estimating the skid numbers of their pavements; and (d) it raises skid-resistance measurements from their present unrealistic isolation and links them with their pavement texture (this may help to deal with the problem posed by the apparent inconsistency of skid measurements of the same pavement obtained by different skid trailers, and also with the problem of correlating skid-resistance measurements, obtained at different times, in different geographic locations).

Because the method does not discard a skid-test result after it has been used for an individual pavement, but continues to use it together with previous and subsequent test results for pavements of the same surface texture, it can be expected that its usefulness will increase as test data accumulate. The method described in this report is an initial attempt at devising a technique for pavement texture analysis that can be used for photo-interpreting skid resistance and it is hoped that it will lend itself to further development and improvement by other workers.

•AT LEAST NINE different types of friction testers are in use for measuring pavement skid resistance, including the ASTM tentative standard skid trailer. Several skid-tester meetings have demonstrated the disparity of test results obtained by different types of testing devices and also by different versions of the same type of skid tester.

The standard skid number of a pavement that would make it possible to relate the measured skid resistance of one pavement to that of another has so far eluded us. Indeed, it is as remote today as it ever was, perhaps because of the complexity of the factors that influence a field skid test (1). It is possible to question if the concept of the standard skid number is realistic, or whether it is erroneous to conceive of one skid

Paper sponsored by Committee on Surface Properties-Vehicle Interaction and presented at the 49th Annual Meeting.

number as a distinct measurable quantity of something as complex as 200 sq ft of pavement surface. Also, the test vehicle is unlikely to retrace the same wheelpath on repetitive tests, and, even though different wheelpaths will have related textures, they generally produce different skid results.

It is therefore suggested that the concept of a standard skid number be replaced by the concept of a skid-resistance range that reflects the surface geometry of the particular pavement. This concept complies with general experience that the surface geometry is the dominant factor among those influencing skid resistance (2). This report presents a method of classifying pavement surfaces according to their geometry and a means of using the classification to estimate the skid resistance as measured by a standard skid trailer.

## ONTARIO PAVEMENT SURFACE CLASSIFICATION METHOD

### Pavement Surface Analysis

The development of a classification system for pavement surfaces began with an attempt to describe the surface characteristics of a small section of pavement. A transparent 15 by 15 cm grid was superimposed over stereophotographs of the surface, and the shapes, sizes, and microtexture of topographical features inside each centimeter square were examined. It was found that the average number of the different features for the 225 one-centimeter squares closely resembled the average for 100, 50, or even 25 one-centimeter squares selected at random. It was also found that the result of the texture analysis was essentially the same for several samples of the same section of pavement. This situation is reminiscent of sampling an aggregate stockpile where one sample may be representative of the stockpile, but several samples, sensibly distributed, give greater assurance of revealing the grain-size distribution of the stockpile.

It seemed feasible, from this early work, that the texture of any pavement surface could be described and classified in a way that would clearly mark its particular identity within the wide variety of present and possible future surfaces. The next objective was to identify the elements of a surface texture whose direct effect on skid resistance could be demonstrated and to classify the elements according to their geometric shapes and sizes.

### Texture Parameters and Texture Code Number

Seven groups of texture parameters, each having a recognizable effect on the pavement's skid resistance, are described in this section of the report. Each parameter group is given a numerical scale of shapes, sizes, or degrees. The numbers on the scale are the individual parameters; the parameters at the lower end of a scale usually, but not always, make the smallest contribution to skid resistance. Seven parameters—one from each group—constitute a texture code number of the pavement that describes and identifies a pavement texture as a whole. Each element of texture has its own scale of sizes.

Height parameter A is measured in millimeters from the top of the background to the top of the projection (Fig. 1).

Width parameter B is measured in millimeters and is the horizontal dimension of the projection. It is measured at the level of the top of the background (Fig. 2).

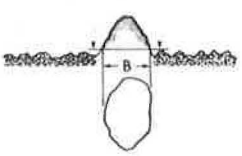


Scale:

| | |
|---|---|
| B0 | 16 mm or greater |
| B1 | less than 16 mm to 8 mm |
| B2 | less than 8 mm to 4 mm |
| B3 | less than 4 mm to 2 mm |
| B4 | less than 2 mm to 1 mm |
| B5 | less than 1 mm to ½ mm |

Figure 1. Height parameter A.

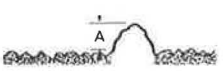


Scale:

| | |
|---|---|
| A0 | 0 mm |
| A1 | greater than 0 mm to ¼ mm |
| A2 | greater than ¼ mm to ½ mm |
| A3 | greater than ½ mm to 1 mm |
| A4 | greater than 1 mm to 2 mm |
| A5 | greater than 2 mm to 4 mm |
| A6 | greater than 4 mm to 8 mm |
| A7 | greater than 8 mm to 16 mm |

Figure 2. Width parameter B.

Angularity parameter C describes the edges of the projections that may come in contact with the tire (Fig. 3).

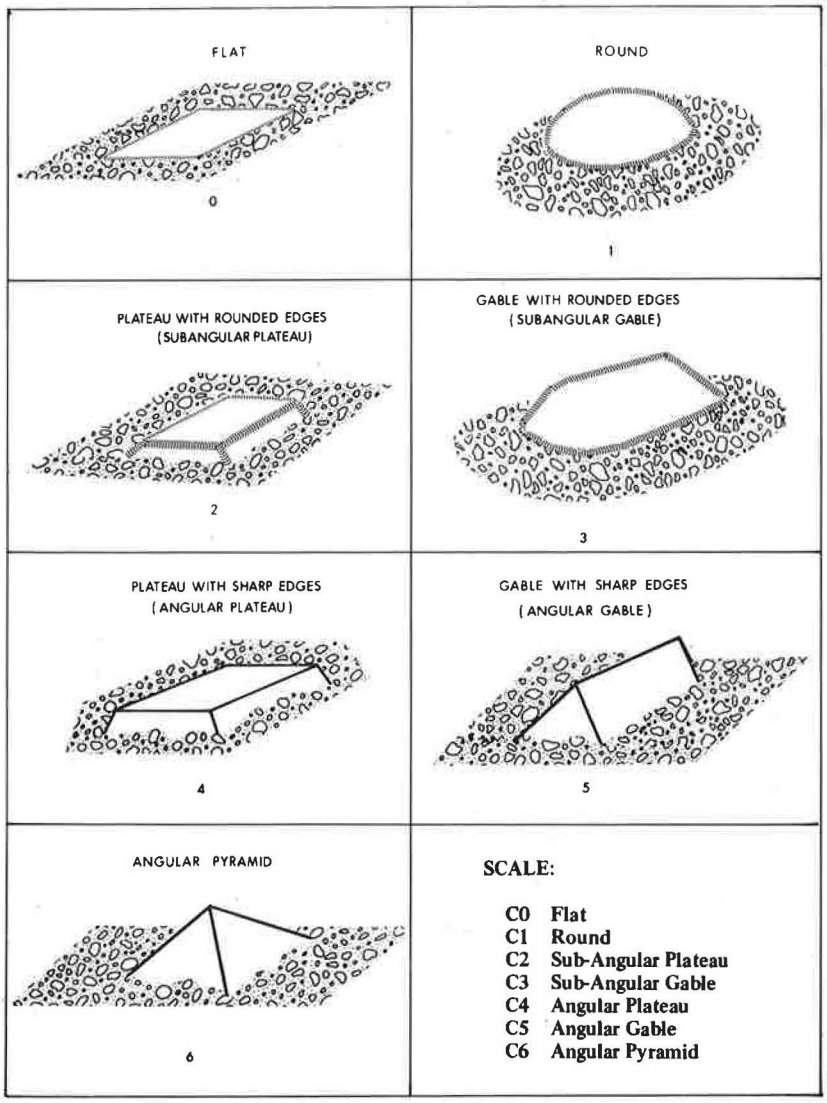


Figure 3. Angularity parameter C.

Density of spacing parameter D is estimated as one would estimate the proportion of occupied seats in an auditorium; i.e., empty (0), one-quarter full (1), half-full (2), three-quarters full (3), and full house (4):

| Scale: | | |
|---|---|---|
| | D0 | No Asperities |
| | D1 | Asperities take up about 25 percent of total area |
| | D2 | Asperities take up about 50 percent of total area |
| | D3 | Asperities take up about 75 percent of total area |
| | D4 | Asperities take up about 100 percent of total area |

Fine texture of projections parameter E denotes size and sharpness or roundness of the microprojections on the surface of the stones (Fig. 4).

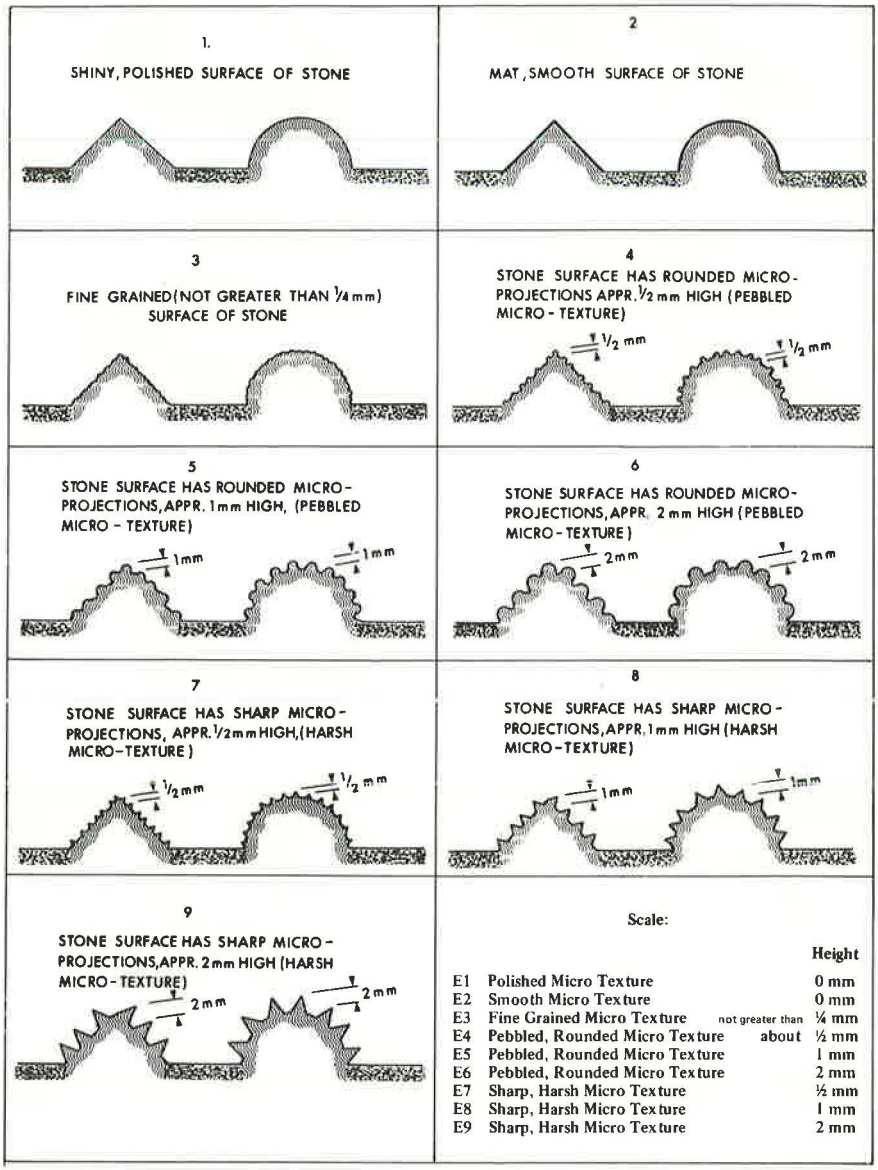


Figure 4. Fine texture of projections parameter E.

Fine texture of background parameter F denotes size and sharpness or roundness of the microprojections in the background (Fig. 5).

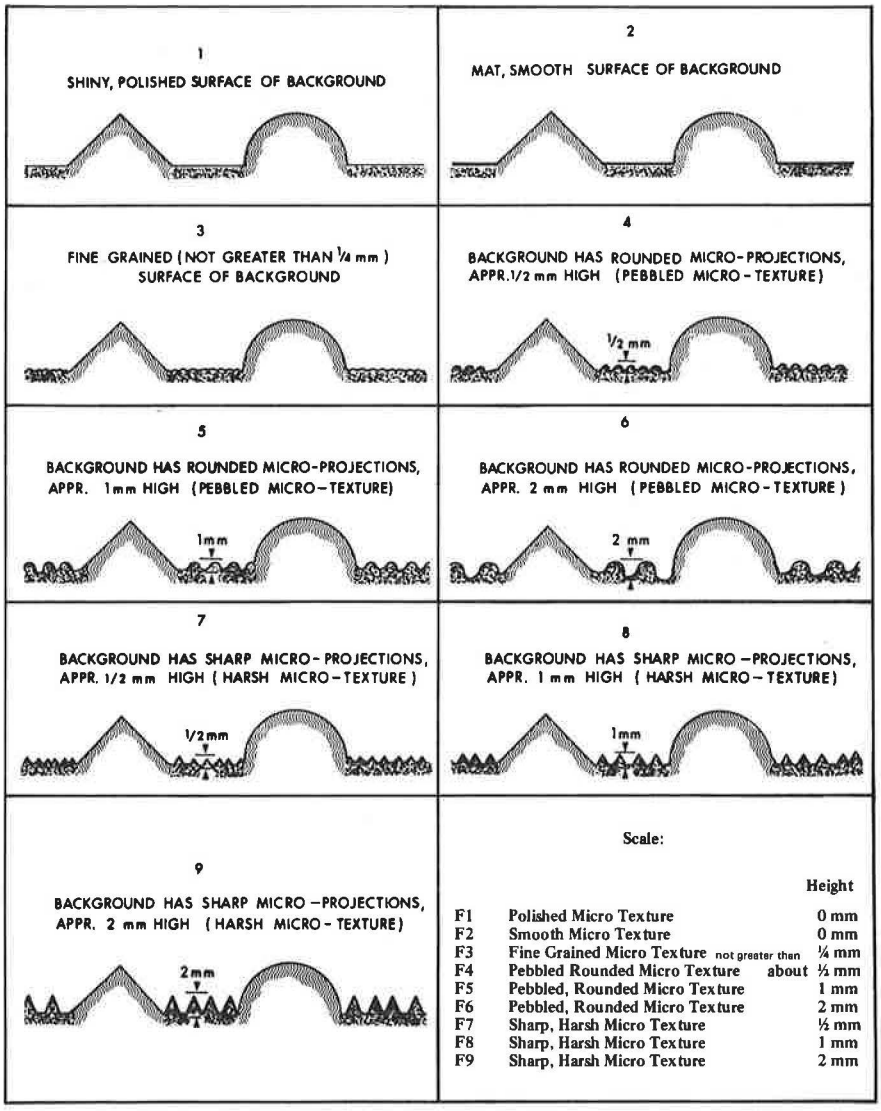


Figure 5. Fine texture of background parameter F.

Undrained cavities parameter G indicates the proportion of cavities (depressions or holes) in the background surface; i.e., none, 1/4, 1/2, or 3/4 (Fig. 6).

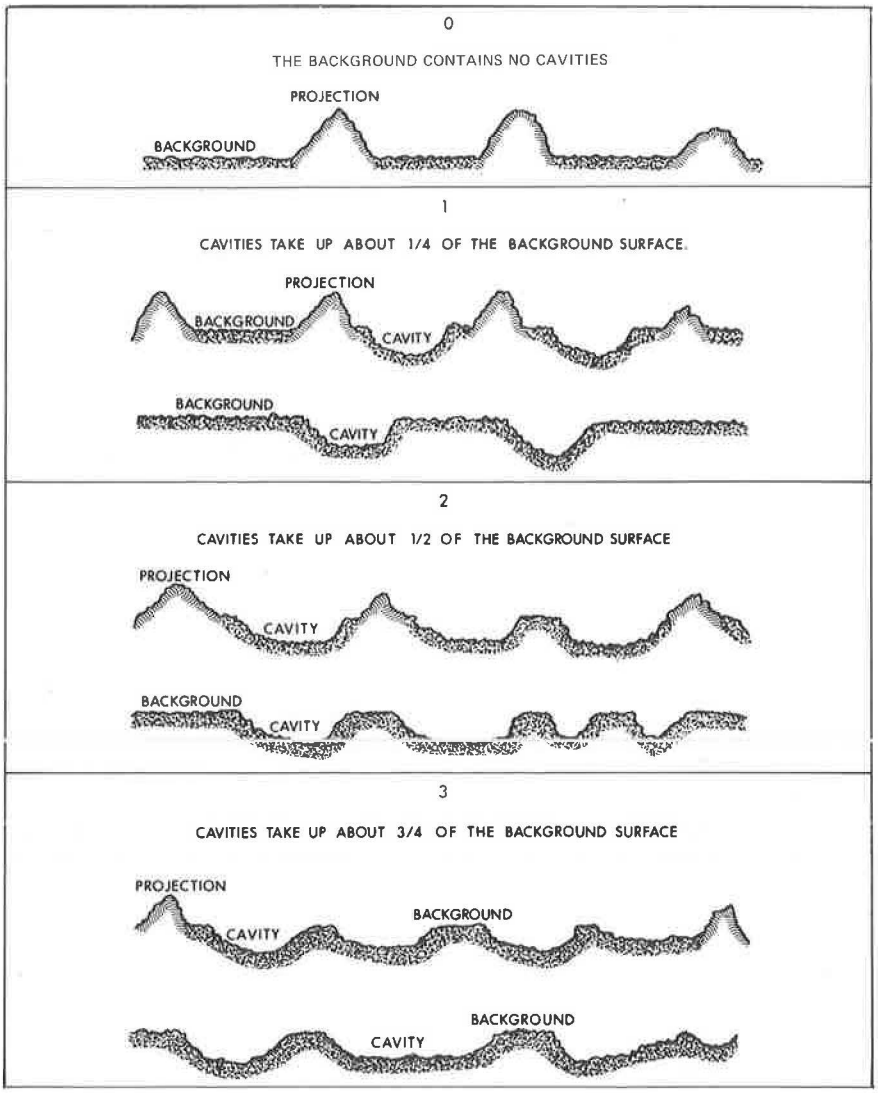


| Scale: | | |
|---|---|---|
| | G0 | No Cavities |
| | G1 | Cavities take up about ¼ of the background |
| | G2 | Cavities take up about ½ of the background |
| | G3 | Cavities take up about ¾ of the background |

Figure 6. Undrained cavities parameter G.

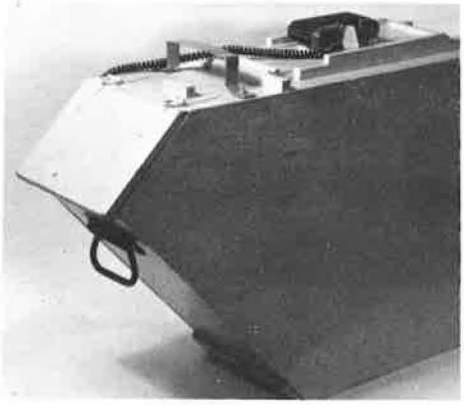

Figure 7. Camera box.

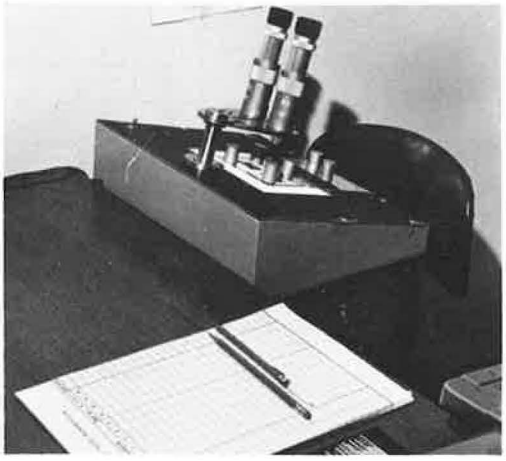

Figure 8. Microstereoscope.

## Examination and Analysis of the Pavement Surface

Color stereophotographs (transparencies) of approximately 6 in. square sections of the pavement surface are obtained by means of a camera box equipped with a 35-mm single-lens reflex camera and a flash attachment (Fig. 7). The pavement sections are identified by numbers placed in the camera's field of view.

Five to ten photographs usually suffice to represent a pavement test section, depending on uniformity and length. The 35-mm transparencies are viewed through a microstereoscope consisting of two 25x linear magnifiers (Fig. 8), and also through a standard stereoscope with a 3x linear magnification (Fig. 9).

The pavement surface is analyzed into texture elements in accordance with the texture parameter table (Fig. 10), and the parameters are entered in a form (Fig. 11) according to the following procedure:

1. Examine the surface projections under the lower magnification stereoscope and note parameter D, which is the density of spacing of the surface projections.
2. Note parameter B, which is the width of the surface projections most prevalent in the photograph. Use the lower magnification stereoscope.
3. Note that parameters A, C, and E should be those of the prevalent projection size, i.e., parameter B.
4. Note parameter A, which is the most prevalent height of surface projections. Use high and low magnification.
5. Note parameter C, which is the prevalent shape of surface projections. Use high and low magnification.
6. Note parameter E, which is the fine texture of surface projections. Use high magnification.
7. Note parameter F, which is the background texture. Use high magnification.
8. Estimate the proportion of holes or depressions below the background level. Use low magnification. It helps to interchange the stereopair by placing the left photograph on the right of the stereoscope, and vice versa. This makes the holes in the surface stand out conspicuously as hills, mounds, or ridges.

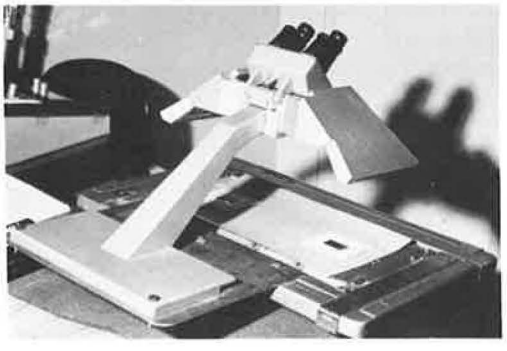

Figure 9. Standard stereoscope.

| PARAMETER NUMBER | PARAMETERS | | | | | | |
|---|---|---|---|---|---|---|---|
| | PROJECTIONS | | | | | BACKGROUND | |
| | A HEIGHT mm. | B WIDTH mm. | C ANGULARITY | D DENSITY PERCENT | E FINE TEXTURE ANGULARITY mm. | F AND HEIGHT | G CAVITIES PERCENT |
| 0 | 0 | >16 | FLAT | 0 | | | 0 |
| 1 | ¼ | 8 | ROUND | 25 | POLISHED | 0 | 25 |
| 2 | ½ | 4 | SUBANGULAR PLATEAU | 50 | SMOOTH | 0 | 50 |
| 3 | 1 | 2 | SUBANGULAR GABLE | 75 | FINE GRAINED | 0 | 75 |
| 4 | 2 | 1 | ANGULAR PLATEAU | 100 | ROUND | ½ | – |
| 5 | 4 | ½ | ANGULAR GABLE | – | ROUND | 1 | – |
| 6 | 8 | – | ANGULAR PYRAMID | – | ROUND | 2 | – |
| 7 | 16 | – | – | – | SHARP | ½ | – |
| 8 | – | – | – | – | SHARP | 1 | – |
| 9 | – | – | – | – | SHARP | 2 | – |

Figure 10. Texture parameter form.

The texture code number is composed of the most prevalent parameters on the examined photograph. If another parameter is present in significant proportion, it should be recorded as a secondary parameter. For instance, if the prevalent angularity parameter C is 5 (sharp edges), and if there is a secondary angularity parameter C3 (round edges), the C parameter will be recorded as $\frac{5}{3}$.

A set of sample photographs is indispensable, especially for the beginner, to serve as a reference in borderline cases, e.g., "smooth" microtexture and "fine-grained" microtexture (E2 or E3), or "round" projections and "subangular plateau" projections (C1 or C2) and the like. (Reproductions of pavement stereophotographs are not included in this report because the screening process required for printing makes them unsuitable for viewing under a magnifier.)

## ESTIMATION OF SKID RESISTANCE

It is well known that the topography of a pavement surface influences skid resistance. Several methods for measuring surface texture have been developed and attempts have been made to correlate pavement texture and skid resistance. Among these are the following:

1. The sand patch method (3) aims at measuring the texture depth of a pavement surface by spreading a known quantity of sand and by measuring the covered area.

| PHOTO NO. | PARAMETERS | | | | | | | SKID NUMBER | | | | COMMENTS |
|---|---|---|---|---|---|---|---|---|---|---|---|---|
| | A | B | C | D | E | F | G | 30 MPH ACTUAL | 30 MPH ESTIM. | 60 MPH ACTUAL | 60 MPH ESTIM. | |
| | | | | | | | | | | | | |
| | | | | | | | | | | | | |
| | | | | | | | | | | | | |
| | | | | | | | | | | | | |
| | | | | | | | | | | | | |
| | | | | | | | | | | | | |
| | | | | | | | | | | | | |
| | | | | | | | | | | | | |
| | | | | | | | | | | | | |
| | | | | | | | | | | | | |
| | | | | | | | | | | | | |
| | | | | | | | | | | | | |
| | | | | | | | | | | | | |
| | | | | | | | | | | | | |

Figure 11. Photo-interpretation form.

2. The print method (4) imprints the image of the pavement's bearing surface on a sheet of paper and also gives some indication of length and width of surface drainage channels.

3. The mold method (3) uses hardening plastics to replicate the pavement surface texture, which can then be used for surface measurements in the laboratory.

4. Pavement cross sections are obtained (3) by covering a pavement sample with plaster of paris, cutting it, and photographically enlarging a cross section of the cast.

5. Multiple sounding needles (3), which are free to move vertically and rest on the pavement surface, define a series of points representing the texture profile.

6. The single sounding needle, combined with an electronic device, has been used for drawing a texture profile.

7. Photogrammetry has been used for measuring pavement surface textures (5). It has the advantage over the sand patch and the texture-printing method of indicating the shape and size of projections.

A satisfactory correlation of pavement surface texture with skid resistance has not emerged from these methods, probably because each method takes into account only one textural feature, whereas the pavement's frictional properties are determined by all textural features acting in concert.

## Texture Code Number and Skid Resistance

The photo-interpretation method developed in Ontario analyzes the pavement surface as a whole, and the resulting texture code number is correlated with the skid resistance measured by an ASTM skid trailer. A survey of skid resistance of Ontario highways was made in 1967. Several thousand skid tests were taken that provided an opportunity for a correlation study of skid resistance and pavement texture. Stereophotographs were taken at five successive points on each section of highway tested. A photograph was only considered to represent the test site if at least three adjacent photographs had the same texture code number. This precaution was taken in order to eliminate non-representative photographs as far as possible. The objectives of the photo-interpretation study were to (a) find suitable surface-texture elements whose effect on skid resistance could be traced, (b) investigate the skid-resistance range of pavements with similar texture code numbers, and (c) investigate the effect on skid resistance of one texture parameter in combination with different parameter groups.

## Friction Weights

The table of friction weights (Table 1) is designed to be used in estimating skid resistance in cases where a pavement cannot be skid-tested, e.g., in sharp curves, at

TABLE 1
FRICTION WEIGHTS

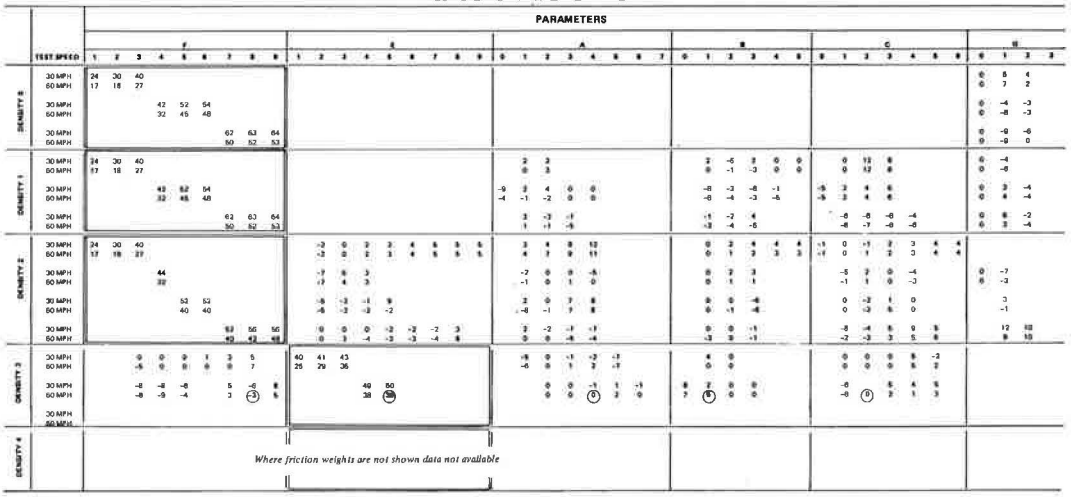

stop-sign locations, or when a skid trailer is not available. The method on which the table is based assigns a weighting to each textural element according to the element's contribution to pavement friction or skid resistance. These friction weights vary according to the other texture parameters present in the texture code number. For instance, the friction weight for a high stone projection is large when it is set in a smooth background, but it is small, or even negative, when set in a harsh background. Because the available amount of correlated skid-test results and texture analyses was not large enough for the development of a regression equation, the friction weights were obtained by trial and error.

The following procedures should be followed in using the table:

1. Note that the pavement textures (texture code numbers) in the table are divided into five groups, i.e., groups D0 through D4 (the D4 group of texture code numbers is not available at present because of a shortage of test data).
2. Find the friction weight of the fine texture parameter inside the thick frame of the table.
3. Find the friction weights of the other six parameters along the same horizontal line as the friction weight obtained in step 2.
4. Obtain the estimated skid number of the pavement texture by adding up all seven friction weights. As an example, the friction weights for texture code number 4123580 are encircled on the table and the estimated skid number in this case is 41 for a speed of 60 mph.

Skid trailer test results and the estimated skid numbers, obtained from Table 1, were plotted and are shown in Figures 12 and 13. The correlation coefficient is 0.9 and the standard deviation is 2.9, for a test speed of 30 mph. At 60 mph, the correlation coefficient is 0.9 and the standard deviation is 2.2. The standard deviation comprises the test error as well as the real variation in magnitude of the skid resistance resulting from variation in the trailer test path, weather, and other conditions. For practical purposes, the standard deviation gives an indication of the skid-resistance range of a pavement surface texture as identified by its texture code number.

## Photo-Interpretation Graphs

The photo-interpretation graphs (Figs. 14, 15, 16, and 17) are the graphical presentation of the friction weights in Table 1. The graphs and table are incomplete at present and are limited to the texture code numbers tested. Because a sufficient number of textures with very closely spaced projections (texture parameter D4) have not yet been encountered, the graphs for this group of pavements cannot be drawn up yet.

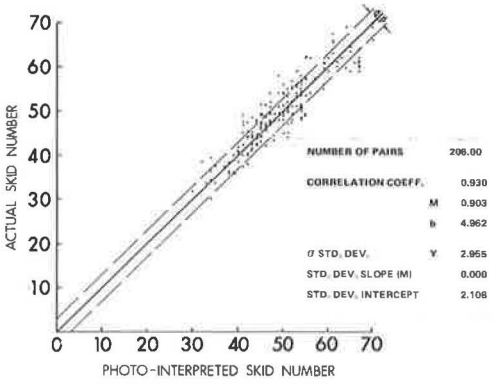


Figure 12. Correlation between estimated skid number and skid-trailer skid number (30 mph).

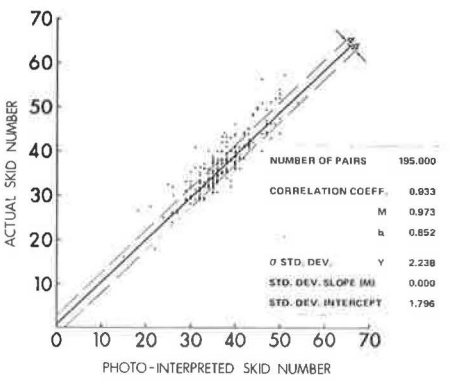


Figure 13. Correlation between estimated skid number and skid-trailer skid number (60 mph).

The graphs can be used as a guide for (a) selecting the most effective stone particle size, if the sand type and the polishing properties of rock or gravel are known; (b) selecting the sand type to suit the coarse aggregate; (c) finding the optimum height of relief if sharpness and harshness of the coarse aggregate and the sand type are known; (d) selecting a suitable chip size and relief height for a precoated chipping surface; (e) assessing the minimum depth of treatment of flushed asphalt pavements; and (f) estimating future decline or increase in skid resistance if the rock type of the aggregate is known. The following two examples illustrate some uses of the graphs.

Example 1—The local sand is sharp, coarse, and has a high silica content. The local gravel contains a large proportion of hard but polishable limestone. There are no quarries in the area. Recommendations: For optimum skid resistance, the high friction weights of an F7 and F9 background texture, i.e., sharp, relatively large microprojections, should be aimed at by incorporating a high proportion (about 70 percent) of the sharp, coarse sand in the pavement surface. Although the stone microtexture (E3 to E0, i.e., fine crystaline to polished particles) is poor, the

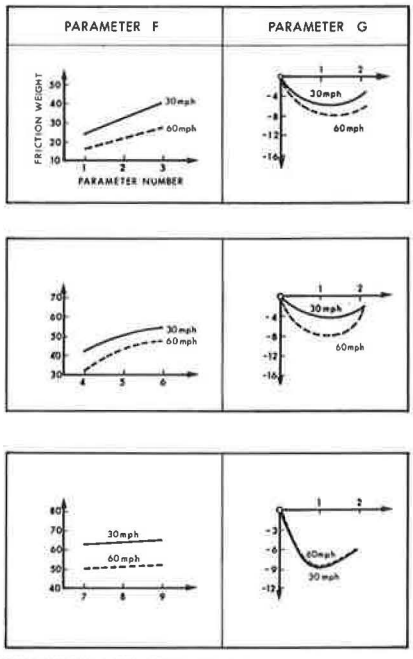


Figure 14. Photo-interpretation graph for density 0.

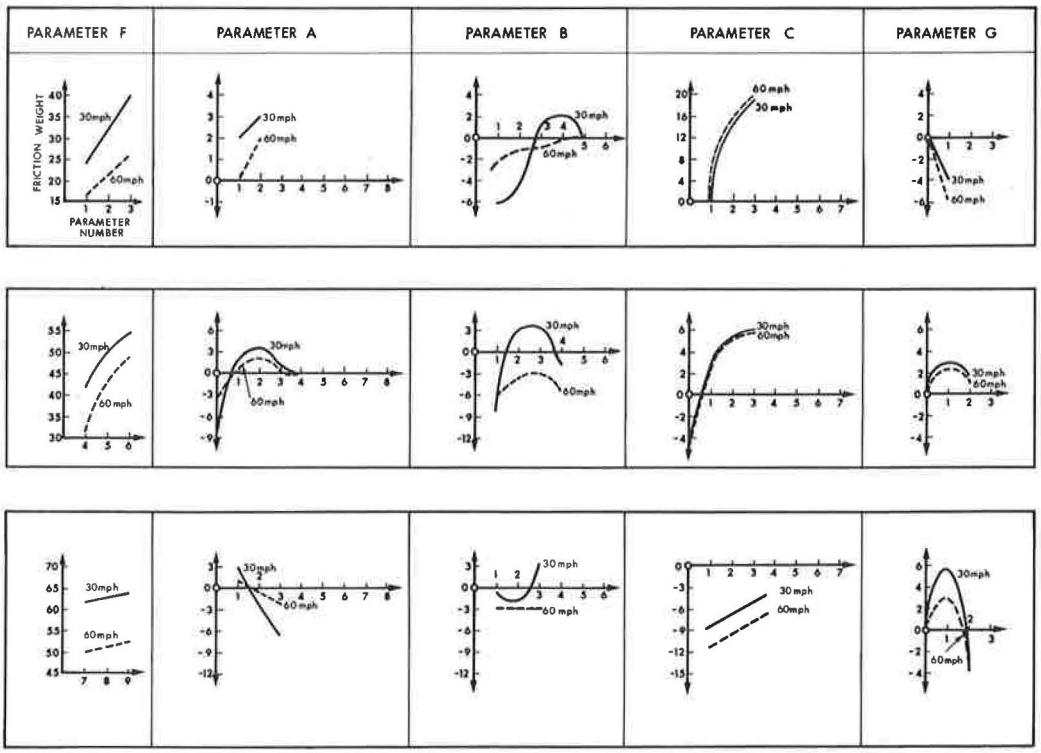


Figure 15. Photo-interpretation graph for density 1.

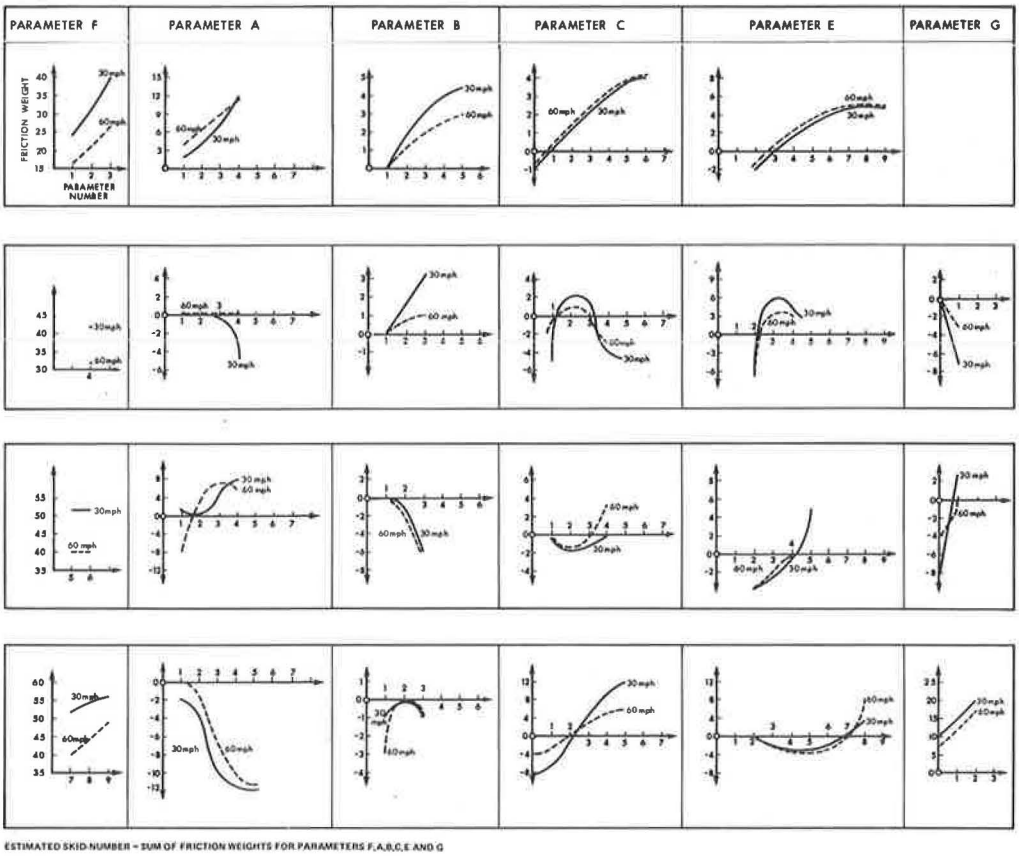


Figure 16. Photo-interpretation graph for density 2.

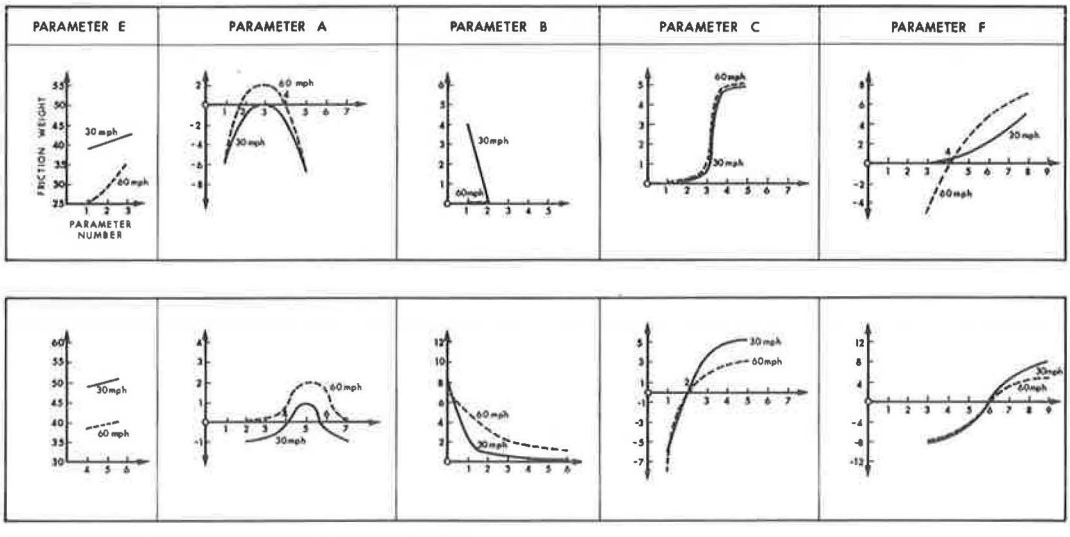


Figure 17. Photo-interpretation graph for density 3.

crushed gravel particles should be relatively large (B1, about 8 mm) and their relief should be kept low (about ¼ mm) to prevent tires of a vehicle from bridging over the sharp, coarse sand. The mix should be as lean as stability will permit. The resulting texture code number would be 1113280. The approximate skid number at 60 mph will be the sum of the following friction weights (Fig. 14):

| Texture Parameter | Approximate Friction Weight |
|---|---|
| F8 | 52 |
| A1 | 0 |
| B1 | 0 |
| C1, polished | -11 |
| Approximate skid number | 41 |

If a mix with a high stone proportion of the same crushed gravel were used, say 70 percent, with 30 percent sand, the projections would be a more densely spaced parameter D3, with an initially good angularity C4. The background texture would still be F8 and the resulting texture code number would be 2143380. The skid number at 60 mph, before traffic wear, would be the sum of the following friction weights (Fig. 17):

| Texture Parameter | Approximate Friction Weight |
|---|---|
| E3, fine crystalline | 35 |
| A2, low relief of new pavement | 0 |
| B1 | 0 |
| C4, good angularity | 5 |
| F7 to F9 | 8 |
| Approximate skid number | 48 |

After traffic wear the resulting texture code number could be 1123170 and the expected skid number at 60 mph would be the sum of the following friction weights (Fig. 17).

| Texture Parameter | Approximate Friction Weight |
|---|---|
| E1, polished | 25 |
| A1, relief of worn pavement | -4 |
| B1 | 0 |
| C2, rounded edges | 0 |
| F7 | 6 |
| Approximate skid number | 27 |

The stoney mix is likely to have the better skid resistance in low-volume traffic locations, but under heavy traffic the skid resistance will decline well below the skid resistance of the recommended mix proportion.

Example 2—The local sand is fine with round particles. The available rock is hard, sharp-edged, and harsh-faced. Recommendation: The stone surface proportion should be large (D3 plus), i.e., the matrix surface should be a minimum. The stone particle size should be large (B0 to B1), and the relief should be about 4 mm (A5). A pavement surface with a texture code number of 4153730 and a skid number of about 39 at 60 mph may be expected.

## STANDARD MEASUREMENT OF SKID RESISTANCE AND STANDARD TEXTURE CODE NUMBER

In the absence of standard skid numbers, the skid resistance of pavement surfaces measured by different skid trailers in different parts of the world cannot be correlated without skid-trailer meetings. It is, however, feasible by means of pavement texture analysis to correlate different skid numbers of the same surface texture code number in the following manner: The skid number of texture code number T, measured by skid trailer $ST_1$, is $SN_1$. The skid number of the texture, $T_X$, measured by skid trailer $ST_2$, is $SN_2$. Therefore, the skid measurements of trailer $ST_2$ in terms of skid trailer $ST_1$ measurements are

$$SN_2 = \frac{SN_1}{SN_2}$$

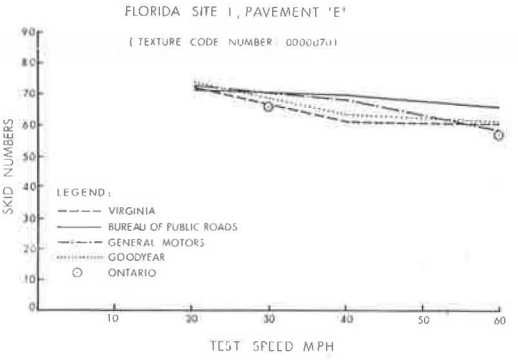


Figure 18. Correlation between skid numbers obtained in Ontario and those obtained by other skid trailers from pavement with similar surface textures (Florida Skid Correlation Meeting, 1967).

This factor may be used for correlating diverse skid-resistance measurements without a meeting of the skid trailers concerned, providing that at least one surface texture was tested by both trailers. As an example, the test results by different skid trailers of a pavement at the Florida Skid Resistance Correlation, 1967, are shown in Figure 18. The texture code number of the surface on test site 1, pavement E was 0000070. The same surface texture was skid-tested in Canada by the Ontario skid trailer. Ontario test results, for a test speed of 60 mph, can be translated into skid numbers obtained by the U. S. Bureau of Public Roads skid trailer by using the skid number ratio, which in this case is

$$\frac{66\ (\text{Bureau})}{57\ (\text{Ontario})} = 1.16$$

On the same principle, the skid number of a simple surface texture, $T_{standard}$, may be rated as 100 percent and the skid resistance of other surfaces may be expressed pro rata, similar to the concept of 100 percent Proctor compaction. For example, the skid resistance of a pavement surface having the surface texture code number 3352370 may be adopted as the standard skid resistance. The skid numbers of this pavement surface as measured by the Ontario skid trailer, 43 at a test speed of 60 mph and 49 at 30 mph, will then represent 100 percent of standard skid resistance. In another geographical location, the same surface texture code number can be adopted as standard and the skid number for 100 percent standard skid resistance can be determined by another skid trailer. If a pavement surface with the adopted standard texture code number is not available for skid-testing, any other surface with a texture code number that has been previously tested by the Ontario skid trailer and for which the percentage of standard skid resistance is known can be used.

## CONCLUSIONS

1. A pavement surface-texture classification method has been devised.
2. Surface-texture parameters have been correlated with skid resistance, and a method for estimating skid resistance from stereophotographs of the pavement surface has been developed that may be a practical alternative to the conventional approach to skid-resistance evaluation based on individual skid tests without reference to past testing experience.
3. By means of the pavement surface analysis described, it will be possible to cor-

relate skid-resistance measurements obtained from different skid trailers in different geographical locations.

## REFERENCES

1. Kummer, A. E., and Meyer, W. E. Tentative Skid-Resistance Requirements for Main Rural Highways. NCHRP Rept. 37, 1967.
2. Croce, K. Mindestwerte fuer Strassengriffigkeit. Strassen- und Tiefbau, Heidelberg, Germany, July 1964.
3. Lucas, J., and Malavialle, M. La Rugosité Géométrique des Revêtements Routiers. Glissance, Special F., Bulletin de Liaison des Laboratoires Routiers Ponts et Chaussées, 1966, pp. 161-175.
4. Kraemer, P. Etat de la Surface des Revêtements Routiers et son Influence sur l'Adhérence. Bitumen-Teere-Asphalte-Peche, No. 11, Nov. 1962.
5. Sabey, B. E., and Lupton, G. N. Measurement of Road Surface Texture Using Photogrammetry. British Road Research Laboratory, RRL Rept. LR57, Crowthorne, Berkshire, England.

# Using a Modified Bureau of Public Roads Roughometer to Measure Pavement Roughness Spectra

B. E. QUINN, Department of Mechanical Engineering, Purdue University;
H. ENGJA, DET Norske Veritas, Oslo, Norway; and
J. L. ZABLE, IBM Corporation, Endicott, New York

A procedure is described by which a BPR roughometer is used to measure pavement roughness spectra. The roughometer is modified by locking the frame rigidly to the axle. A spring-mass system in the form of a cantilever beam is attached to the roughometer. Strain gages mounted on the beam detect the motion induced in the beam when the roughometer is towed over the pavement. The signal from the strain gages provides the input to a special electronic circuit that gives a voltage proportional to the ordinate of the pavement roughness spectrum curve after a fixed interval of time. The frequency (or wavelength) associated with this ordinate is computed from the natural frequency of the cantilever beam and the towing velocity of the roughometer. Different ordinates are obtained by repeating the test at different velocities. The important characteristics of the mechanical and electrical systems are discussed. The roughness spectra of four pavements are included that were measured using this procedure together with the corresponding BPR roughometer ratings.

•IN RECENT YEARS the use of a pavement roughness spectrum for describing the condition of a pavement has attracted considerable interest (1). One reason for this interest is the fact that a pavement roughness spectrum can be used with the appropriate vehicle characteristics to predict certain types of vehicle behavior. It is thus theoretically possible to predict the vertical acceleration that the passengers in a vehicle will experience or to predict the dynamic tire forces that a vehicle will exert on the highway if an accurate pavement roughness spectrum and the necessary vehicle characteristics are available.

Because the Bureau of Public Roads roughometer has been used extensively to measure pavement conditions, the question has been raised as to whether this device, with suitable modifications, could be used to make pavement roughness spectrum measurements. An investigation has indicated that this can be done, provided that certain minor changes are made in the roughometer and that additional mechanical and electrical components are added. This paper deals with the problems encountered in modifying the BPR roughometer for the purpose of measuring a pavement roughness spectrum.

It may be helpful to briefly consider some of the problems experienced in computing a pavement roughness spectrum for a selected pavement. One of the most controversial steps is that of obtaining a suitable measurement of the pavement roughness. If a rod and level survey is conducted along a highway, elevation measurements in a wheelpath can be obtained. These measurements will be affected by the pavement roughness because patches, potholes, and faulting will cause more variation between adjacent

Paper sponsored by Committee on Surface Properties-Vehicle Interaction and presented at the 49th Annual Meeting.

elevation measurements than in the case of a smooth pavement. On the other hand, the established grade line of the highway will also cause successive elevation measurements to differ (even if the pavement surface is perfectly smooth) if the highway is going up or down a hill. The problem therefore arises of extracting from the survey data the variation in the pavement profile that is due to roughness.

One procedure (2) in common use is to establish a running mean by taking the average of several elevation measurements on each side of the elevation measurement under consideration. This average is then subtracted from the elevation measurement to obtain a deviation that is assumed to be related to the pavement roughness. A power spectral density analysis is then made on the deviations thus computed for a selected length of pavement to obtain the pavement roughness spectrum.

Typical pavement roughness spectra are shown in Figure 1. Extensive information is available in the literature (3) concerning the details of the calculations required to compute this type of characteristic, so no attempt will be made in this paper to cover this procedure.

The pavement roughness spectrum indicates the extent to which various wavelengths in the pavement profile contribute to the pavement roughness. The area bounded by the curve, the horizontal axis, and any two selected ordinates represents the contribution to the total mean square value of roughness that is made by the wavelengths lying between the two selected ordinates.

In discussing the profile of a pavement, it is convenient to refer to the wavelengths that may be present. In making a power spectral density analysis of the deviations just described, it is more convenient mathematically to deal with the reciprocals of the wavelengths and to refer to them as frequencies. Normally one associates the use of the word "frequency" with a phenomenon in which time is a variable. In defining a highway profile, purely geometric quantities are used. As a result, the frequency that is used in connection with a pavement roughness spectrum is a distance-based frequency having the units of cycles per foot. This quantity is actually the reciprocal of the wavelength and is more convenient to use in this type of analysis than the wavelength itself.

The total area under a power spectrum curve (calculated from the deviations previously described) represents the total mean square roughness of the pavement in units of feet squared. The ordinate of the roughness spectrum is, however, in units of feet squared per cycle per foot and, as such, represents a roughness density. The area between two selected frequencies thus represents the contribution that this band of frequencies makes to the total pavement roughness. The ordinates, as such, of a roughness spectrum curve are of secondary interest because it is theoretically impossible to refer to the roughness contributed by only one wavelength in a pavement profile.

Different investigators have used different techniques for computing the pavement roughness from elevation measurements, and thus different roughness spectra can be obtained from the same set of elevation measurements (4). An example of this is shown in Figure 1 in which the two broken-line curves repre-

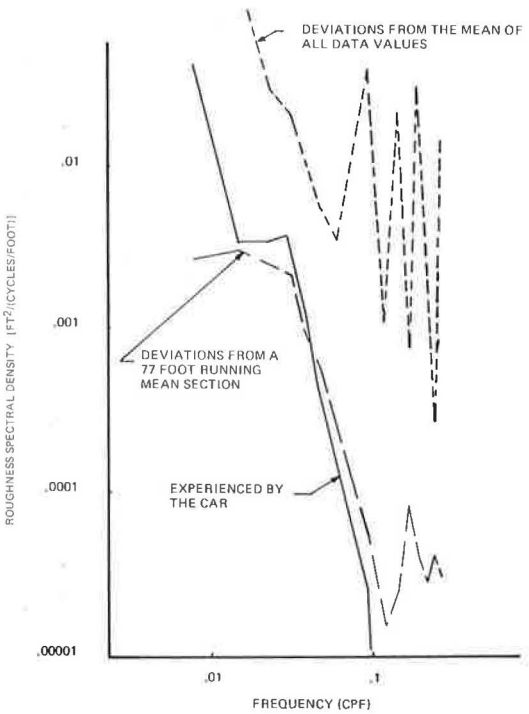


Figure 1. Pavement roughness power spectrum curves.

sent two different pavement roughness spectra calculated from the same set of pavement elevation measurements. It would be nice to say that this problem is completely avoided when the BPR roughometer is used to measure a pavement roughness spectrum, but this is not true. The problem is still encountered, but in a different manner.

The solid curve shown in Figure 1 represents the roughness spectrum actually experienced by a vehicle operated over the highway in question. It is interesting to note that both procedures used for calculating the roughness spectrum from elevation measurements have overestimated the actual roughness experienced by the car at high frequencies. Moreover, one procedure overestimates the magnitude of the roughness experienced by the car at very low frequencies, whereas the other procedure underestimates this value for the same frequencies.

The principal attraction of the BPR roughometer for measuring pavement roughness spectra lies in the fact that the roughometer will separate the roughness of the pavement from variations in the grade line in much the same manner as will an actual vehicle. This is one of the main reasons for using the BPR roughometer for this purpose.

## FUNDAMENTAL CONSIDERATIONS

The basic idea underlying the use of the BPR roughometer for measuring pavement roughness spectra can best be discussed in reference to Figure 2. In this figure a length of the highway profile is shown that contains a well-defined wavelength as indicated. On this highway is placed an ideal trailer having one wheel. In this case an ideal trailer is defined as one that will follow the highway profile exactly and that will introduce no natural frequencies into the resulting records. On this trailer is mounted a spring-mass system that contains an appropriate amount of damping. Although constraints are not shown in Figure 2, it is understood that only vertical motion is possible for this mass.

As the trailer is towed over this highway at the velocity V, a periodic motion will result at the point at which the spring-mass system is mounted to the trailer. The frequency of this vertical motion will depend on the velocity of the trailer. A high velocity will result in a high frequency, whereas a low velocity will result in a low frequency. The spring-mass system mounted to the bed of the trailer as shown will have a certain natural frequency of vibration, $f_n$, depending on the magnitude of the mass, on the stiffness of the spring support, and, to a limited extent, on the amount of damping existing between the mass and the bed of the trailer. There exists a velocity at which the vertical motion of the bed of the trailer will have the same frequency as the natural frequency of the spring-mass system. At this velocity, resonance will occur in the spring-mass system. This will result in large displacements of the mass in the system shown. The

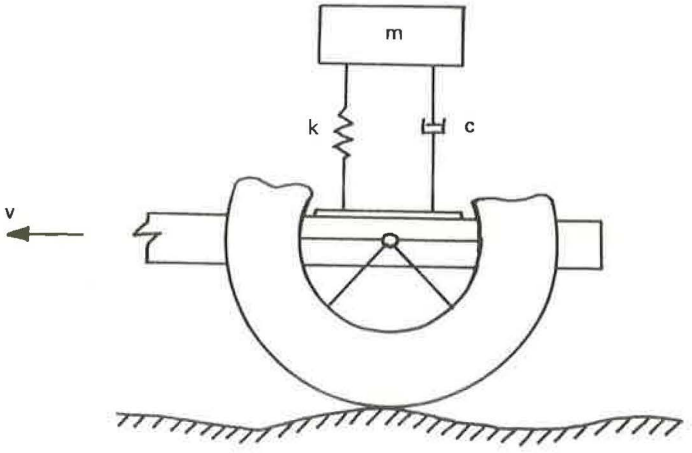


Figure 2. Schematic representation of spring-mass system mounted on an ideal vehicle.

actual wavelength, $\lambda$, of the undulation shown in the pavement in Figure 2 can thus be determined by observing the motion of the mass and by noting the vehicle velocity at which the largest amplitude of motion exists. This wavelength can be computed using the relationship

$$\lambda = \frac{V}{f_n}$$

At speeds corresponding to frequencies greatly above or greatly below the natural frequency of the spring-mass system, relatively little motion will occur between the mass and the bed of the trailer. Thus the natural frequency of the system and the trailer velocity can be used to calculate the wavelength causing the disturbance.

If the pavement undulation has high peaks and low valleys, a much larger motion of the mass will result than if the undulation is relatively smooth. If the heights of the peaks and valleys are taken as a measure of pavement roughness, then a large amount of roughness will produce large motions of the mass, whereas a relatively small amount of roughness will produce relatively smaller motions.

Consider the system shown in Figure 2, and assume that the natural frequency of the spring-mass system is 1 cycle per second (cps). If this system is towed at 20 feet per second (fps) over a pavement that contains a wavelength of 20 ft, this wavelength will induce resonance in the system. As a consequence, large amplitudes of motion will occur between the frame of the vehicle and the suspended mass. If this wavelength has a large amplitude, the mass will vibrate violently; if the wavelength has a small amplitude, there will be relatively little motion induced in the mass. If the vehicle is towed at 45 fps over the same pavement, then the wavelength of 20 ft will induce relatively little motion in the mass. A wavelength of 45 ft, however, would again be in resonance with the spring-mass system and would thus induce large amplitudes of motion.

The wavelength being measured therefore depends on the velocity with which this system is towed over the pavement and on the natural frequency of the spring-mass system. The amplitude of this wavelength is indicated by the amplitude of the vertical motion induced in the mass. This is the basic principle underlying the operation of the modified BPR roughometer for use in measuring roughness spectra. Suitable spring-mass systems are attached to the roughometer to simulate the ideal system shown in Figure 2. Electronic circuits are used to measure the motion of the mass relative to the roughometer and to obtain from these measurements a value for the ordinate of the pavement roughness spectrum curve. As will be shown later, actual tests indicate that the BPR roughometer thus modified can be used for this purpose.

## ROUGHOMETER MODIFICATION

In many ways the BPR roughometer is well qualified for use as the vehicle in making these measurements. It is of relatively simple construction, and its suspension characteristics can be easily measured and modified. In addition, the roughometer is sufficiently heavy to maintain contact with the pavement at higher towing velocities. Moreover, it is presently being operated by many state highway departments and is therefore readily available to many people who may wish to make this type of measurement.

One modification is made on the BPR roughometer in order to use it for this purpose. The roughometer introduces a natural frequency into the measurements that is caused by the motion of the sprung mass of the roughometer relative to the axle. Moreover, this motion is nonlinear because of the nature of the hydraulic shock absorbers that connect the mass to the axle. This frequency can easily be eliminated by locking the sprung mass of the roughometer to the axle, and this can be done by using a simple rigid mechanical connection. The roughometer also introduces another frequency into the measurements that consists of the bouncing of the roughometer on its tire. This frequency cannot be removed mechanically, but it can be removed electrically, as will be described later. Aside from connecting the axle rigidly to the frame and inflating the tire to the proper pressure, no further changes must be made in the existing roughometer. It is, of course, necessary to add the spring-mass system described in the next section.

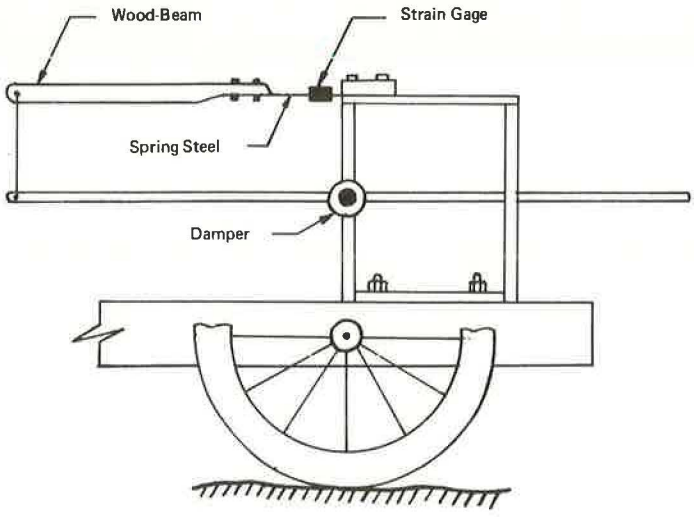


Figure 3. Beam and damper assembly.

## FACTORS INFLUENCING THE SELECTION OF A SPRING-MASS SYSTEM

The spring-mass system used for this purpose must be rugged, simple, and designed in such a manner that the damping coefficient can be easily adjusted. The idealized spring-mass system shown in Figure 2 was approximated by the use of a cantilever-beam system shown in Figure 3. A composite cantilever beam was connected to a rigid base as indicated. The tip of this beam was attached to a long arm mounted below the beam as shown. The center of gravity of the arm was located at the axis of rotation of the arm relative to the base. This had the effect of reducing the natural frequency of the beam while not increasing the static deflection. Moreover, a variable damping element was mounted at the axis of rotation of the arm as shown in Figure 3. This provided variable damping for the system without changing other characteristics. Strain gages were mounted on the spring steel strip that provides the elasticity for the beam.

The system shown in Figure 3 actually responds to more than one wavelength for a given vehicle velocity. It responds to a range of wavelengths controlled by the damping and natural frequency of the mechanical system and the characteristics of the associated electronic system (discussed next). Figure 4 shows the relationship between the range of wavelengths, $\Delta\lambda$, being measured at a particular vehicle velocity, V, and the natural frequency of the beam being used to make the measurements. In these tests two cantilever beams were used having natural frequencies of 2 and 9.33 cps respectively.

The longest wavelength that can be measured in a pavement profile depends on the highest towing velocity that can be used together with the lowest natural frequency that can be realized in the spring-mass system. The shortest wavelength depends on the highest natural frequency of the spring-mass system and the lowest vehicle velocity that can be utilized. For the parameters selected in these experiments, Figure 4 shows the wavelengths that are measured at the indicated towing velocities. Using the beam having a natural frequency of 2 cps, the range of wavelengths that will be measured using a towing velocity of approximately 46 mph is indicated by $\Delta\lambda_4$ in Figure 4. A towing velocity of $V_3$ can then be utilized to measure the next band of wavelengths indicated by $\Delta\lambda_3$. Four different towing velocities are shown in Figure 4 that will result in a continuous coverage of wavelengths ranging from the maximum to the minimum when the 2-cps beam is used.

At a towing velocity of $V_1$, a minimum wavelength of approximately 9 ft can be measured using the 2-cps beam. The measurement of the power associated with shorter wavelengths will require abnormally low vehicle velocities that are not practical. In order to measure the power or roughness associated with shorter wavelengths, it is

necessary to use a higher frequency beam. Such a beam is shown in Figure 4 by the dotted line; it has a natural frequency of 9.33 cps. If the towing velocity is then increased to the maximum value indicated by $V_4$, the range of wavelengths that will be measured using the high-frequency beam is indicated by the lower portion of Figure 4. Continuous coverage of all wavelengths, from the highest to the lowest, requires the proper selection of the natural frequency of the spring-mass system and the proper towing velocity. Figure 5 shows two cantilever strips mounted on the BPR roughometer ready for highway testing. In actual highway operation it is necessary to protect these beams from the effect of the wind, and a wooden cover encloses the entire mechanical system, protecting it from the weather.

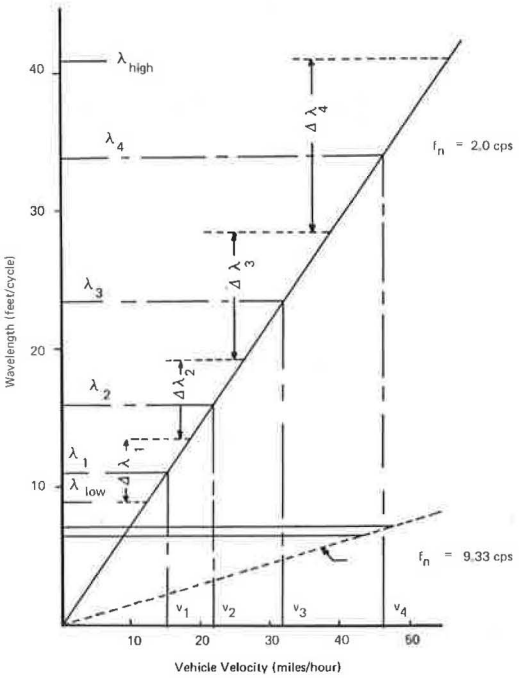


Figure 4. Effect of vehicle velocity and beam frequency on range of wavelengths contributing to roughness power spectrum.

## ELECTRONIC SYSTEM REQUIREMENTS

When the cantilever beams are mounted on the BPR roughometer as shown in Figure 5 and the roughometer is towed over a highway, the motion of the cantilever beams is detected by strain gages mounted on the spring steel element of the beams as shown in Figure 3. In this investigation only one beam was active during a run in order to minimize the investment required in the electronic circuits.

The signal from the strain gages is amplified by the first portion of the electronic system. This signal as it comes from the strain gages contains the natural frequency of the beam together with the natural frequency of the roughometer bouncing on its tire. As mentioned previously, this frequency of the roughometer could not be eliminated mechanically, but at this point it is removed electrically through an appropriate circuit; an electronic filtering process is thus used to remove the undesired frequency introduced mechanically by the roughometer.

The remaining signal, containing only the natural frequency of the beam, then enters a squaring circuit, as shown in Figure 6. Care must be taken in designing this circuit to be sure that large values of the input signal do not exceed the maximum capacity of the squaring circuit, because saturation can easily result if excessive inputs are encountered.

Some types of squaring circuits do not operate satisfactorily on very low values of input voltage. It is therefore necessary to select a circuit that does not arbitrarily cut off low values of input voltage. Moreover, some squaring circuits will not accept negative voltages, and circuits of this type are not suitable for this purpose. A squaring circuit used for this purpose should there-


Figure 5. Two cantilever beams mounted on modified BPR roughometer for measuring pavement roughness spectra.

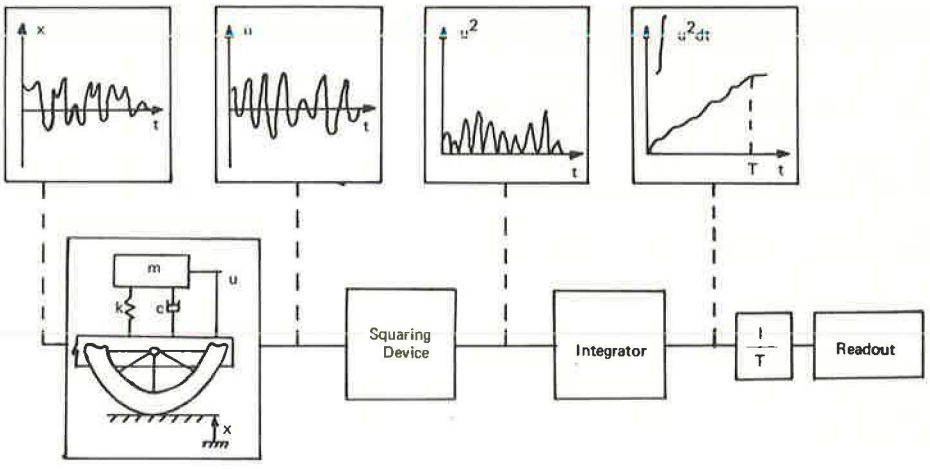


Figure 6. Block diagram (with typical waveforms) for electronic system used with modified BPR roughometer to measure pavement roughness spectra.

fore be able to accept either positive or negative voltages, should not exclude low voltages close to zero from the squaring operation, and should permit a large amplitude of input voltage before saturation occurs.

The output of the squaring circuit is then integrated over an arbitrary period of time, as indicated in Figure 6. In the construction of these electronic circuits, commercially available operational amplifiers of a relatively inexpensive type were used. These proved satisfactory for every circuit except the integrating circuit. Early road tests indicated that a relatively high-quality operational amplifier would be needed in order to avoid excessive drifting during the time of integration. A stabilized operational amplifier was therefore found necessary in order to obtain satisfactory integration of the signal.

The entire electronic system, with the exception of the integrating circuit just noted, was made with commercially available components together with relatively inexpensive operational amplifiers. This system has been very reliable, and no problems of any consequence resulting from faulty operation of the electronic equipment have been encountered. A source of 110-volt current is presently required for the operation of the electronic circuits. This is due primarily to the special requirements of the stabilized amplifier in the integrating circuit. It appears possible, however, by suitable design to eliminate the need for the 110-volt power supply and to operate entirely on batteries. The present level of funding has not made this possible yet.

The integrated value of the signal, mentioned previously, is read from a meter and is multiplied by a constant to give a value for an ordinate of the pavement roughness spectrum. The vehicle velocity at which this reading is taken establishes the wavelength and thus the frequency associated with this value.

Of particular importance in the design and operation of the electronic system is the bandwidth associated with the signals that are processed. The bandwidth of the system depends on the characteristics of the electronic circuit and on the damping in the mechanical vibrating system. This bandwidth is used to establish the constant by which the meter reading is multiplied to get the value of the roughness spectrum. Further discussion of this relationship is beyond the scope of this paper.

## HIGHWAY OPERATION OF MODIFIED ROUGHOMETER

The system was operated in the following manner after checking to make sure that the mechanical and electrical systems were functioning. The roughometer was brought up to the speed associated with the range of wavelengths to be measured (Fig. 4). When the roughometer reached the selected pavement section, a switch was thrown and the

integrating process was started. After 1 minute of elapsed time, another switch was thrown that preserved the integrated value of the output (Fig. 6) on a voltmeter. This value, together with the velocity, was recorded and another run was undertaken.

The roughometer was again brought up to the speed associated with the next wavelength to be measured. When the roughometer crossed the starting line of the pavement section, the integrating switch was again thrown. Integration was continued for a period of 1 minute, at the end of which the integrated value was read from the voltmeter. Because the integration process is carried out for the same period of time regardless of the vehicle velocity, different lengths of pavement are traversed at different speeds. This requires that a statistically significant pavement section be used when these measurements are made, and that no significant change in pavement condition occur within the pavement section undergoing these measurements. The same conditions are involved when pavement roughness spectra are to be computed from elevation measurements, and hence no new limitations are imposed on the measurements of pavement roughness spectra when the modified BPR roughometer is used.

No adjustments were needed on the electronic circuit once the testing program had begun. It was necessary, however, to shift from a low-frequency filter to a high-frequency filter when the high-frequency beam was used in place of the low-frequency beam to make roughness spectrum measurements.

## RESULTS

The use of two spring-mass systems in the form of cantilever beams was discussed earlier. Subsequent research yielded a mechanical device that could provide the equivalent of three spring-mass systems. Use of this device on a roughometer in place of the two cantilever beams made it possible to measure wavelengths from 96 to 4 ft.

The results of tests conducted on four different pavements are shown in Figure 7. For each pavement the roughness spectrum is shown by the designated curve. In addition, the area under each curve is given in a table that also includes the Bureau of Public Roads roughometer ratings (BPRR).

Cumberland Avenue is a rigid pavement with faulted joints and tilted slabs. Passengers in a car experience an extremely unpleasant sensation when riding over this pavement. The roughometer rating of 153 in. per mile is quite appropriate. Cherry Lane is a rigid pavement in good condition. Slight cracking of the slabs is evident, but this does not produce any significant motion in a vehicle. State Route 26 is a flexible pavement with a good surface but with a discernible low-frequency (long-wavelength) undulation in its longitudinal profile. At low vehicle velocities this condition is not evident, but at higher velocities a passenger experiences excessive vertical motion. Lindberg Road is a flexible pavement in excellent condition that serves as the local drag strip. This fact alone attests to its desirable surface properties. It has a roughometer rating of 70 in. per mile.

As mentioned previously, the area under the roughness spectrum curve represents the mean square value of the pavement roughness. If this is used as a criterion of pavement condition, misleading conclusions may be drawn. This would indicate that State Route 26 is the roughest of the four pavements and that Cumberland Avenue and Lindberg Road are of approximately the same roughness. This is not true, and for the pavements under consideration the roughometer ratings give an accurate description of pavement condition.

A vehicle moving over a pavement is very sensitive to certain wavelengths. If these wavelengths make a large contribution to the pavement roughness, then excessive vertical motion will be induced in the vehicle. This will result in an unpleasant ride and in large dynamic tire forces. The value of a pavement roughness spectrum is that it indicates the extent to which various wavelengths contribute to the total pavement roughness.

With this in mind, consider the roughness spectrum of Cumberland Avenue. At frequencies ranging from 0.02 to 0.25 cycles per foot (wavelengths ranging from 50 to 4 ft), this pavement has from 3 to 100 times the roughness of Lindberg Road. Under prevailing traffic conditions, vehicles are very sensitive to these wavelengths and thus the unpleasant ride associated with Cumberland Avenue. On the other hand, at wavelengths

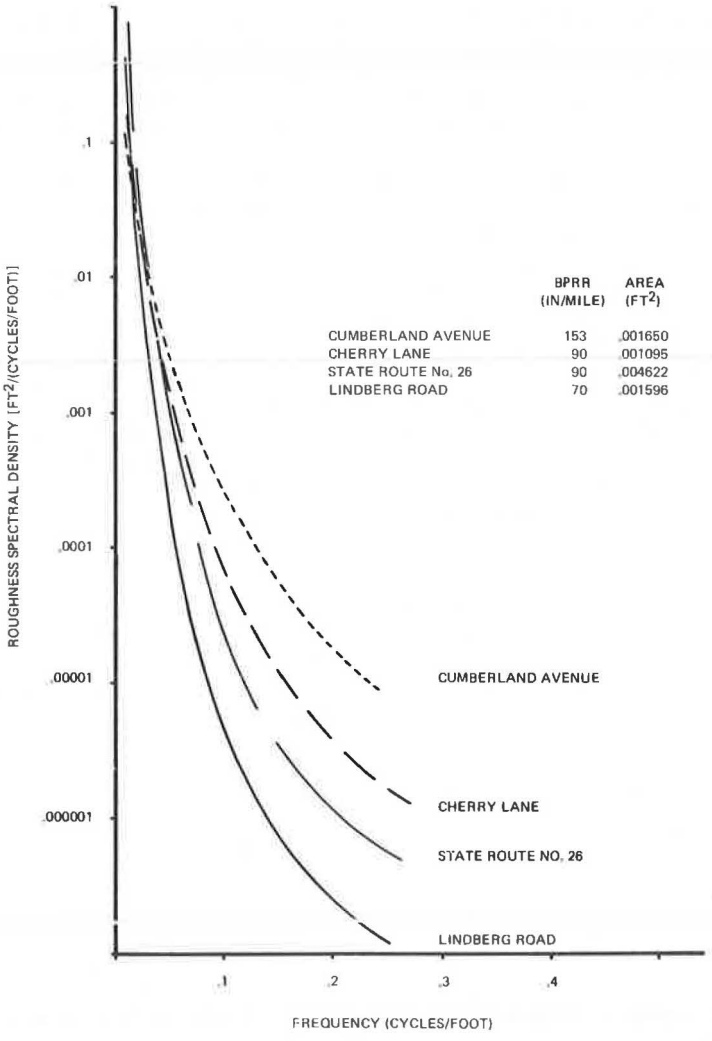


Figure 7. Pavement roughness spectra obtained using modified BPR roughometer.

in excess of 70 ft, Lindberg Road is rougher, but vehicles are not as sensitive to this excitation. Further information concerning the relationship between pavement roughness spectra and vehicle characteristics is given elsewhere (5).

One further observation is appropriate concerning Figure 7. It should be noted that the roughness of long wavelengths is several orders of magnitude greater than the roughness associated with short wavelengths. Areas under roughness spectrum curves are therefore not greatly influenced by relatively large differences in roughness in the high-frequency (short-wavelength) region.

## CONCLUSIONS

A method is available for making pavement roughness spectrum measurements using a modified BPR roughometer. A spectrum obtained using this equipment is relatively free from the arbitrary decisions that are required when such a spectrum is to be calculated from highway profile measurements obtained using a wide variety of devices.

Further effort is required, however, to optimize the mechanical and electronic components, to increase the sensitivity, and to extend the range of wavelengths that can be measured with this equipment. Breadboard circuits that are satisfactory for experimentation must be made suitable for highway operation.

Previous research (5) has shown that it is possible to predict dynamic tire forces if a pavement roughness spectrum is available along with the proper vehicle characteristics. Using the same basic procedure, it is also possible to estimate the extent to which cargo may be damaged and to predict whether or not the ride on a pavement will be satisfactory. These predictions have as their starting point a knowledge of a valid roughness spectrum for the pavement under consideration. A BPR roughometer, modified as indicated in this report, gives great promise of being able to supply this information for a modest investment of funds and effort.

## ACKNOWLEDGMENTS

The authors wish to thank the U.S. Bureau of Public Roads for encouragement and advice, as well as for support of this research. They also wish to thank Ali Sattaripour for valuable supporting effort in conducting laboratory and highway tests.

## REFERENCES

1. Walls, J. H., Houbolt, J. C., and Press, H. Some Measurements and Power Spectra of Runway Roughness. NACA Tech. Note 3305, 1954.
2. Thompson, W. E. Measurements and Power Spectra of Runway Roughness at Airports in Countries of the North Atlantic Treaty Organization. NACA Tech. Note 4303.
3. Blackman, R. B., and Tukey, J. W. The Measurement of Power Spectra. Dover Publications, 1958.
4. Quinn, B. E., and Hagen, K. Problems Encountered in Using Elevation Power Spectra as Criteria of Pavement Condition. Highway Research Record 189, 1967, pp. 166-181.
5. Quinn, B. E., and Van Wyk, R. A Method for Introducing Dynamic Vehicle Loads Into Design of Highways. HRB Proc., Vol. 40, 1961, pp. 111-124.

# A Road Profile Data-Gathering and Analysis System

ROGER S. WALKER and W. RONALD HUDSON, Center for Highway Research, University of Texas at Austin

A profile data-gathering and analysis system developed for the Texas Highway Department is described. This paper presents details of the overall system and demonstrates that rapid and effective data processing is essential for a usable system. The analog-to-digital data conversion and processing subsystem used in conjunction with a surface dynamics profilometer is described. The operating procedure used for gathering and validating data is presented covering both the profilometer and analog-to-digital subsystems. The analysis of the overall system includes an experiment conducted to check the authenticity of the calibration signals and detect errors in the digitization process. Many of the problems encountered during development of the overall system and corrections required to keep the system operational are described. Suggestions for needed modifications, including a noncontact sensing wheel, are discussed.

•THIS PAPER describes a road profile data-gathering and analysis system that provides quantitative records of a road profile at speeds up to 60 mph and thus can be used without causing undue traffic interference. The two major components of the road profile data system (Fig. 1) are a surface dynamics (SD) profilometer and an analog-to-digital (A-D) data conversion and processing subsystem, which is essential for effective use of the gathered data.

The SD profilometer was developed by General Motors Corporation for gathering analog profile data to use in vehicle ride simulation. However, there was widespread interest in it, and K. J. Law Engineers, Inc., was licensed to manufacture it. The SD profilometer used in this road profile system was the first one delivered by Law.

The other major component of the system is the A-D subsystem, two versions of which are available: an SDS 930 general-purpose computer with an A-D peripheral unit owned by the University of Texas, and a Hewlett-Packard 2115 computer, purchased for use with the system. The HP 2115 system is just becoming operational and is not described here. It does, however, maintain complete compatibility with the SDS equipment.

The profile data recorded in analog form by the SD profilometer could be processed in several ways, including analog and digital, but digital processing was chosen for this system to give increased flexibility and because a digital computer was available. Analog processing is satisfactory if only processing techniques such as harmonic analyses and power spectral density are to be used, but digital processing has advantages if other techniques such as variance of slope or roughness indexes, which are more difficult to obtain in analog form but lend themselves to digital processing, are to be used.

Development of the overall system brought out a variety of problems, many of them concerned with the profilometer. They are discussed here together with modifications required to keep the system operational and suggestions for permanent solutions.

Paper sponsored by Committee on Pavement Condition Evaluation and presented at the 49th Annual Meeting.

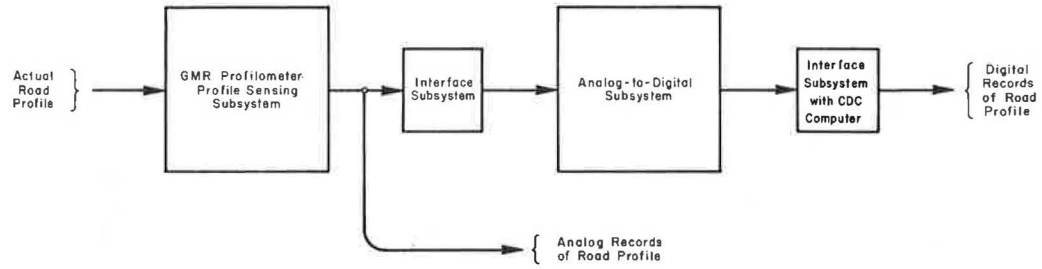


Figure 1. Profile-measuring system.

## SYSTEM DESCRIPTION

The objective in developing a high-speed profile data-gathering and analysis system was to provide a capability of measuring highway profiles at highway speeds and using the resulting data in such ways as (a) evaluating the serviceability index of new or existing pavements; (b) establishing pavement maintenance priorities; (c) conducting research, such as determining whether continuously reinforced concrete pavements provide better serviceability than jointed pavements; and (d) possibly establishing roughness levels for acceptance of new construction.

A standard procedure for use in gathering and analyzing road profile data was developed. Figure 2 shows the measurement process. To determine the profile for a particular pavement, the SD profilometer is driven to the section to be measured, the proper filter and speed combinations are determined, and the electronic equipment is calibrated. The profilometer then is driven over the pavement section and the road profile measurement is recorded in continuous form by a strip chart recorder, which provides a permanent visual record of the profile, or on an analog magnetic tape recorder, or both. To obtain a digital record of this profile, the analog tape is sent to a laboratory, where the A-D subsystem computer converts the road profile measurements to discrete digital values at desired equidistant intervals for processing. Computer programs are then used to summarize the data in the form required for profile analysis. A detailed block design for the road profile data-gathering and analysis system is shown in Figure 3.

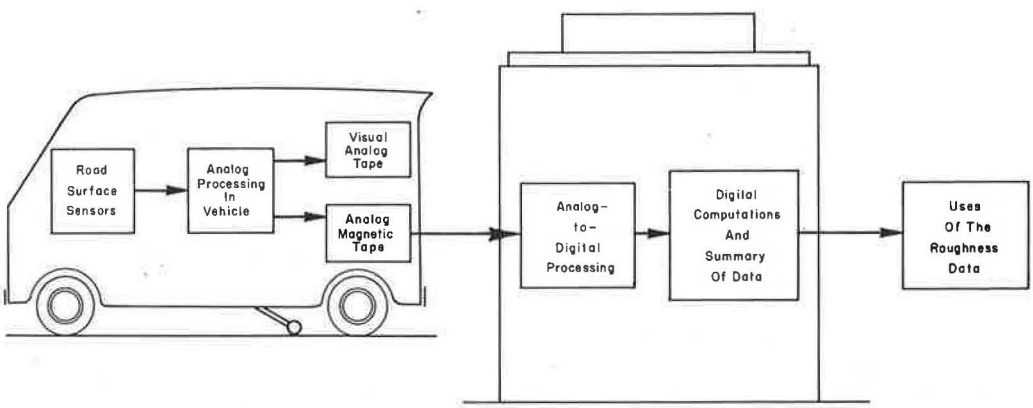


Figure 2. Measurement process.

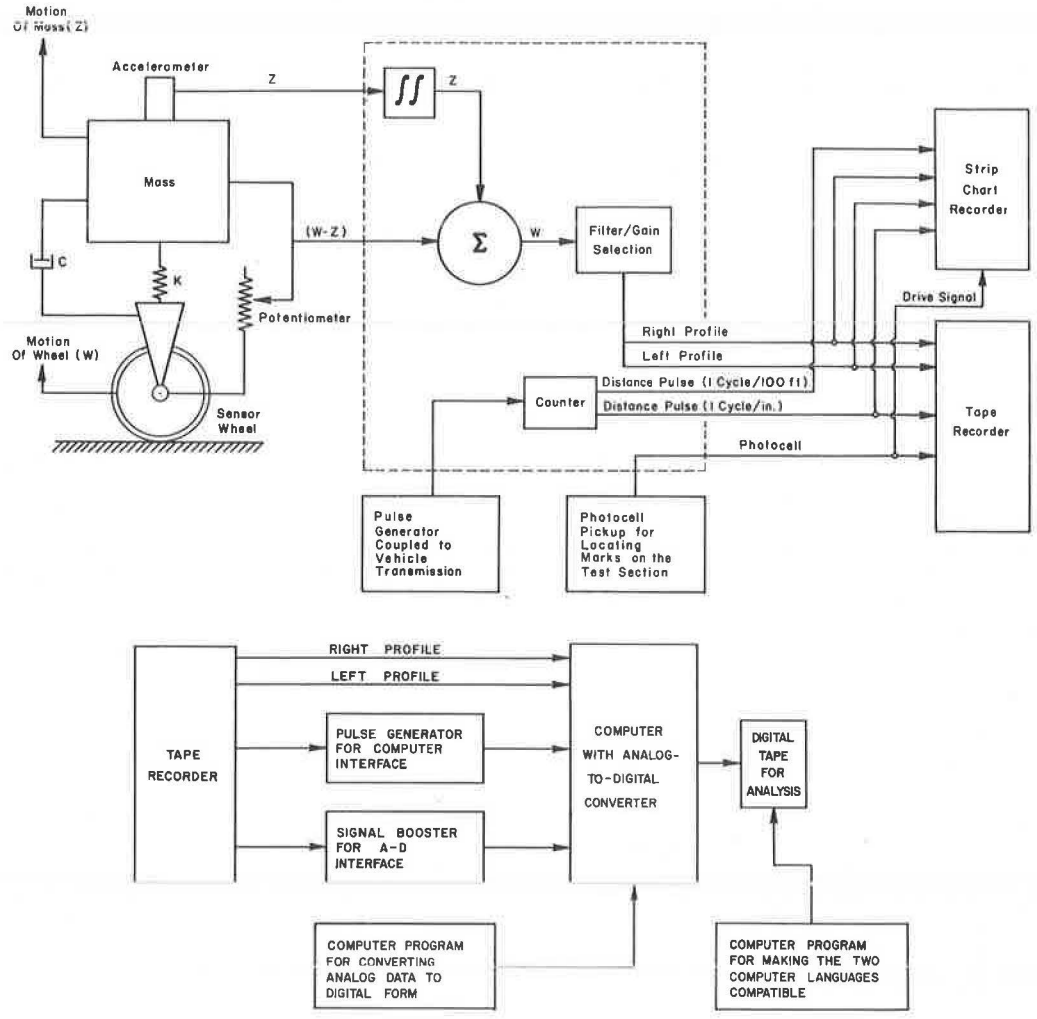


Figure 3. Detailed block diagram of measurement system.

## Measuring Technique and Equipment

The SD profilometer contains all the necessary sensors and equipment to obtain an analog signal directly proportional to a roadway profile: two road-following wheels (each mounted to the vehicle and held firmly in contact with the road by a 300-lb spring force exerted by a torsion bar and a linear potentiometer), an accelerometer, and a small analog (profile) computer to sense and record data. A linear potentiometer is mounted between a sensor wheel and the vehicle body, and the difference in sensor wheel and vehicle body displacements, W - Z, is obtained by the potentiometer. The accelerometer, mounted directly above the potentiometer, induces a voltage proportional to the vertical vehicle body acceleration, $\ddot{Z}$, and the analog computer double-integrates the vertical body acceleration to obtain the vertical body displacement, Z. A voltage directly proportional to the vertical wheel movement (the road profile) is then obtained by the analog summing of the vertical body displacement, Z, and the sensor wheel and body displacement difference, W - Z. An active high-pass filtering network is used in the integrator and summing circuitry for filtering low-frequency or long-wavelength profiles, such as those of hills. Two independent measuring subsys-

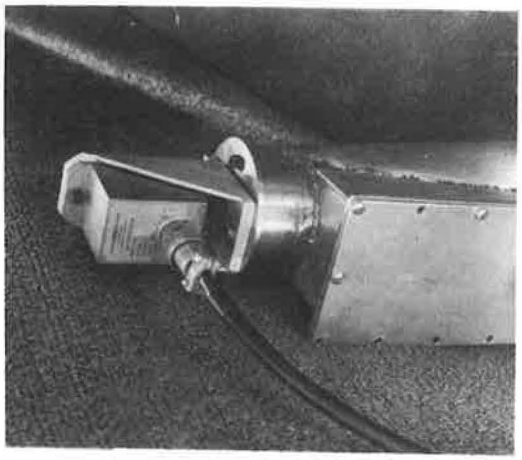

Figure 4. Systron-Donner accelerometer.


Figure 5. Road-following wheel and assembly.

tems are used for measuring profiles, one right and one left. Complete details of the measuring technique are given elsewhere (1).

The device used to measure the difference in wheel and body displacements is a Markite linear potentiometer, which its manufacturer considers to have "substantially infinite" resolution. The potentiometer output signal is scaled in the profile computer so that a 1-in. displacement of the potentiometer shaft is equivalent to 1 volt.

Vertical vehicle body acceleration is obtained with a Systron-Donner model 4310 servo-accelerometer (Fig. 4) with a ±2 g range. The output from this accelerometer is large enough so that signal amplification in the profile computer is not necessary.

A spring-loaded arm, which holds a road-following or sensor wheel in contact with the road surface, is shown in Figure 5. The figure also shows the potentiometer mounted above the sensor wheel on a wheel support and attached to the vehicle body directly above the wheel. The trailing arm can rotate about the transverse and vertical axes, but rotation about the transverse axis is constrained by the torsion bar springs. Further details of the trailing arms are given elsewhere (2).

Each sensor wheel is specially constructed, with a high strength-to-weight ratio. The natural rubber tire is molded to the wheel rim, and the outside diameter is ground to be concentric with the wheel shaft. Experience has indicated that wheel road wear is a significant factor, as is discussed later in an analysis of the system.

Road-distance measurement is obtained with a Veeder-Root rotary pulse generator coupled to the speedometer drive. The strip chart has an optional drive that can be run off a fixed-time base or by the distance pulses for a direct-distance scaling of the pavement surface.

Operation of the profilometer requires two persons—a driver and an operator—for the electronic equipment. The driver has controls for turning on warning lights, raising or lowering the trailing arms, and indicating specific events, and also has visual and audio alarm systems for indicating vehicle-speed errors and computer overloading. Pertinent data such as test section identification information and filter-gain combinations can be recorded on the voice channel of the Honeywell 8100 FM tape recorder. The vehicle has an automatic speed control system. Variations in the speed selected in the profile computer by the operator can be observed on a speed-error meter calibrated so that variations within ±5 mph of the selected speed result in full-scale meter deflections. Speed variations can also be indicated by an audio alarm provided by the profile computer. The amount of speed variation is indicated by the intensity of the signal. The intensity of the audio signal decreases as the vehicle speed approaches the selected speed and increases in proportion to an increasing difference from the selected speed.

Further information on the profilometer output signals is provided in the section on the profile computer subsystem. Two independent power systems are included in the profilometer: the standard vehicle power system and an independent supply for the profilometer equipment.

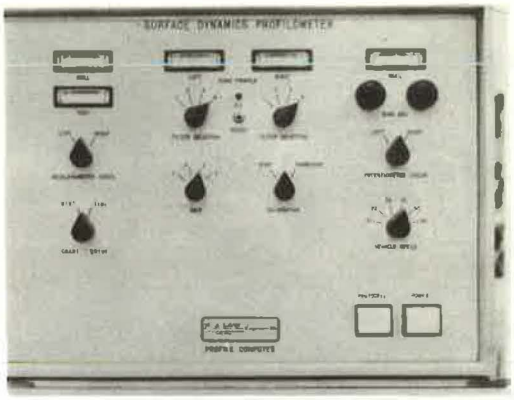


Figure 6. Profile computer.

## Profile Computer

The profile computer has inputs for (a) body acceleration for right and left sides of the vehicle, (b) sensor wheel and body displacement difference for both sides of the vehicle, (c) distance traveled as denoted by pulses per foot, and (d) photocell-sensing for location of marks on the test section (Figs. 6 and 7). The computer then provides as outputs (a) the right and left road profile measurements, (b) distance traveled denoted by approximately 1 pulse per inch, (c) distance traveled denoted by 1 pulse per hundred feet, (d) a photocell-sensing signal (logical), and (e) a speed-error audio reference signal. There are three selectable parameters that affect the right and left profile measurement outputs. These are high-pass filter selection, gain or measurement sensitivity selections, and vehicle operating speed selection.

The four high-pass filter selections are used for attenuating frequencies below 0.3, 0.6, 1.0, and 3.0 radians per second. The four gains of 0.2, 0.5, 1, and 2 volts per inch are available for selecting profile gain sensitivity. As may be noted from the measuring sensors, the long-wavelength profiles affect the vehicle body and thus are sensed primarily by the accelerometer. The short wavelength profiles, such as bumps and potholes, are sensed primarily by the traveling wheel. The vehicle suspension system dampens the effects of the high-frequency, small-magnitude bumps. Because the magnitudes of the longer wavelengths vary considerably, as noted from the varied elevations of hills and dips, profile scaling, or gain selection, is necessary. By the use of the four filter selections, attenuation of the undesirable long wavelengths is possible. Because the measuring speed determines the frequency of the long-wavelength components, careful selection of a speed-filter-gain combination is required to make the best measurement of a particular section.

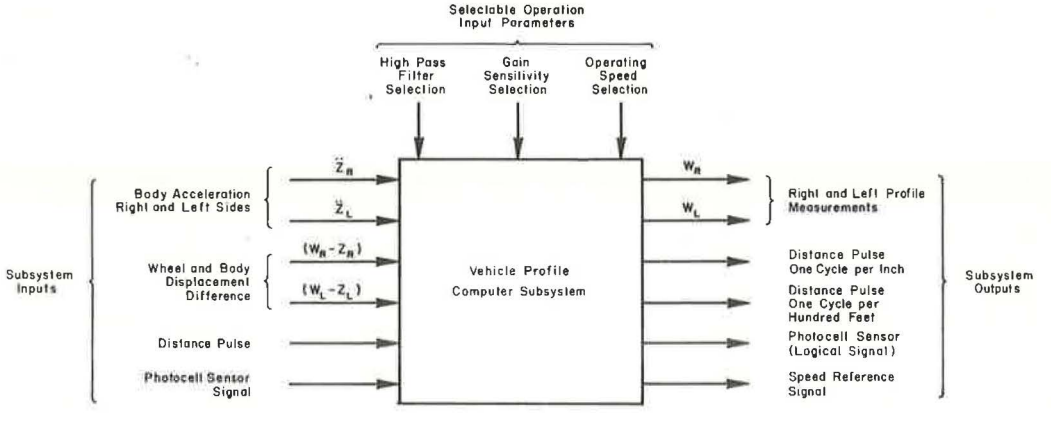


Figure 7. Profile computer subsystem.

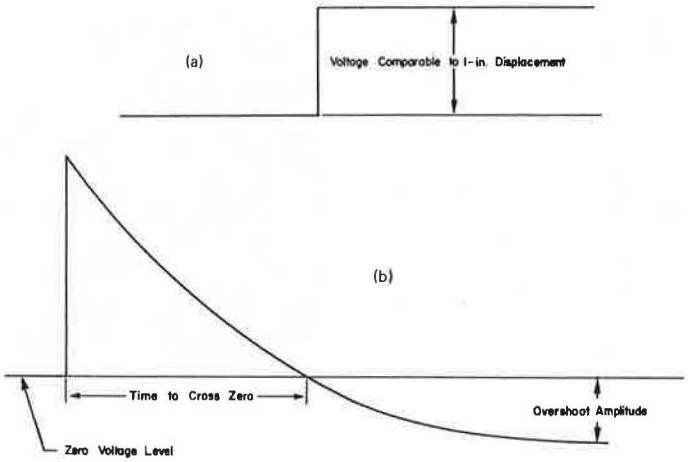


Figure 8. Typical calibration signals: (a) 1-in. displacement for scaling data; (b) transient for filter validation.

The six speed selections on the vehicle profile computer (10, 20, 34, 40, 50, and 60 mph) are used to provide a reference for the speed-error meter display so that adjustments of the vehicle cruise control can be made to reach the desired speed.

In considering the speed-filter-gain relationship from an electronic viewpoint, it should be noted that integration of dc or near-dc signals by electronic integrators results in an unbounded output as time increases without bound. Thus, the four filters help maintain stability of the profile computer by attenuating the long wavelengths. Even with these selections, however, low-frequency profile components of sufficient duration and magnitude can saturate the integrator amplifiers. To prevent this, an overload circuit was designed to short the integrating capacitors and reinitialize the subsystem. When this occurs, however, the profile signal obtained at that time and for a few seconds thereafter is erroneous.

The analog computer subsystem uses two calibration signals for scaling and filter information. The voltage amplitude comparable to a continuous 1-in. profile displacement (Fig. 8) is obtained by a simple control switch on the front panel of the computer. Similarly, the free response of the system can be obtained by a transient switch, which when activated excites the system with a voltage pulse comparable to a 1-in. impulse displacement. The high-pass filter selection can then be checked by noting the zero crossover point. When recording a 1-in. step or transient, the vehicle is normally stationary, and thus the distance pulse is zero. To provide a sampling signal for the A-D process and also a drive signal for the strip chart recorder, a constant 500 Hz signal replaces the distance pulse via a time-distance switch on the profile computer.

## Recording Equipment

The strip chart recorder, a Brush Mark 280, provides an immediate permanent visual copy of the road profile. It is a two-channel analog recorder with two event pens and pressure ink-writing system providing 0.5-millivolt per chart division maximum sensitivity capability. The analog channels display the right and left road profile measurements. The 100-ft distance pulses and the photocell-sensing signal are displayed on the two event channels. Pulses from the Veeder-Root rotary pulse generator trigger the paper drive in the distance mode of operation.

The Honeywell 8100 magnetic tape recorder records information for subsequent analog or A-D processing. It is equipped with eight FM record/reproduce channels and four recording speeds. An FM compensation channel for playback compensation is

provided, as is a voice monitor channel. Four of the eight channels record right and left profile measurements, 1-in. distant pulses, and the photocell-sensing signal. A fifth channel is used to record the system ground. The remaining channels are available for any additional requirements. The voice channel is used for section identification, for speed-filter-gain selection, and for calibration information. The 42-dB signal-to-noise ratio of the FM tape system allows 8-bit resolution of digitized data reproduced from the analog tape.

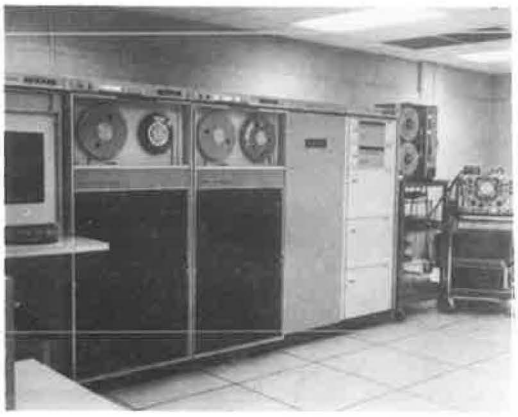

Figure 9. SDS 930 computer console and equipment hookup for A-D processing.

## Analog-to-Digital Subsystem

The A-D subsystem is used to digitize the analog profile signals, which are gathered by the profilometer, for digital computer analysis. The process is accomplished with an SDS 930 general-purpose computing facility. The A-D process involves the Honeywell 8100 analog tape recorder for data playback, an HP 214A pulse generator, a photocell signal-booster unit, an SDS 930 computer facility (Fig. 9) with an A-D peripheral unit, and an A-D program. The right and left profile signals are digitized into 12-bit (11 bits plus sign) data words in accordance with the distance or sampling signal. The HP 214A pulse generator is used to interface the sampling signal with the SDS 930 computer. The photocell signal-booster unit interfaces the photocell signal with the SDS facility. The digitized 12-bit data words are then written on standard digital tape in 1,500-word blocks at 556 bits per inch.

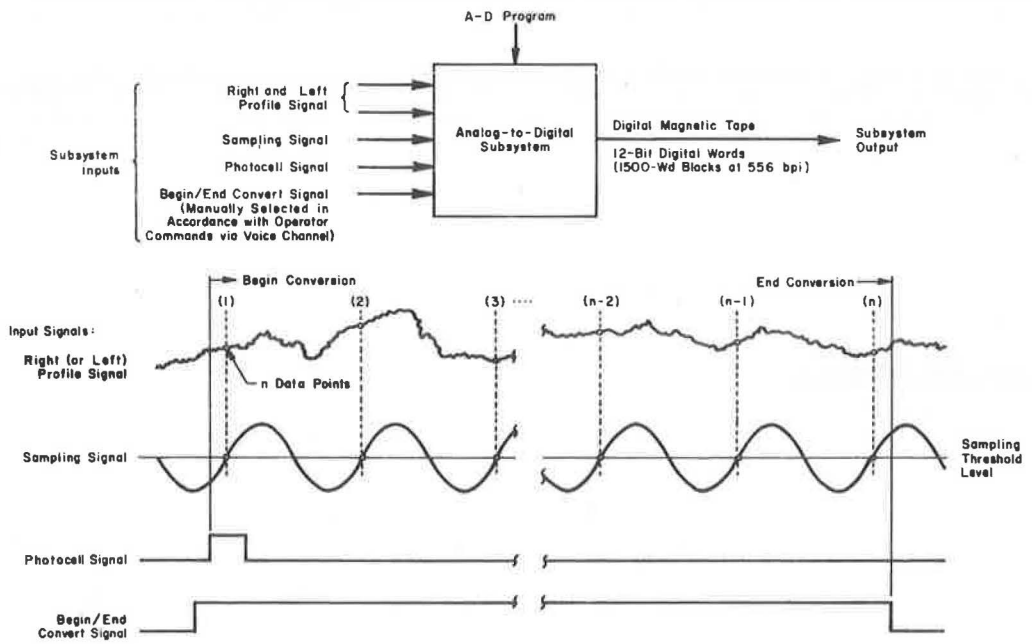


Figure 10. Analog-to-digital subsystem with inputs.

## Analog-to-Digital Process

There are four primary signal inputs to the A-D subsystem (Fig. 10). Either the photocell-sensing signal and the begin/end conversion signal or the begin/end conversion signal is necessary to begin the A-D process. The begin/end conversion signal comes on first, initializing the system, and the program waits for the photocell signal to be sensed, indicating the beginning of the section to be measured and thus the beginning of the conversion process. If the photocell signal is not used, A-D operations are controlled by the begin/end conversion signal. The conversion process continues in accordance with the sampling signal until the begin/end conversion signal drops, indicating the end of the conversion process and thus the end of the digitized data file. The begin/end conversion signal is initiated and terminated manually on command from the profilometer operator via the voice channels on the Honeywell recorder.

As the analog data are digitized, they are stored in 1,500-word blocks, after which they are written on digital magnetic tape at 556 bits per inch. Thus, two memory buffers are used by the computer, one for inputting the digitized values and the other for outputting the data on the digital tape. On receipt of the end of conversion signal, a five-word identification record followed by an end-of-file is written to signify the end of the conversion process and thus the data file.

The SDS A-D subsystem has the following characteristics:

1. Sample resolution of 11 bits plus a sign bit.
2. Up to eight channels at sampling rates up to 16/N kHz per channel, where N is the number of channels.
3. Sampling rate externally driven at any external rate or reduced multiple of this rate; i.e., sampling rate equals external rate divided by W, where W is any positive integer from 1 to 2,048. For example, with a 2 kHz external sampling signal and W = 4, the sampling rate will be 2 kHz/4 or 500 Hz.
4. Sample rate internally controlled by the HP 214A pulse generator.
5. Conversion process controlled by the photocell signal and the begin/end conversion signal or simply the begin/end conversion signal.

## Analog-to-Digital Program

Both FORTRAN and symbolic languages are used in the A-D program, for which the general flow chart is shown in Figure 11. Briefly, the general flow of the program is as follows:

1. The program is loaded and the operator enters various operation parameters, such as (a) whether a new or old data tape is used (e.g., if the tape is not a new data tape, the last data file or any other desired file is located and the tape is positioned to begin after that file), (b) whether the control mode is automatic or manual (e.g., if a conversion process is desired for beginning and ending the conversion process by a series of control signals and thus, without entering any new file identification information, the automatic control mode is selected), and (c) whether or not the photocell signal is to be ignored (i.e., whether or not the conversion process will be initiated and terminated solely by the begin/end conversion signal).
2. The program waits for the begin conversion and/or photocell signal command for initiating the A-D process.
3. The program uses two 1,500-word buffer areas so that one buffer is being filled by the A-D input operations while the other is emptying on the magnetic tape.
4. A new read command is immediately initiated after 1,500 words have been read to ensure that the required sampling rate is maintained.
5. The 1,500 12-bit words in buffer 1 are written in binary on the magnetic tape.
6. The procedure is repeated (i.e., the filling and emptying of alternate buffers from the A-D unit to the magnetic tape continues until the end of the analog record or section being measured is detected).
7. The conversion process is terminated by the sensing of the begin/end conversion signal when the analog record has been completed, and a five-word identification rec-

ord is written at the end of the last data record. If the next analog record is to be read soon after the end of the last record and no additional identification information is desired (i.e., if the automatic control mode was specified), the program automatically increments the data file number and waits for the next begin conversion command(s). If not, or if other identification is required, the program stops and waits for further information or commands from the operator.

8. Each data set (data records plus identification record) is separated by an end-of-file. Two end-of-files are written at the end of the last data set on the magnetic tape.

Each data set or file has an identification record generated during the A-D process that includes (a) a data file number used by the program for identification and positioning of the data tape when adding, replacing, or deleting additional data files; (b) the number of converted 1,500-word records in the data file; (c) the number of converted data words in the last record; (d) the total number of conversions in the data file; and (e) a 24-bit identification tag for additional operational information, such as filter-speed-gain selection and date.

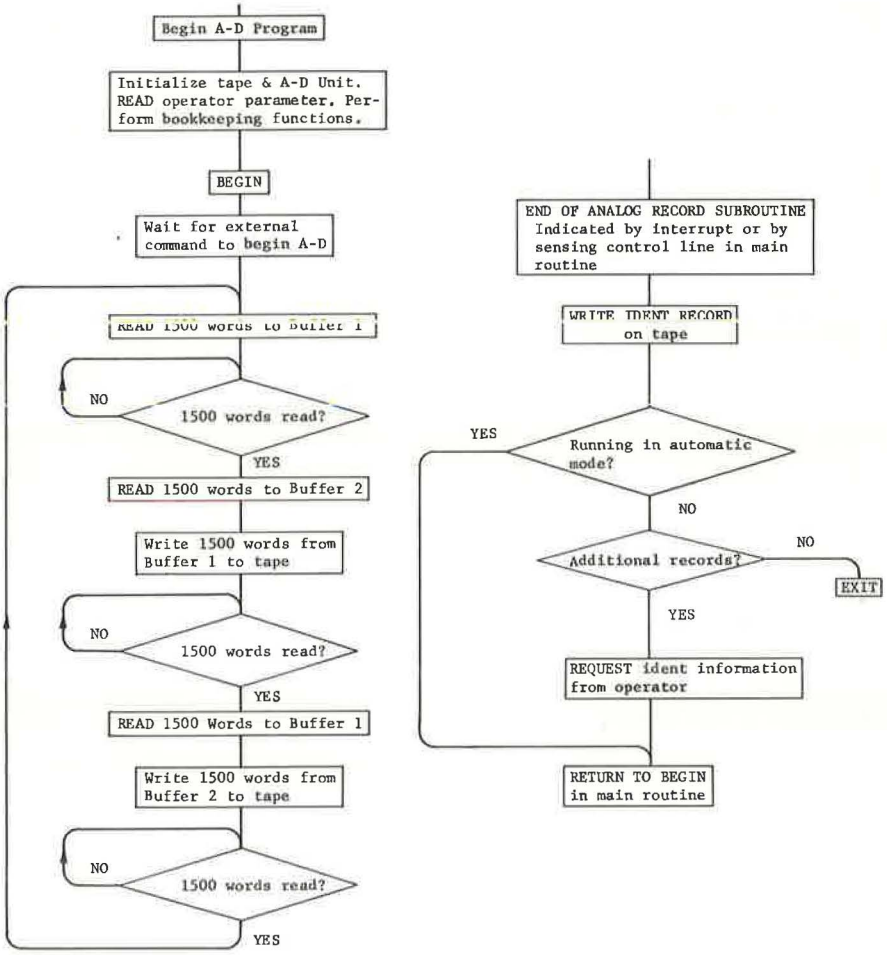


Figure 11. Analog-to-digital program for SDS computer.

Control Data Corporation 6600

After the profile data have been digitized and written on a digital tape by the SDS computer, they must undergo a transformation to make them compatible with the computer performing the data analysis. Current data analysis at the University of Texas at Austin is performed on a Control Data Corporation 6600, and therefore the SDS profile data are made compatible with the CDC 6600 data analysis programs. The changes can be made on either the SDS 930 or the CDC 6600. The compatibility program currently used is run on the CDC 6600. The program performs the following steps to transform the SDS binary data words into CDC 6600 binary data:

1. The program examines the data for possible parity errors. A continuous conversion process from beginning to end of a road section is required because of the analog tape recording. Consequently, time is not available during the digitizing process to check for bad digital tape writes. Thus, parity errors are possible when the digital tape is read. The effects of these errors may vary in statistical analysis of large samples of data, particularly if errors are omitted or replaced by approximations, and thus the importance of identifying the locations and numbers of these errors is realized.
2. The program reverses the order of each set of five 12-bit words, from one to five to five to one. This change is necessary because of the characteristics of the CDC data channel and the SDS binary write operations.
3. The program changes the 12-bit SDS binary words into 60-bit CDC binary words.
4. The program changes each binary word from the two's complement mode as used in the SDS machine to a one's complement mode as used by the CDC machine.

## FILTER-SPEED-GAIN SELECTION CRITERIA

The filter and speed selection used in measurement of a road profile effectively fixes the profile wavelengths that will be measured. The response curves (4) denote the gamut of frequencies in which the system introduces no attenuation or phase shifts. Speed and wavelength are related to these frequencies by

$$\lambda = \frac{V}{f} \tag{1}$$

where

$\lambda$ = wavelength, in ft;
$V$ = velocity, in ft/sec; and
$f$ = frequency, in Hz.

To determine a speed-filter combination for measurement of a road profile, it is necessary to determine which profile wavelength measurements are wanted. Then the proper filter-speed combination for phase shifts of 10 and 135 deg (0.7 or 3 dB attenuation) is obtained from a graph (Fig. 12). If only those wavelengths smaller than 10 ft with no phase shifts exceeding 10 deg are of interest, filter-speed selections of filter 3 at 10 mph or filter 4 for the remaining speeds of 20 to 60 mph can be used. Similarly, beginning with a given speed or filter, the necessary combinations, in accordance with Eq. 1 and the system frequency constraints of Walker, Roberts, and Hudson (4), can be found.

Four gain selections are provided by the profile computer for profile data scaling. The computer is designed for a voltage operation of ±10 volts. Voltage amplitudes exceeding this range overload the computer and cause erroneous data. For a given data run, maximum resolution is obtained when the profile voltage amplitudes are as large as possible, but it is necessary to take care not to exceed the ±10-volt range of the computer to avoid jeopardizing the entire data run. The ±10-volt critical magnitude can be violated easily if the full-scale reading is too close to this ±10-volt critical magnitude, because the accelerometer and thus the voltage output changes are quite sensitive to speed variations.

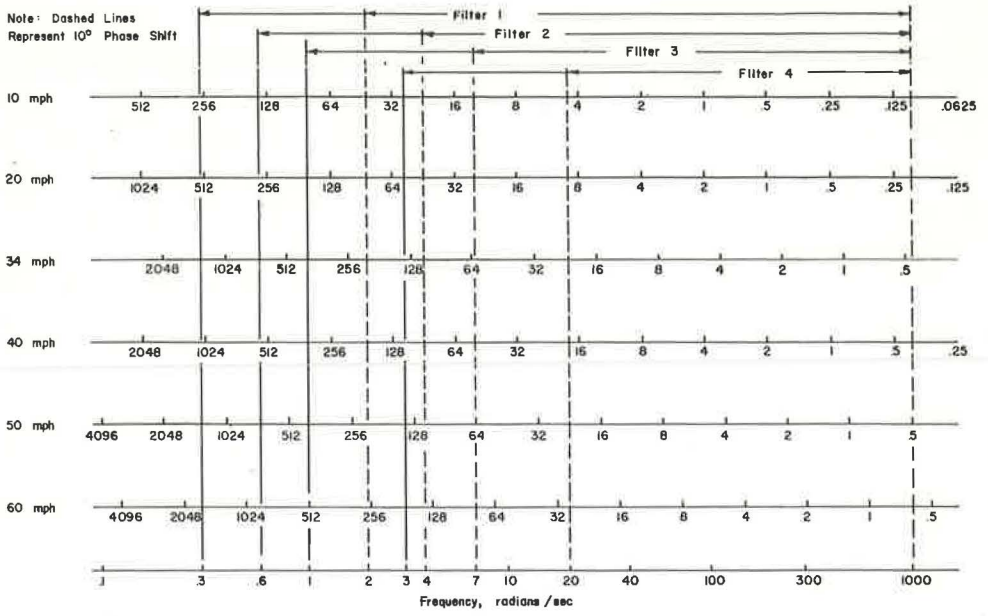


Figure 12. Filter-speed wavelength selection graph.

## ANALYSIS OF THE SYSTEM

Various system analysis techniques were used to determine the authenticity of the data obtained by the profile-measuring system. A system analysis procedure was used to ensure the validity of the profile data at the various stages in the data-measuring flow path. It was instrumental in development of the total measuring system and is currently used for isolating equipment problems or failures. The digitizing process was examined closely to determine if significant errors that could lead to misleading or erroneous road profile measurements were introduced. An experiment conducted to establish the significance of any such errors is described in the following section. To examine the sensitivity of the measuring subsystem to typical environmental conditions such as weather and operating techniques, an experiment was conducted to determine the sensitivity of the major electronic components of the profile computer to typical changes in the operating environment. The sensor wheels were analyzed also to determine a solution to the problem of rapid wear. The frequency response of the system was also checked and is documented elsewhere (4).

### System Analysis Procedure

Because of the size and complexity of the profile-measuring system, a systematic procedure was developed for use in the early detection of system failures and to aid in the initial system development (Fig. 13). Basically, this analysis procedure identifies the most likely failure areas and the facilities available for rapid detection of the failure. A typical example of the need for such a procedure is the early detection of a noisy channel in the analog recording unit that could lead to misleading results when the road profile data are being analyzed. To develop the test procedure, checkpoints along the data flow path were selected where subsystem failure could affect the measurement process; thus, each checkpoint could be used to verify the system operation to that point. The entire test procedure should be followed as standard operating practice to ensure satisfactory system operation and, if a failure occurs, as a guide for isolating the problem cause.

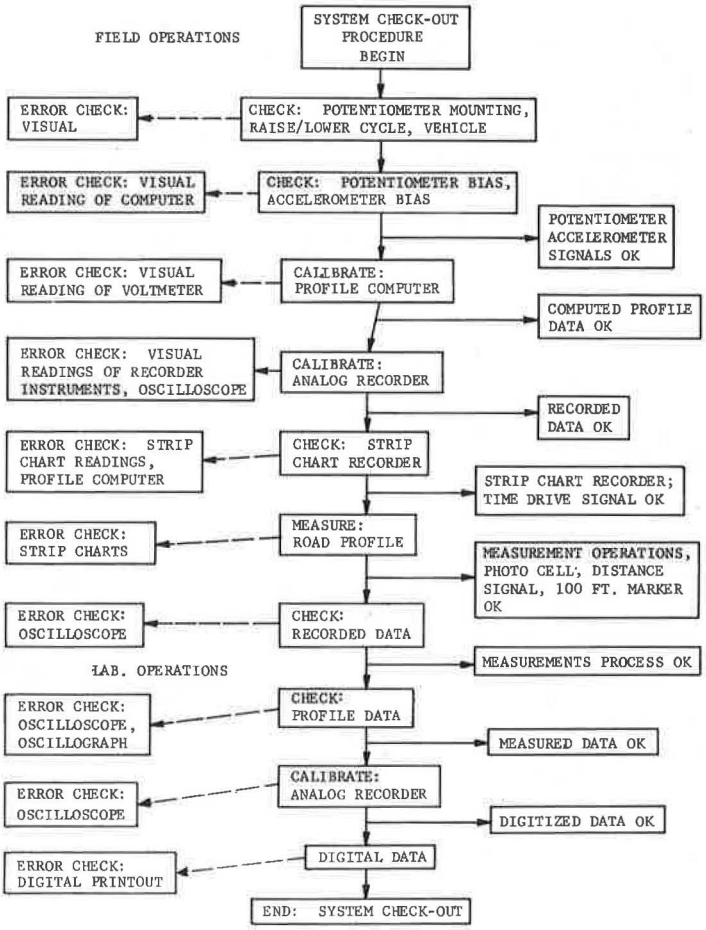


Figure 13. Schematic of system analysis procedure.

The procedure is as follows:

1. Examine the potentiometer mounts and wheel assembly for possible breakage. Check the raise/lower cycle to ensure that the wheels raise, lower, and latch properly. An inoperative road-following wheel will give erroneous profile data or introduce considerable noise.
2. Test the potentiometer and accelerometer for proper bias and operation with the test switches on the profile computer. A failure in either potentiometer or accelerometer can result in erroneous data, frequent computer overloads, or considerable noise in the data.
3. Verify operation of the profile computer by balancing the operational amplifiers. Test the filters by observing the transients on either the oscilloscope or the strip-chart recorder. Erroneous profile data or noise can be introduced by a malfunctioning profile computer.
4. Calibrate the Honeywell 8100 analog tape recorder to ensure proper recording. An inoperative recorder can result in the complete omission of a channel or can introduce noise in the data.
5. Calibrate the strip-chart recorder; once it is set up properly, it can be used for continuously checking the operation of the measuring process.

6. Validate the operation of the photocell, the time-distance pulse, the 100-ft event maker, and the right and left profile data by making a test run of the vehicle with the strip-chart recorder in use.

7. Periodically play back the Honeywell recorder via both the strip-chart recorder and the oscilloscope to ensure proper recording. The oscilloscope check ensures that noise was not introduced into the data.

8. Check the profile data, photocell signal, and timing or sampling signal brought back to the laboratory for A-D processing by using the oscilloscope and the light-beam oscillograph. The light-beam oscillograph (wide-band response) provides a high-frequency hard-copy output for comparison with the strip-chart (limited bandwidth) records.

9. Calibrate the Honeywell 8100 analog tape recorder to ensure proper playback operation for the A-D process. An inoperative recorder can result in the playback of data with considerable noise or no signal at all.

10. Make periodic checks of the digitized data to confirm the validity of the digitizing process. Malfunctions in this process can add noise, provide erroneous data, or intermittently fail to sample the data signals.

## Redigitization

An experiment was conducted in which a known signal was recorded and then redigitized several times to ensure that system accuracy, as determined by the least accurate subsystem, the Honeywell 8100 tape recorder, was maintained in the digitizing process. The results indicated that the accuracy of the digitizing process was within the accuracies of the Honeywell 8100 recorder, i.e., 8 bits ± least significant bit.

In the experiment, a 1,000-Hz signal was recorded on two channels of the Honeywell 8100 magnetic tape recorder. The 1,000-Hz frequency is considered to be the upper limit of the sampling frequencies for typical data runs. The upper limit was selected because of the nature of the digitizing techniques—i.e., the greater the sampling frequency, the less the expected system resolution capability. The two channels were then played back into the SDS 930 computer facility, one channel into the analog input for sampling and the other into the external interrupt input to initiate the sampling process (Fig. 14).

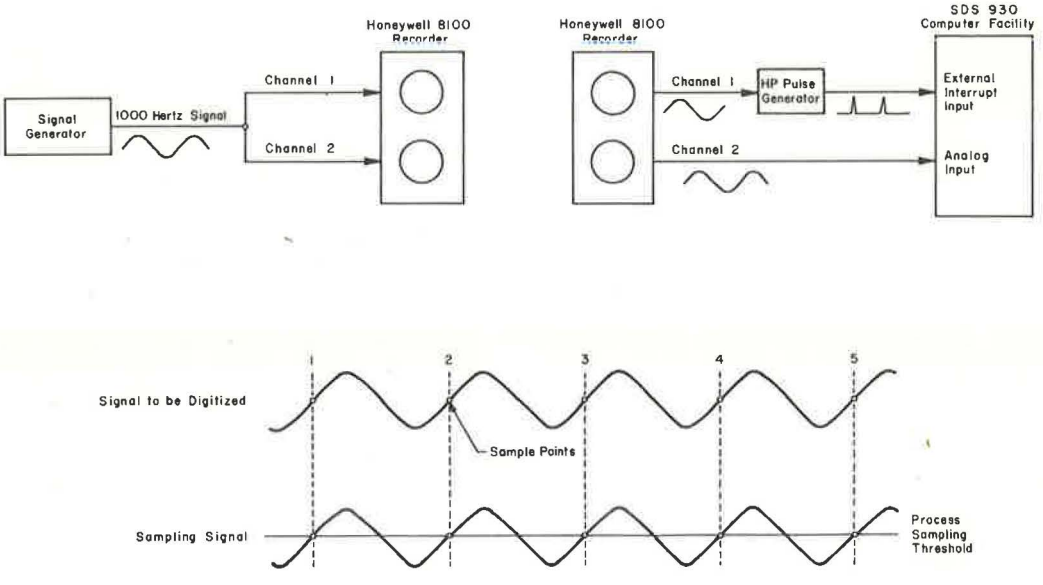


Figure 14. Sampling configuration.

As noted before, the computer samples the analog input channels in accordance with the sampling signal; i.e., each cycle of the sampling signal is used to interrupt the computer, which in turn initiates a conversion process to read and store the 12-bit digitized value. By using the same signal for both the signal to be digitized and the sampling signal, a consistent set of digitized results can be obtained. This signal was digitized five times, beginning at the same point each time, to check the repeatability of the digitizing process. The 8-bit results were converted from the 12-bit values by adding 8 to each 12-bit word and then dividing by 16. The largest variation between successive redigitizing was of the magnitude of one, which is the best accuracy that can be expected from the recording device, i.e., 8 bits ± least significant bit. Thus, it was assumed that the digitizing process was within the system accuracies as established by the Honeywell 8100 recorder, and redigitization of subsequent data runs confirmed these results.

It should be emphasized that the accuracy of interest is of the entire digitizing process—i.e., using a recorded sampling signal to signal the computer to initiate the conversion process—and not in a single digitization, because the SDS converter is accurate to within 12 bits ± the least significant bit. The A-D converter is checked periodically by standard SDS diagnostic programs.

## Scale Factor Sensitivity

To scale the profile data from volts to inches, the profile computer can provide a calibration voltage proportional to a 1-in. change in road profile. This 1-in. voltage signal, recorded prior to each profile measurement run, is digitized along with the respective profile data for a particular section. The magnitude of the digitized 1-in. step is the difference between the average of the points before the voltage step and the average of the points after the voltage step, as shown in Figure 15. Once this magnitude has been determined, the digitized road profile points are divided by this scale factor value to obtain a set of scaled road profile deflections in inches. It was noted that, when the 1-in. steps were recorded, there were variations in the magnitudes of these steps between right and left profiles for different filter-gain combinations, as well as between the same channels with the same combinations for subsequent readings. The concern for such variations is easily understood if it is realized that (a) these same variations could probably be expected in the profile signal itself, because many of the

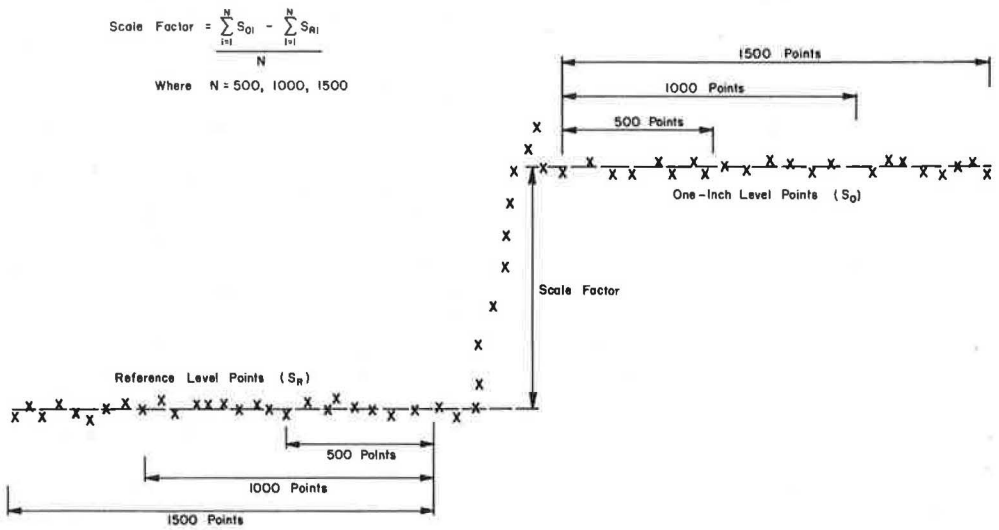


Figure 15. Schematic of scale factor computation.

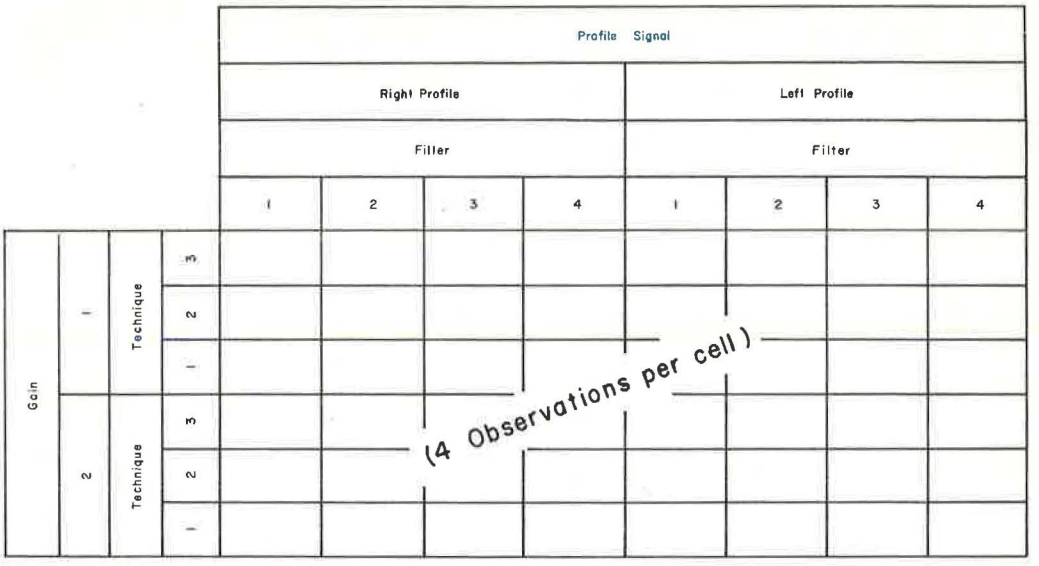


Figure 16. Scale factor experiment design.

electronic components are shared by the calibration circuitry and the profile-measuring circuitry, and (b) all the profile measurements are scaled by these 1-in. calibration steps.

To determine the significance of these variations on the measuring system, an experiment was conducted in which several 1-in. steps for the various filter-gain combinations were randomly obtained (Fig. 16). Because electronic components are typically heat-sensitive, the experiment was conducted during the middle of an unusually warm day, when the variations should be at a maximum. The 1-in. calibrations were obtained and recorded in a fashion similar to that used during a typical profile-measuring operation. An accurate 1-volt signal obtained from a dc power supply as a base for computing the difference in gain selections was recorded with these calibration signals. The 1-in. steps were digitized and their respective scale factors were determined. Three averaging techniques (500-, 1,000-, and 1,500-point averaging) were used to determine if the number of points used had any effect in the scale factor computing technique (Fig. 15). Table 1 gives the analysis of variance used for obtaining the previously mentioned results. The analysis of variance was run on the difference between the scale factor obtained from the digitized measured calibration voltage and the actual value.

From this experiment, it was concluded that (a) the variation was well within the measuring accuracy of the system and it made no difference which filter-gain

TABLE 1

ANALYSIS OF VARIANCE SCALE FACTOR EXPERIMENT

| Source | dF | SS | MS |
|---|---|---|---|
| Filter (F) | 3 | 195.97 | 65.32 |
| Gain (G)* | 1 | 487.05 | 487.05 |
| F × G* | 3 | 1,715.58 | 571.86 |
| Side (S) | 1 | 213.36 | 213.36 |
| S × F | 3 | 258.00 | 86.00 |
| S × G | 1 | 140.77 | 140.77 |
| S × F × G | 3 | 516.98 | 172.32 |
| Error (a) Replication (R), R × F, R × G, R × F × G, R × S, R × S × F, R × S × G, R × S × F × G | 45 | 2,723.69 | 60.70 |
| Technique (T) | 2 | 0.71 | 0.36 |
| T × F | 6 | 9.26 | 1.54 |
| T × G | 2 | 8.29 | 4.14 |
| T × F × G | 6 | 45.93 | 7.65 |
| T × S | 2 | 3.54 | 1.77 |
| T × S × F | 6 | 4.78 | 0.80 |
| T × S × G | 2 | 2.70 | 1.35 |
| T × S × F × G | 6 | 54.52 | 9.09 |
| Error (b) T × R, T × R × F, T × R × G, T × R × F × G, T × R × S, T × R × S × F, T × R × S × G, T × R × S × F × G | 96 | 268.70 | 2.80 |
| Total | 191 | | |

*Significance is expected because the gain is a multiplication factor.

combination was used for the scale factor, and (b) no difference existed in the averaging technique used for computing the scale factor. Subsequent experiments revealed that 100-point averaging provided adequate scale factor results and it is currently used in determining scale factors. Obviously, the gain selection should be made in accordance with the gain used when measuring the road profile, but the filter selection need not be the same. In fact, it was found that a usually better calibration reading was obtained with the filter 4 selection. This would be expected, considering that the higher cutoff frequency of filter 4 causes a more rapid attenuation of the system to the zero equilibrium point, which is used in the scale factor computing technique as the base or reference value.

### Sensor Wheel Analysis

As noted, the life of the sensor wheels has been much shorter than expected; they have had to be replaced after 400 to 500 miles of road use. Because the cost of a wheel is about $500, this wear is considered excessive, and consequently investigations are currently in progress to find a less expensive, but usable, wheel. Two substitute wheels currently being evaluated cost less than $50. From initial test runs, it appears that there are some differences between the upper frequencies of the profile made with one of the replacement wheels and those of the profile made with the original equipment wheel. Further analysis will indicate whether or not these differences are within acceptable error limits of the overall system. It is hoped that these investigations will also provide some measure of the amount of wear a wheel can be subjected to and still provide meaningful results.

Investigations are also in progress to identify the influence of wheel characteristics, such as wheel bound, on the measured data. Use of the profilometer to date has indicated the existence of some periodic wave forms in much of the data. This wave is generally more prevalent in roads with rough textures, such as those with surface treatments. Power spectral analysis and coherence on selected combinations of various surface treatments and road types and analysis of variance are some of several analysis techniques being used to identify and determine the significance of these wheel characteristics.

## SYSTEM PROBLEMS

As in all newly developed systems, a number of problems had to be solved before a workable road profile data-measuring system could be developed. The majority of these problems occurred in the profilometer, but, as noted, the profilometer used was the first one manufactured. For that reason, these problems were not considered to be unreasonable, although there did appear to be an unusually large number of them associated with the vehicle engine. The problems often resulted in considerable frustration and delays. Some of the more serious problems encountered, together with the steps taken to alleviate them, are given in the following.

### Potentiometer

1. Failure of the potentiometer wiper shaft connection to the wheel assembly required that the connection be redesigned for a male-type connector.
2. Inability of the sleeves on the wiper to maintain their structural integrity made it necessary for the sleeves, which were originally sweated on, to be welded on.
3. Damage to the bearings for the wiper shaft when the wheel assembly was raised, because of excessive travel in the hydraulic actuator, required that limit switches be replaced to provide positive limit adjustments.

### Distance Pulse Generator

1. Intermittent loss of the distance pulse because of poor connection of some of the leads in the pulse generator made it necessary that the leads be resoldered.
2. Loss of the distance pulse signal because the temperature environment of the Veeder-Root generator exceeded the design requirements made it necessary for the Schmitt trigger circuit, which was breaking down, to be bypassed.

Photocell

1. Severing of the power leads on the photocell lamp necessitated replacing the leads.
2. Continual breakage of the photocell lamp made it necessary to develop a better mounting technique.

Automatic Speed Control

Improper operation of the speed control unit required that the motor and drive gear in the speed control unit be replaced.

Power Supply

Because the Brush equipment failed to operate on the square wave 500 va inverter, a "Power Com" sine wave inverter for the Brush equipment was installed and the Brush pulse generator repaired.

Trailing Arm Hydraulic Life

1. Failure of the trailing arms to catch properly in some situations made it necessary that limit switches, the hydraulic actuator, and the timing control switch be adjusted.
2. Because the trailing arm stabilizer spring failed frequently, an inexpensive spring was found and large quantities were purchased for replacement.
3. Frequent failure of the potentiometer shaft mount yokes on the trailing arms required that the support brackets be welded to yokes.

Tape Recorder

1. Recorder was inoperative when delivered by the manufacturer and it was sent to Honeywell for repair.
2. Failure of discriminator and record zero adjustment trim-pot made it necessary for Honeywell to replace all trim-pots.

Profile Computer

1. Failure of capacitor mounts because of vibrations made necessary the redesign of mounting brackets to withstand vibration.
2. Failure of the integrated circuit and an R-S flip-flop in counter circuit made it necessary to replace the integrated chip.

Vehicle Engine

1. Valves and rod bearings were burned out when the vehicle was delivered, and the engine had to be rebuilt.
2. Because of frequent overheating the fan was changed and a shroud was installed over the fan.
3. The timing gear had to be replaced.

## SUMMARY AND CONCLUSIONS

A detailed description of a high-speed road profile data-gathering and analysis system, including general operating criteria, analog-to-digital operations, and system checkout and data validation techniques, is presented in this paper.

The profilometer, which is a major part of the overall system, provides an accurate record of low-frequency components in the road profile, but higher frequency data have been found to be somewhat distorted because of wheel bounce at operating speeds above 34 mph. The amount of distortion is a function of vehicle speed and profile roughness, and studies are continuing in order to determine the amount and significance of these distortions.

A second significant noise problem that has been found is due to tape flutter that occurs when the vehicle is driven over roads that are rough but not considered to be excessively so. Experiments are under way to find a better mounting technique to eliminate this problem.

In general, the time required for processing profile data with the A-D subsystem and profile summary routines is often lengthy, especially when immediate results are desired. It appears that there would be some advantage to providing a profile summary device, for use in conjunction with the profile computer, that would provide immediate estimates of road roughness or other such characteristics while a profile run is being made. The accuracies of such a device would, of course, have to be carefully determined.

The weakest link in the overall system appears to be the sensor or road-following wheels. Considering their high cost, the usable life of about 500 miles is too short. The wheels have been found to be too susceptible to cutting, and the frames are often damaged when measurements are made on rough portland cement concrete pavements. To remedy this problem, two substitute wheels are currently being evaluated.

Extreme care is required in general operation of the road profile data system because of the many possibilities for introducing erroneous mechanical and electrical noise into the profile. For this reason, the data for this study have been monitored after data runs with an oscilloscope and oscillograph because of the inability of the Brush recorder to respond to most high-frequency noise.

Although the profilometer has been found to be useful to the research engineer, it is a subsystem, and considerable care in planning and analysis must also be given to the overall system if accurate road profile data are to be obtained.

## APPLICATION OF RESEARCH RESULTS

Because an adequate operating manual for the SD profilometer was not provided by the manufacturer, a detailed calibrating and operating manual was developed for future use (4). This paper provides some of the information described in the report and may be of use to other users of the profilometer.

The road profile data-measuring system will continue to be used to evaluate the pavement serviceability index, pavement roughness, and road profile. Specific uses in the future include the following:

1. Aid in establishing priority for major maintenance, reconstruction, and relocation. Roughness values obtained with this equipment, along with information from traffic studies, could be used to make objective rankings for various pavement sections.
2. Aid to the design engineer in determining the degree of success with which his design has met the design criteria and to help him learn the causes for failure. To successfully evaluate a design system, accurate measurements of the system output function should be made during the entire design life of the pavement. Such measurements would provide an objective indication of the performance and the success of the particular design.
3. Aid in establishing levels of roughness that are acceptable for new construction.

To make the system more useful, further studies should be conducted to determine differences between profile data and erroneous data introduced from wheel bounce and noise. Assistance in achieving this can be provided by use of analysis techniques recently developed at the Center for Highway Research that will help to establish undesirable frequency ranges. Briefly, the procedures for the analysis would involve removing various frequency ranges by the use of digital filtering techniques and noting the effects on the resulting profile data and summary statistics. Power and cross-power spectrum analysis, regression analysis, and analysis of variance are useful tools in determining the significance of these effects.

Studies to develop better techniques for data validation during the measuring process, for early detection of noise or equipment malfunction, should be continued as well. In pursuing the problem, a suitable in-vehicle summary device could be used as an indicator of erroneous profile data; it would also be of great value in providing

rapid road-profile evaluation. Although the accuracy may be less than with existing processing techniques, the device would significantly enhance the use of the SD profilometer.

## ACKNOWLEDGMENTS

The findings discussed in this paper are those obtained from research on Project No. 3-8-63-73, "A Feasibility Study for High-Speed Road Profilometer Equipment". Support is gratefully acknowledged from the Texas Highway Department and the U.S. Bureau of Public Roads. The opinions, findings, and conclusions expressed are those of the authors and not necessarily those of the Bureau of Public Roads.

## REFERENCES

1. Spangler, E. B., and Kelly, W. J. GMR Road Profilometer—A Method for Measuring Road Profiles. Engineering Mechanics Dept., General Motors Corp., Research Publ. GMR-452, Dec. 1964.
2. The Surface Dynamics Profilometer. K. J. Law Engineers, Inc., Detroit.
3. Hudson, W. R. High-Speed Road Profile Equipment Evaluation. Center for Highway Research, Univ. of Texas at Austin, Research Rept. No. 73-1, Jan. 1966.
4. Walker, R. S., Roberts, F. L., and Hudson, W. R. A Profile Measuring, Recording, and Processing System. Center for Highway Research, Univ. of Texas at Austin, Research Rept. 73-2, May 1969.

# An Examination of Concrete Pavement Structural Performance

L. F. HOLBROOK, Research Laboratory Section, Michigan Department of State Highways

This paper argues that concrete pavement deterioration survey variables (such as blowups, spalls, and cracks) must be combined in a single index if general structural performance is to be defined and reliably measured. To this end, a mathematical definition of pavement structural performance is developed from a factor analysis of the survey variable-construction project matrix. All projects are then evaluated using this index, thus facilitating the search for causal determinants of structural performance. Highway projects are then classified by the estimated coarse aggregate carbonate content and the average daily commercial traffic volume. The structural performance of projects in these classes is then compared. It is found that good performance is associated with high carbonate content and low commercial traffic volume (ADT). Moreover, the relationship with traffic is supported by a comparison of divided highway traffic and passing lanes.

More intensive investigation reveals that performance is more closely associated with the percentages of soft, nondurable particles in the coarse aggregates. Using these findings, a mathematical model is developed that is designed to predict structural performance for up to 15 years of service using only percentage of soft, nondurable particles and commercial ADT. It is found that the present serviceability index (PSI) is not significantly related to either structural performance (as defined in this study) or to the materials and usage variables mentioned. This is because of the PSI's dependence on pavement wheel-track roughness—a measure only weakly related to structural performance variables.

•THIS PAPER is derived from an investigation of postwar concrete pavement performance in Michigan. The basic data were obtained from pavement condition surveys conducted during the period 1951 to 1963. These surveys, together with all readily available construction, environment, and use information, provided the basis for an analysis of the extent and causes of pavement deterioration sponsored by the U. S. Bureau of Public Roads under the Highway Planning and Research Program.

## PERFORMANCE PHILOSOPHY: NEED FOR A STRUCTURAL INDEX

Often one finds that the available basic field or research variables are not directly and simply related to the property for which causal information is sought. The desired information contained in each basic variable may be totally lost because of the masking influence of other variables either not measured or not controlled. Under these conditions, the use of a general index composed of two or more basic variables may be

Paper sponsored by Committee on Pavement Condition Evaluation and presented at the 49th Annual Meeting.

helpful. General indexes are designed to amplify the desired information weakly expressed in the directly measured and specific survey variables. By a suitable weighting of these highly specific variables, it is hoped that an index can be constructed that will serve as a more powerful research tool in the investigation of more general properties. The structural performance of highway pavements is an example of this kind of measurement problem: Each condition survey variable measures a particular type of pavement distress and therefore is not in itself a complete indicator of overall structural performance. In short, structural performance is a concept we cannot directly, physically measure but would like to define.

The manner in which condition survey variables are used in a performance definition depends on the kind of performance considered important, as well as the methodological preferences of the investigator. Thus, there can be considerable disagreement concerning the proper formulation and use of these composite variables. Nevertheless, the simplicity and utility of a single, overall performance index justify almost any approach, provided that its composition and assumptions are in clear view.

A pavement structural performance index can be used for the following purposes:

1. To summarize the essential information contained in the condition survey variables, thereby effecting a simplified measure of performance (although the index equation may be complex—i.e., some linear equation of the basic condition survey variables—once it is calculated, the structural performance of a length of highway is characterized by only one figure rather than a dozen or more);
2. To serve as a convenient tool in the search for possible "causes" of structural deterioration;
3. To anticipate the pavement's ability to continue in service; and
4. To indicate the need for maintenance or improvements to forestall excessive deterioration.

Each condition survey variable is unique and ideally could be uniquely associated with the relevant variables of design, materials, construction, or environment, provided that they were all known and measured with precision at the proper time. Because this amount and quality of information is usually not available, it is expedient to take the view that most condition survey variables express varying degrees of common performance information, and this redundancy makes the complicated and tedious in-depth consideration of each variable by itself unnecessary.

Although indexes can be computed for almost any length of pavement, computations for this study are for full construction projects. Thus, the computed performance is considered general, in that it pertains to an entire project and not to a smaller subsection. This is not to say that short stretches of light or excessive deterioration associated with local conditions, such as subbase, drainage, and joint construction, are of no interest. These factors, although affecting the general index, may not be linked with such general conditions as climate, materials, and traffic that are set aside as possible determinants of performance. Consequently, these stretches are best investigated by the case history approach where all relevant local conditions are exhaustively examined. To this end, general performance indexes may be used to spot extremes of deterioration, thereby reducing the number of projects requiring intensive investigation.

Performance is generally considered to be a positive concept, and deterioration its polar opposite. Thus, the emphasis in this paper will be on the negative of performance, i.e., deterioration. Performance indexes used to measure highway structural deterioration will display the same advantages and shortcomings encountered with their use in other areas of research. If one wishes to measure very general concepts, such as standard of living, economic activity, intelligence, or even cardiac condition, he must decide on some abstract criterion of indirect measurement. What one usually finds available are many direct and specific empirical measures, none of which uniquely expresses the more general property subject to definition. Notwithstanding each measure's individual importance, there is often good reason to think of these variables in relation to the more general property, with the presumed degree of relationship determining each variable's ultimate influence on the overall criterion.

## OBJECTIVE RATING APPROACH

In contrast with the AASHO Road Test's present serviceability rating (PSR) and hence present serviceability index (PSI), an attempt will be made in this paper to devise a structural performance rating index on "objective" rather than "subjective" grounds (1). By stressing the subjective aspect of performance, the PSI approach could weight the basic survey variables in such a way as to obscure the causes of structural distress. The technique of factor analysis used in this study (2) does not utilize the differential subjective importance of the survey variables or public or professional subjective evaluation of serviceability. Rather, the empirical intercorrelations found among the survey variables provide the only basis for a performance equation. The key methodological assumption is that, if the survey variables linearly measure in varying degrees general structural performance, they will be intercorrelated accordingly. It is assumed that the degree to which a given variable is correlated with the others in a group reflects the extent to which it expressed the "common" performance characteristic. Because this method of performance fabrication does not utilize any form of subjective evaluation, its chief contribution is in delineating basic, nonjudgmental categories of pavement deterioration which simplify the search for assignable causes. For the present study, the survey variables are reduced first to a single, more general category of performance (deterioration), from which is developed a single performance index. Although more specific categories can be subsequently extracted, their generality will decrease and they will account for diminishing amounts of survey variable intercorrelation.

Another advantage of this type of rating is that the sets of intercorrelations for the 5-, 10-, and 15-year survey periods can be considered separately. Consequently, the changing pattern of intercorrelations reflecting the evolutionary or retrogressive importance of each variable in respect to the underlying causes of deterioration can be acknowledged in different rating equations for each survey period. This is not usually possible with any of the subjective approaches. The PSI equations are invariant with time, thereby disallowing corrections for changes in each variable's relationship to general performance or to the underlying system of causes. On the other hand, there are occasions when strict continuity of performance measurement is desirable, thus requiring a uniform performance measure. The PSI can be computed at any time in a project's life, thereby providing a historical record of performance. Consequently, projects can be compared on the basis of their performance-time histories. This latter advantage was considered very important, and the present analysis was conducted accordingly, using a single performance equation for all survey periods.

## OBJECTIVE RATING MODEL

The principal axis method of factor analysis based on the survey variable intercorrelation matrix yielded the following structural deterioration index, I:

$$I = [0.004\,(LC) + 0.005\,(TC) + 0.006\,(D) + 0.106\,(BU) + 0.011\,(CBJ) + 0.410\,(CBTC) + 0.013\,(SJ) + 0.359\,(STC) + 0.043\,(RS)] \quad (1)$$

where

LC = longitudinal cracks per mile,
TC = transverse cracks per mile,
D = disintegration in square feet per mile,
BU = blowups per mile,
CBJ = corner breaks at transverse joints per mile,
CBTC = corner breaks at transverse cracks per mile,
SJ = spalls at transverse joints per mile,
STC = spalls at transverse cracks per mile, and
RS = remaining spalls per mile.

Even though a pavement in perfect structural condition would have an index value of zero, there is no limit to the degree of deterioration measurable with the scale.

Unlike the PSI, the structural index, I, has a ratio scale status and therefore can be mathematically manipulated without attention being paid to scaling assumptions. (Ratio scales have "zero points" that can be interpreted, thereby allowing the calculation of ratios having physical meaning.)

Index values can be computed for any year for which a condition survey is available. Substitution of a series of surveys taken during a project's service life in Eq. 1 will show the structural deterioration trend as well as the project's condition at the end of any service period. Figure 1 shows the structural deterioration index history for a project for which the 5-, 10-, and 15-year surveys are available. It is characteristic of this project, and others in general, that the index history is nearly linear when plotted on log-log coordinates. Therefore, it is assumed that a close approximation to the index history could be made with the following power function:

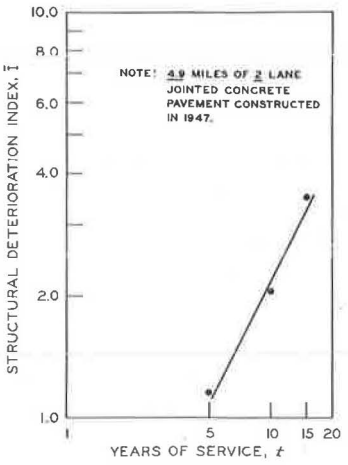


Figure 1. Structural deterioration index (I) history for project 17-1 C6.

$$\log \hat{I} = A \log t + \log B$$

or

$$\hat{I} = Bt^A \tag{2}$$

where

$\hat{I}$ = structural deterioration index estimate,
t = service time in years, and
A, B = fitting constants unique to each project and determined by least squares.

The structural deterioration index, I, and its estimate, $\hat{I}$, can be computed by Eqs. 1 and 2 for any specific time, t. However, condition at a point in time is generally of minor interest; one usually wishes information on the rate of deterioration so that performance can be evaluated. In the present case, however, the negative of performance (called "depreciation") will be calculated. To evaluate total depreciation, D, over each project's service life, $\hat{I}$ was summed over time as follows:

$$dD = \hat{I}\, dt = Bt^A dt$$

and

$$D_T = B \int_0^T t^A dt = \frac{A}{A+1} T^{A+1} \tag{3}$$

where

$D_T$ = structural depreciation from time of construction to terminal rating, and
T = elapsed time in years to terminal rating.

Using Eq. 3, one can evaluate each pavement's structural depreciation from construction to any time up to 15 years. (Survey data beyond 15 years were not available; therefore, Eqs. 2 and 3 can be applied only to this period.)

The structural depreciation index, $D_T$, accomplishes first the pooling of correlated information (survey variables) on pavement distress into a time-dependent measure of pavement deterioration, and second, the summarization of this deterioration over service life. Thus, the deterioration index, $\hat{I}$, and the depreciation index, $D_T$, provide single measures of structural condition and performance respectively. It was hoped that these very general measures would facilitate the search for associated materials, environment, and construction variables.

## DISCUSSION OF RESULTS

A general analysis of variance suggested the existence of relationships between average daily commercial traffic (ADT), coarse aggregate, and deterioration, I. As shown in Figure 2, gravel aggregates containing high proportions of carbonates and pure crushed limestone or dolomite perform best (generally lower I values) over the 15-year service period. [The number of projects surveyed for each period was determined by the distribution of construction over the years and the capabilities of the survey program. There are more 10-year surveys available because, when analysis was begun, many projects were not old enough for 15-year examination.] At 15 years of service, the average I is about 2½ times greater for those projects built with aggregates of relatively low carbonate content. More refined examination of these aggregate groups shows that further subdivision is possible: Of the projects constructed with aggregates containing 80 to 100 percent carbonates, those using 100 percent pure crushed limestones and dolomites had the smallest I values. Also, the gravels containing no carbonates performed somewhat better than other aggregates in the 0 to 60 percent carbonate group. This suggests that aggregate heterogeneity and not merely carbonate content is more closely associated with pavement performance.

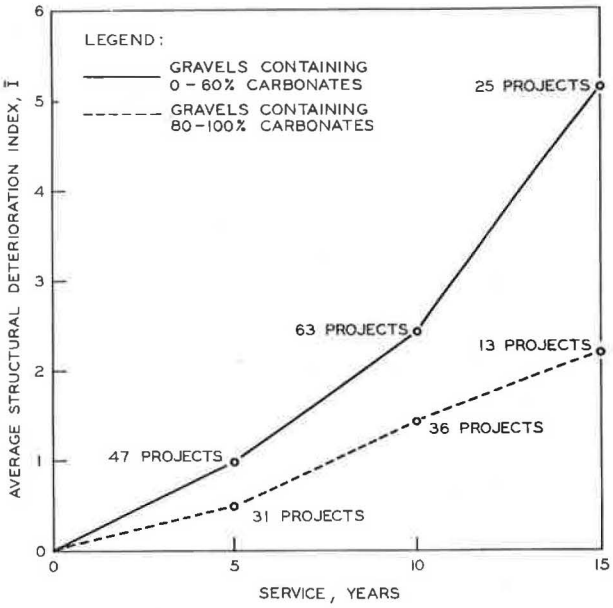


Figure 2. Relationship between deterioration (I) and time for coarse aggregate categories.

A rough attempt to quantify this possibility was made with the formula $H = \sin(P\pi)$, where H is defined as coarse aggregate heterogeneity and P is the proportion of carbonate in the coarse aggregate. Thus, 100 percent pure crushed limestone and 100 percent pure igneous rock gravel will have an H value of 0.0, whereas an aggregate composed of 50 percent carbonate and 50 percent other rock types will have the maximum H value of 1.0.

Figure 3 shows that, in general, performance tends to deteriorate as carbonate-gravel heterogeneity increases. This is especially the case after 15 years of service, where aggregate classes show wide performance variance. However, very general graphic comparisons, such as those just discussed, are usually unreliable and, in any event, rarely sufficient in themselves to pinpoint the causal mechanism involved. Clearly, many local conditions such as faulty joint construction or subgrade support relate to each particular case and type of deterioration, and we oversimplify matters when we speak of one cause alone. Moreover, even if a single factor is identified, it may not be causally important but only statistically associated with the real cause of poor performance. Because the relationship is empirical, the possibility always exists that the statistical finding is misleading, the real mechanism being masked by the complex interrelationship between statistically associated variables. The relationship of aggregates to performance is a case in point; the poorer performance of the heterogeneous aggregates could be due to the differential thermal expansion rates of the several components in the aggregate or to some other variable associated with aggregate heterogeneity. Past research indicates that the latter possibility is more likely (3). Cherts, soft nondurable particles, hard absorbent particles, and the like have long been suspected

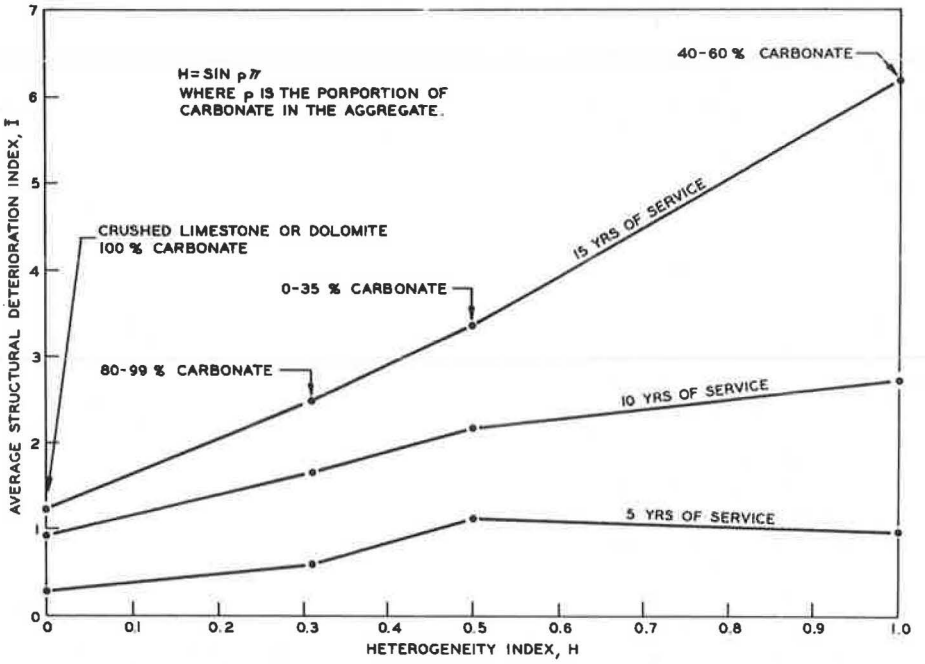


Figure 3. Effect of coarse aggregate heterogeneity (H) on structural performance (I).

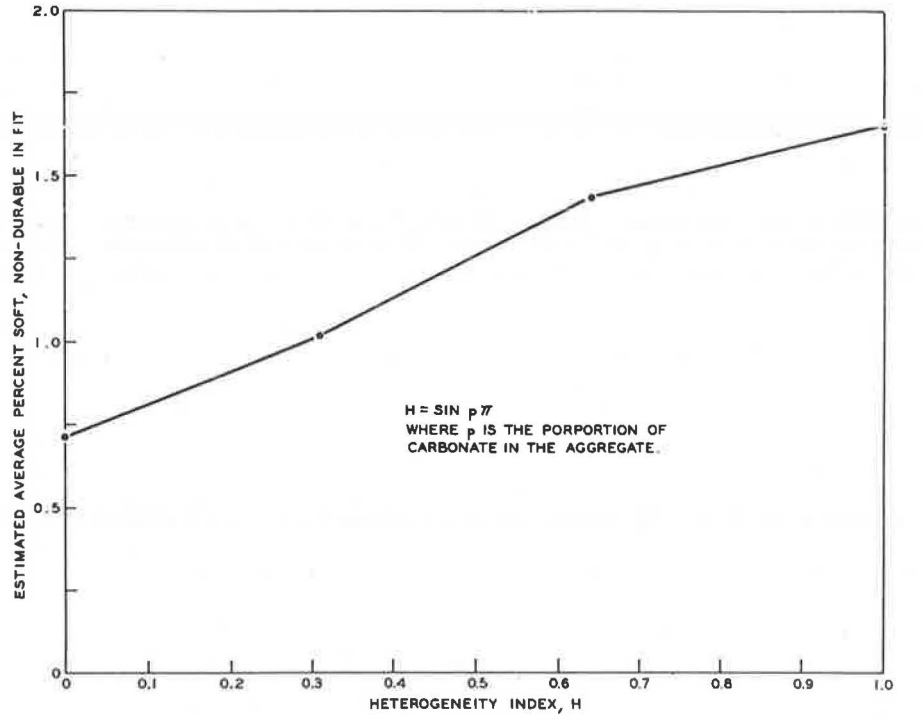


Figure 4. Relationship between coarse aggregate heterogeneity (H) and soft nondurable content (S).

as causes of various kinds of pavement deterioration. The absorption and expansion properties of these materials have inspired attempts at performance forecasts through laboratory freeze-thaw tests. Soft nondurables seem to be present in Michigan's heterogeneous aggregates (Fig. 4) and may, as suggested by other research, be responsible for the structural performance differences encountered (4, 5, 6, 7). As defined by Michigan specifications, soft particles include shale, soft sandstone, ochre, iron-bearing clay, weathered schist, shells, floaters, partially disintegrated particles, cemented gravel, and any other particles that are structurally weak or that fail to meet the soundness test. Michigan specifications for 4A and 10A aggregates used in concrete pavement call for a 3 percent maximum.

Because of past work in these areas and the evidence shown in Figure 4, it was considered unlikely that the simple gravel-limestone aggregate classification used in the preceding examinations would sufficiently define the performance-materials relationship. For this reason, I and PSI values were examined in connection with available soft particle and chert information. Projects for which construction field tests were available provided the basis for analysis. From these records, averages of field test results for soft nondurable and chert percentages were obtained and used as an estimate of the overall content of these materials in the coarse aggregate. Neither I nor PSI showed significant dependence on the chert content; however, correlations appeared to exist between soft nondurable content and I. It is known that the PSI depends largely on roughness, a performance measure only tenuously related to structural distress (8). This is because roughness is not particularly sensitive to such structural deterioration variables as transverse cracking where reinforcing has prevented faulting. Also, other variables such as corner and centerline spalling are generally not picked up directly by the roughometer wheel.

Using the soft nondurable (S) and average daily commercial traffic (ADT) medians, all projects were classified as to either high or low S and either high or low ADT. Figures 5, 6, 7, and 8 show averages for 5-, 10-, and 15-year periods of I and PSI for these

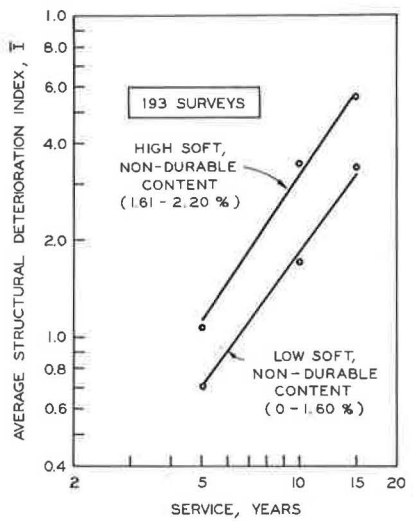


Figure 5. Average structural deterioration (I) for projects with low and high soft nondurable content (S).

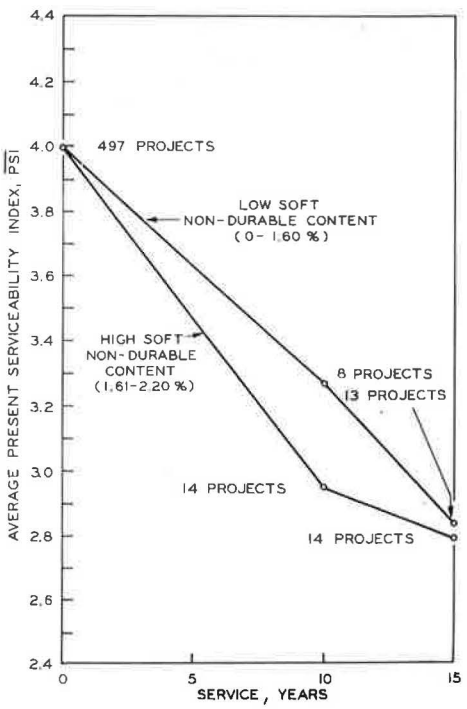


Figure 6. Present serviceability index (PSI) for projects with low and high soft nondurable content (S).

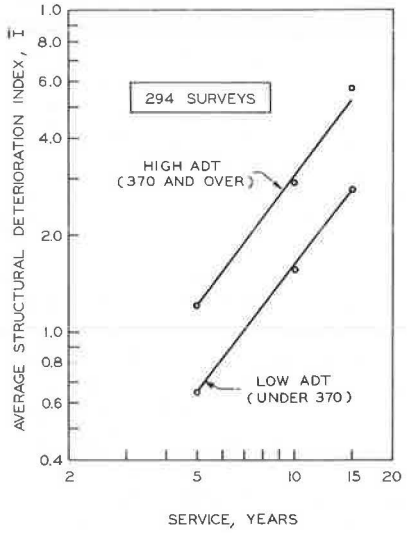


Figure 7. Relationship between average daily commercial traffic volume (ADT) and average structural deterioration (I).

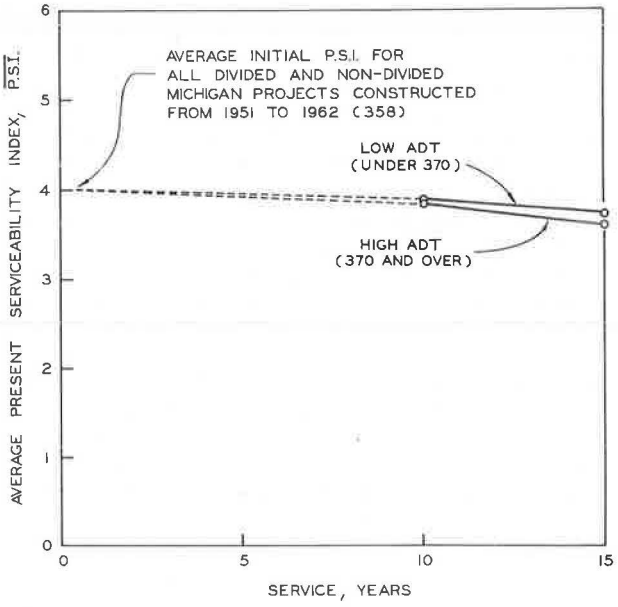


Figure 8. Relationship between average daily commercial traffic volume (ADT) and average present serviceability index (PSI).

classifications using data from all available nondivided roadway projects. Notice that low ADT and low S values are associated with better performance for both indexes. However, I is affected considerably more than PSI. To show the effects on I in more detail, moving averages of I are plotted against both ADT and S for the 5-, 10-, and 15-

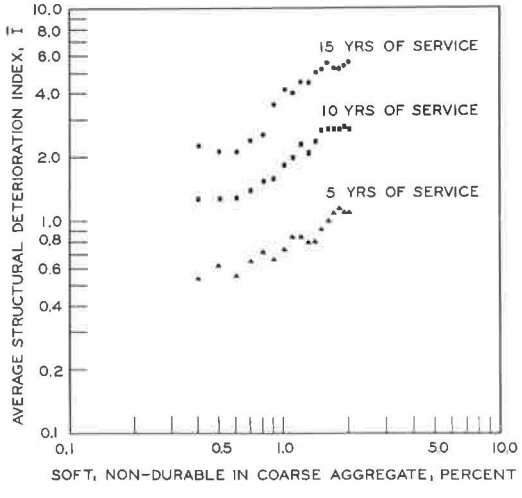


Figure 9. Relationship between soft nondurable (S) and average structural deterioration (I).

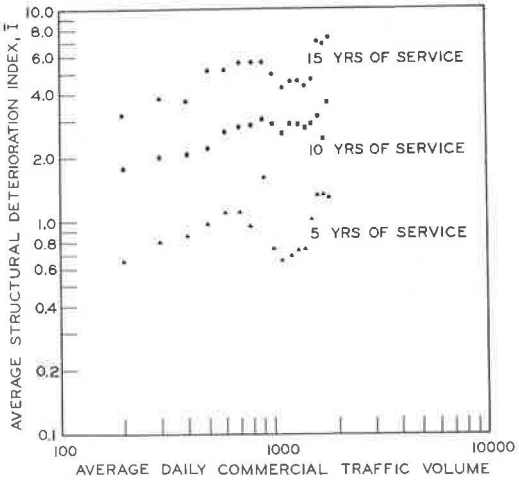


Figure 10. Relationship between average daily commercial traffic volume (ADT) and average structural deterioration (I).

year service periods in Figures 9 and 10. Log I appears to increase with both log S and log (ADT) at about the same rate for each service period. These moving averages, while showing predominant trends, remove considerable scatter from the data—correlations are of the order of only 0.40 to 0.50. Correlations would be higher but for only 5 or 6 projects (out of nearly 100). These projects either had low traffic or low soft content (or both) and showed excessive deterioration early in their service life. No reason could be found, but it is assumed that local soil conditions are responsible. Also, the data used for ADT estimates resulted from only a single 24-hour sample taken during the service life of each project. Because these data are so weak, the influence of traffic on performance requires further examination.

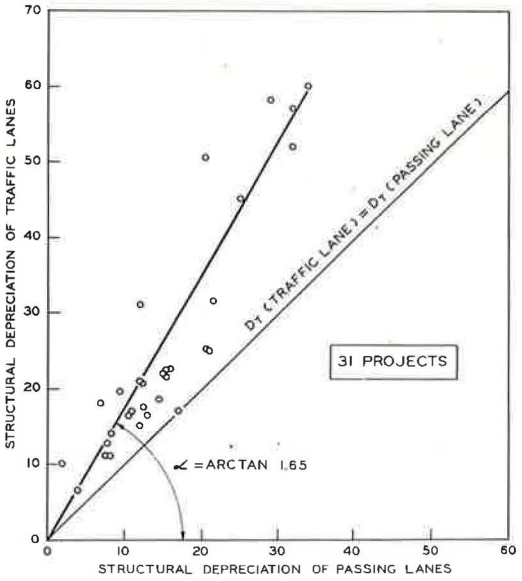


Figure 11. Comparison of structural depreciation for traffic and corresponding passing lanes.

Four-lane divided expressways provide an excellent opportunity to evaluate lane-performance differences attributable to differential usage. For these pavements, all construction, environment, design, and materials variables are identical and thus any difference in performance between traffic and passing lanes can be unequivocally assigned to differences in traffic load. A quantitative, between-lane difference in traffic load was generally not available for the projects examined herein. However, it is well known that traffic lanes experience more loading than the corresponding passing lanes and that the traffic lane can probably be assigned from 70 to 90 percent of the total in one direction.

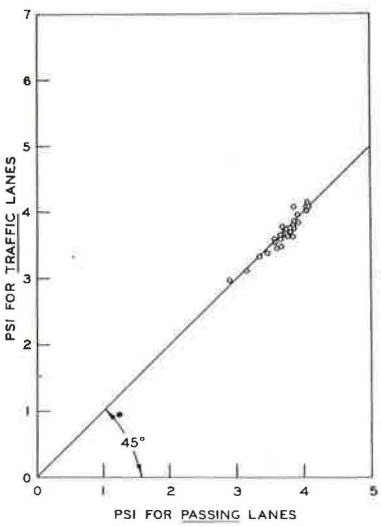


Figure 12. Comparison of present serviceability index (PSI) for traffic and corresponding passing lanes.

Figure 11 shows the depreciation index, $D_T$, computed for the traffic and corresponding passing lanes for each of 31 divided-roadway projects. Also shown is a 45-degree line, which, of course, indicates equal depreciation for each lane. The traffic-passing lane and structural depreciation relationship, although linear, definitely does not have the slope of 1.0 that is necessary if both lanes perform equally. Overall, the traffic lanes show about 65 percent more structural depreciation (as measured by $D_T$) than the corresponding passing lanes.

As with overall traffic volumes, PSI's for matched traffic and passing lanes do not show appreciable differences attributable to vehicle distributions even after 15 years of service (Fig. 12). As could be expected, those survey variables that are heavily weighted in the structural performance index, i.e., corner cracking and spalling together with transverse and longitudinal cracking, do not noticeably influence PSI in the traffic wheelpaths where roughometer measurements are made. Only after more extensive deterioration has taken place (much of which may stem from the initial failures measured by these variables) would roughness measurements be substantially

affected. Because of the failure of the PSI to adequately measure structural performance differences, further analysis using this criterion was not undertaken. (All survey variables except blowups in Eq. 1 had larger average values in the traffic lane.)

It should be pointed out that all projects examined herein were considered to have adequate subgrade support. Either they were constructed on natural sand and gravel subgrades with good natural drainage, or proper subbases with adequate thickness were constructed to improve drainage. If structural performance is measured by the PSI, one would conclude from the traffic versus passing-lane study that because commercial traffic does not perceptibly influence structural performance, the pavement system must be adequate (Fig. 12). However, if structural performance is measured by structural condition variables collectively in indexes such as D, one would conclude the opposite. Because pavement performance, even with quality subgrade, is substantially affected by commercial traffic, the pavement system could be improved. [Since these projects were constructed, the Michigan subbase requirements have increased from 12 to 14 and later to 15 in. of granular material. Also, contraction joint spacing has been decreased from 99 ft to 71 ft 2 in.]

## STRUCTURAL PERFORMANCE MODEL

Assuming that the effects of soft nondurable particles and average daily commercial traffic volume on performance are real, it seems reasonable to construct a performance prediction equation. Figures 5, 7, 9, and 10 suggest the following relationships:

$$\log \hat{I} = K_1 \log S + \log K_2 \tag{4}$$

$$\log \hat{I} = K_3 \log (ADT) = \log K_4 \tag{5}$$

$$\log \hat{I} = K_5 \log t + \log K_6 \tag{6}$$

where

$\hat{I}$ = estimate of structural deterioration index, I;
S = percentage of soft nondurable particles in coarse aggregate;
ADT = average daily commercial traffic volume;
t = age of pavement in years; and
$K_1, \ldots, K_6$ = fitting constants with $K_2$ and $K_4$ dependent on the survey year.

Ideally, these variables would be combined by multiple regression techniques. In the present case, however, a complete data matrix was not available because many projects did not have complete records for soft nondurable content or condition surveys for all three service periods. Consequently, these variables were combined geometrically by first estimating the slopes for each variable by simple linear regression and then summing the three equations (the geometric average results in a simpler model than the arithmetic average). Thus, we have in general

$$\log \hat{I} = \frac{K_1}{3} \log S + \frac{K_3}{3} \log (ADT) + \frac{K_5}{3} \log t + \log K_7$$

From Figures 5, 7, 9, and 10 we can estimate that $K_1 = K_3 = 0.54$ and $K_5 = 1.56$. Therefore,

$$\hat{I} = K_7 S^{0.18} (ADT)^{0.18} t^{0.52}$$

Estimates of $D_T$ can be obtained by integration:

$$\hat{D} = \int_0^T \hat{I}\, dt = K_7 S^{0.18} (ADT)^{0.18} \int_0^T t^{0.52}\, dt$$

and

$$\hat{D}_T = K_8 S^{0.18} (ADT)^{0.18} T^{1.52} \tag{7}$$

In order that both traffic and passing lanes of divided expressways could be included with the two-lane pavements, the commercial ADT, given for only the roadway, had to be distributed between the lanes. An approximate distribution formula was obtained as follows by Eq. 5:

$$\hat{I} = K_4 (ADT)^{K_3}$$

and

$$\hat{D}_T = \int_0^T \hat{I}\,dt = K_4 (ADT)^{K_3}\, T$$

Dividing $\hat{D}_T$ for the traffic lane by $\hat{D}_T$ for the passing lane and substituting the slope from Figures 10 and 11, we have

$$\frac{D_T\,(\text{traffic lane})}{\hat{D}_T\,(\text{passing lane})} = \left(\frac{\text{ADT traffic lane}}{\text{ADT passing lane}}\right)^{0.54} = \arctan \alpha = 1.65$$

Therefore,

$$\frac{\text{ADT traffic lane}}{\text{ADT passing lane}} = (1.65)^{\frac{1}{0.54}} = 2.52$$

Because the percentages in the traffic and passing lanes must add to 100, we have ADT traffic lane = 0.72 ADT and ADT passing lane = 0.28 ADT. These formulas were used to divide the total roadway ADT volumes for each lane, thereby permitting the incorporation of both lanes of divided expressway into the final analysis.

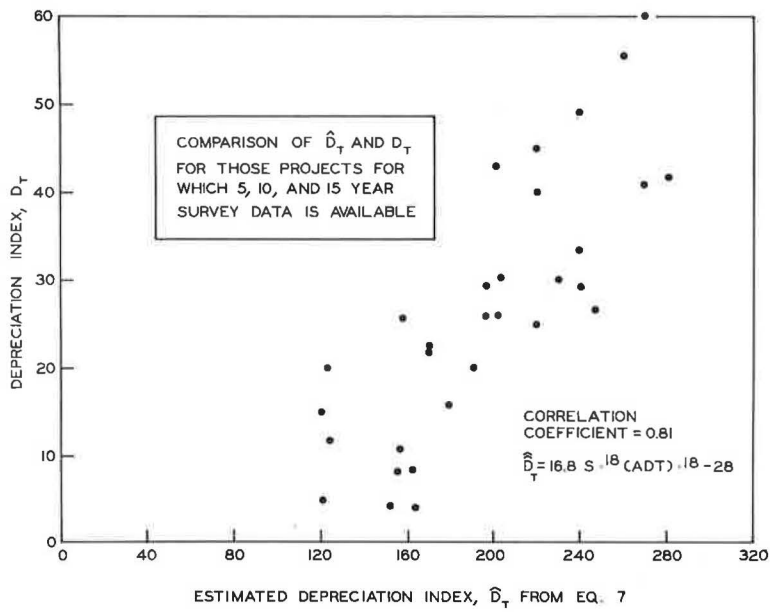


Figure 13. Comparison of D and $\hat{D}$ for those projects for which 5-, 10-, and 15-year survey data are available.

$K_8$ of Eq. 7 can now be determined by the regression of $\hat{D}_T$ on $D_T$, that is,

$$\hat{\hat{D}}_T = K_9 \hat{D}_T + K_{10}$$

which gives

$$\hat{\hat{D}}_T = 0.33\ S^{0.18}\ (ADT)^{0.18}\ T^{1.52} - 28 \qquad (8)$$

The correlation coefficient for the regression is +0.77, which for the number of points (111) is highly significant.

Figure 13 is a plot of $D_T$ and $\hat{D}_T$ for all projects for which 5-, 10-, and 15-year data were available, including divided expressways. This is presented to show the structural depreciation predicting power of S and ADT independently of time, when reasonably stable (3 survey years available) $D_T$ values can be calculated. Considering only these projects, Eq. 7 becomes

$$\hat{D}_T = 0.28\ D_T - 28 = 16.8\ S^{0.18}\ (ADT)^{0.18} - 28$$

and the correlation for the regression of $\hat{D}_T$ on $D_T$ is a highly significant +0.81 for the 31 projects. Thus, when projects having 5-, 10-, and 15-year surveys are considered, 65 percent of the structural depreciation variance can be "explained" by the variables of soft nondurable percentage and average daily commercial traffic volume. Presumably, if more surveys could be incorporated, thereby allowing more reliable time-deterioration curves, a somewhat better relationship could be established. The main point is, however, that both percentages of soft nondurable particles in the coarse aggregate and commercial traffic have been shown to have structural performance prediction power. This does not ipso facto "prove" a causal relationship. However, background information on these variables (such as traffic versus passing-lane comparisons and the AASHO Road Test) suggests that the present correlations are meaningful, and that these variables are not merely "standing in" for the "real" causes.

These examinations suggest four conclusions:

1. Of all deleterious materials examined, the soft nondurable content of coarse aggregate is the best predictor of concrete pavement structural performance as measured by "objective" indexes based on condition survey variables.
2. Average daily commercial traffic is definitely associated with concrete pavement structural deterioration as measured by the same indexes. This is shown to be the case for both four-lane divided highways and two-lane roadways.
3. The PSI is not effectively related to structural performance. Also, neither soft nondurable content in coarse aggregate nor average daily commercial traffic volume shows any significant relationship to the PSI. This may not be true for service periods beyond 15 years, when structural deterioration is presumed to significantly affect roughness. However, up to 15 years of service, condition survey variables combined in indexes appear to be the most reliable early predictor of concrete pavement structural deterioration.
4. Based on sampled soft nondurable percentages in the coarse aggregate and anticipated commercial traffic volume, a mathematical model can be constructed that will predict with moderate precision concrete pavement structural condition at a specified future time, or total performance up to 15 years of service.

## ACKNOWLEDGMENTS

This research project was conducted by the Research Laboratory Section of the Michigan Department of State Highways in cooperation with the U. S. Bureau of Public Roads. The opinions, findings, and conclusions expressed in this report are those of the author and not necessarily those of the Bureau of Public Roads.

## REFERENCES

1. The AASHO Road Test. HRB Spec. Rept. 61A, 1961.
2. Harman, H. H. Modern Factor Analysis. Univ. of Chicago Press, 1960, pp. 1-23, 154-157, 337-348.
3. Walker, R. D. Identification of Aggregates Causing Poor Concrete Performance When Frozen—Interim Report. NCHRP Rept. 12, 1965.
4. Reagel, F. V. Chert Unfit for Coarse Aggregate. Engineering News-Record, Vol. 93, No. 9, 1924.
5. Legg, F. E. Freeze-Thaw Durability of Michigan Concrete Coarse Aggregates. HRB Bull. 143, 1956, pp. 1-13.
6. Schuster, R. L. A Study of Chert and Shale Gravel in Concrete. HRB Bull. 305, 1961, pp. 51-75.
7. Swenson, E. G., and Chaley, V. Basis for Classifying Deleterious Characteristics of Concrete Aggregate Materials. Jour. American Concrete Institute, Proc., Vol. 52, No. 58, 1956.
8. Yoder, E. J., and Milhous, R. T. Comparison of Different Methods of Measuring Pavement Condition—Interim Report. NCHRP Rept. 7, 1964.

# Four Years' Experience at the Brampton Test Road

W. A. PHANG, Research Branch, Department of Highways, Ontario

In 1965, 36 short, experimental sections of flexible pavement were constructed on Highway 10 near Brampton to compare five types of base materials laid in four thicknesses on three thicknesses of subbase. The base materials are asphalt concrete, crushed stone, crushed gravel, emulsion-stabilized sand, and cement-treated sand. Measurements of Benkelman beam rebound, rut depths, longitudinal and transverse profile, and frost depth penetration and frost heave have been made periodically. A summary of the results from 1965 through to 1969 is reported.

Analysis of peak annual deflection has yielded layer equivalency factors and deflection-thickness relationships, and, although these change from year to year, they are valuable indicators of performance. Observations of frost penetration and frost heave are presented and their effect on the behavior of the different materials is discussed. The performance of the pavement sections is described in terms of rutting, cracking and patching, and roughness of ride. The behavior of materials in rutting is discussed and some anomalous behavior is reported. The degree and extent of cracking and patching are described, and comparisons of pavement roughness are made in terms of pavement performance ratings. Some preliminary conclusions on the relative values of the base materials appear warranted.

•A FULL-SCALE ROAD EXPERIMENT was constructed on 2 miles of the north-bound lanes of Highway 10, approximately 5 miles north of Brampton, Ontario, in August and September of 1965. The main objectives of this experiment were (a) to enable the Department of Highways, Ontario, to benefit from the results of the AASHO test by extending these results to the most commonly used materials and the environment of the province; (b) to evaluate the standard pavement designs used in the province; and (c) to observe the structural performance and the performance under traffic of five types of base material and a sand cushion subbase and, if possible, to develop equivalency values for these materials.

The experiment consists of 36 test sections of pavement, each 2 lanes wide by 200 ft in length and separated by 50-ft transitions. A uniform light clay subgrade was ensured by placing selected borrow over the existing ground. The sand subbase was laid either 6 in. or 18 in. in thickness. No subbase was used with four of the asphalt-concrete base sections and with one section each of bituminous and cement-treated bases.

The main experiment compares equal thicknesses of five types of base material; asphalt concrete, crushed limestone gravel, crushed dolomitic limestone rock, bituminous-stabilized sand, and cement-treated sand (both sands similar to that used in the subbase). These materials were laid in thicknesses of 2, 4, 6, and 8 in. One duplicate section of each type was laid at either the 4- or 6-in. thickness.

Paper sponsored by Committee on Pavement Condition Evaluation and presented at the 49th Annual Meeting.

The asphalt concrete surfacing was placed in two layers to a total thickness of $3\frac{1}{2}$ in. over all sections except four, where an additional 2-in. layer was placed to provide $5\frac{1}{2}$ in. of surfacing. Two of the sections were of thicknesses equal to the standard DHO design, one with crushed-gravel base and the other with crushed-rock base. The sections were randomized in location and base thickness, but replicated sections were placed adjoining each other. A detailed layout of the sections is shown in Figure 1. Details of the construction and records of material testing and weather data have been published in an earlier report (1). The experimental sections were opened to traffic in October 1965 with southbound traffic using the northbound lane for approximately 3 weeks while the two southbound lanes were reconstructed.

## MATERIALS AND CONSTRUCTION

At least 3 ft of selected light clay borrow was placed over the existing ground to provide uniformity of materials in the subgrade. Uniformity of the top 6 in. of the subgrade was further ensured by reworking this material with a pulvemixer not more than 24 hours prior to placing the overlying layers, and recompacting at optimum moisture with a sheepsfoot and vibrating steel-wheeled rollers.

The sand subbase consisted of a well-graded medium sand with about 15 percent passing the No. 200 screen. It was placed by spreader box and compacted in 6-in. lifts by vibratory steel- and pneumatic-tired rollers. The asphalt concrete base was a standard binder mix utilizing a $\frac{3}{4}$-in. maximum size coarse aggregate with 58 percent passing the No. 4 screen and 3 percent passing the No. 200 screen. Six percent of an 85-100 penetration grade asphalt cement was used and the mix had an air voids content of 7 percent after compaction. The mix was compacted in 2-in. lifts with steel-wheeled breakdown and finish rollers and with a pneumatic intermediate roller.

The crushed-rock base was a quarried dolomitic limestone of standard $\frac{3}{4}$-in. grading, with 50 percent passing the No. 4 screen and 9 percent passing the No. 200 screen. The crushed-gravel base of limestone gravel was essentially of the same gradation as the crushed rock, but it had only 7 percent passing the No. 200 screen. Both the crushed-rock and crushed-gravel base materials were laid by asphalt pavers and compacted by vibratory steel- and pneumatic-tired rollers.

The bituminous-stabilized base utilized a well-graded sand from the same source as the subbase sand, but with only 6 percent passing the No. 200 screen. The binder was 3 percent of an SS-1h emulsion, and the materials were plant-mixed and laid with an asphalt paver. A combination of vibratory steel and pneumatic rollers was used to compact each layer to a finished thickness of 2 in. The sand used for the cement-treated

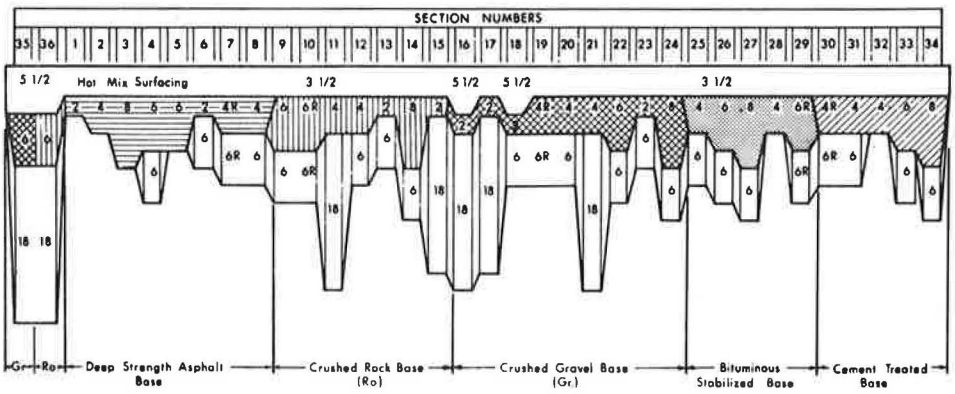


Figure 1. Layout of experimental pavement sections: R = replicated (i.e., duplicated design); Gr = crushed-gravel base; Ro = crushed-rock base.

base was similar to that used for the bituminous-stabilized base. Four percent portland cement was added. The materials were plant-mixed, laid by asphalt paver, and compacted with vibratory steel and pneumatic rollers.

The asphalt concrete surfacing consisted of a 2-in. lift of a binder course of mix properties similar to the asphalt concrete base courses, followed by a $1\frac{1}{2}$-in. lift of a finer surfacing mix in regular use in the southern part of the province. Further details of the material properties are given in Appendix A; construction and other data are available in an earlier report (1).

## INSTRUMENTATION AND MEASUREMENTS

### Reference Pins for Transverse Cross Sections

As soon as the surface course was completed and before the experimental sections were opened to traffic, three transverse rows of steel pins were embedded in each test section—at the middle and 30 ft from each end. Each row of pins began 6 in. from the pavement edge; the pins were spaced at 12-in. intervals across the two traffic lanes. The hole for each pin was predrilled and the pins were set flush with the pavement surface with an epoxy cement. To facilitate reading the levels of the pins, the head of each pin was recessed to receive a special shoe attached to the leveling staff. Precise leveling was carried out on these reference pins four or five times each year.

### Benkelman Beam Measurements

Benkelman beam deflection measurements were made on the experimental sections in accordance with the procedures developed by the Canadian Good Roads Association (2). The deflection readings on all sections were measured once weekly during the spring months and once monthly during the rest of the year. The deflections were measured every 20 ft in the outer wheelpaths of both driving and passing lanes. In each test the 9,000-lb wheel load, on standard dual tires, is located on a painted mark and the probe tip is placed between the dual tires just a few inches ahead of the axle. The truck is then driven to the next mark and the maximum deflection and the final reading are recorded. The mean value of the 10 deflections per section is noted as well as the standard deviation and the temperature of the road surface. No temperature corrections are made to these deflections at this time.

### Profilometer Measurements

The profilometer used in this study is a replica of the one developed by the British Road Research Laboratory (3) and is similar to that used by the Canadian Department of Transport, Air Services Construction. This 16-wheel, 22-ft long vehicle provides a floating datum representing the average road surface. A central wheel moving relative to the datum is used to trace a profile of the road surface and to activate counters at amplitudes of the vertical movement of from 0.1 to 1.5 in. in increments of 0.1 in. The number and amplitudes of the bumps over some measured distance is converted to inches of vertical movement per mile, and is denoted as the classifier or q value. The profilometer q value has been correlated with panel ratings (4, 11) and with road-user opinion (5), but for this experiment present performance ratings (PPR) are derived from profilometer q values by the equation

$$PPR = 12.73 - 4.53 \log q$$

Although the correlation work used profilometer measurements taken over longer distances, the repeatability of the measurements obtained from the 200-ft test sections was found to be satisfactory for the purposes of this experiment. The present performance rating used by the CGRA (2) is comparable to the present serviceability index (PSI) developed at the AASHO Road Test except that the PPR uses a rating scale of 0 to 10 instead of the scale of 0 to 5.

## Rut-Depth Gage

During the early stages of the experiment, it was thought that rutting could be measured from the plotted transverse cross sections obtained by precise leveling on the transverse cross-section pins. However, because of the small rut depths during the early months, inaccuracies in the plotting and drawing made this method unreliable, and a rut-depth gage was constructed in 1967 to the design used at the AASHO Road Test (6). The gage measures the depth of rutting midway between two points 4 ft apart. Rut-depth measurements were made on each test section at 20-ft intervals in both the inner and outer wheelpaths. The average value of the 20 measurements per section was recorded as the rut depth for that section.

## Crack and Patching Records

Pavement cracking and patching of each test section is recorded cartographically at periodic intervals, so that the growth and severity of cracking and patching can be observed for any desired time.

## Frost-Depth Gages

Measurements of frost penetration were made during 1967 and 1968 at five test sections (sections 4, 9, 22, 26, and 33) with similar construction thickness but with different base materials. The graduated frost-depth gages, which are installed under the pavement surface, contain a methylene-blue indicator solution that becomes white when frozen, thus providing a clear indication of the frost line.

# TRAFFIC

The 2-mile section of Highway 10 where the experimental pavement is located has only one minor intersection, so that each test section is subjected to substantially the same loading and traffic volume. To assess the amount of loading imposed on the test sections, traffic and vehicle classification counts were carried out periodically. As a result of a 1967 loadometer survey, and utilizing load equivalency data from the AASHO Road Test, load factors were determined for converting each class of vehicle into equivalent 18,000-lb single-axle loads. Figure 2 shows a plot of the accumulated number

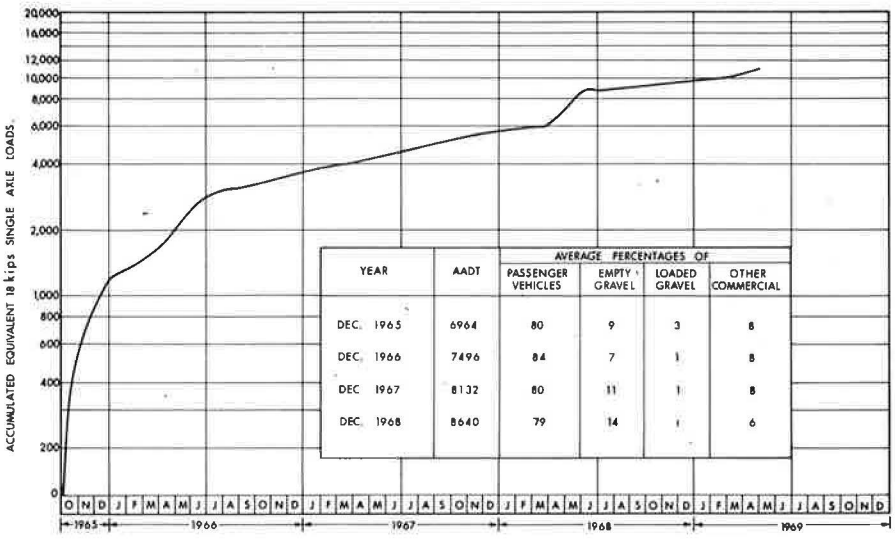


Figure 2. Accumulated equivalent 18,000-lb single-axle loads in northbound driving lane.

of equivalent 18,000-lb single-axle loads passing over the driving lane of the test sections for each month. The relatively low total of 18,000-lb single-axle loads so far experienced, in spite of an AADT of over 8,000, probably explains why the weaker sections started to fail at a much later date than expected.

## LOAD RESPONSE CHARACTERISTICS

Deflection measurements made in accordance with the CGRA Benkelman beam rebound procedure give a measure of the response of the pavement to a standard load. The rebound varies quite considerably even in what is considered a uniformly constructed length of pavement, and the CGRA procedure for analyzing the test results uses all the measurements in a section to calculate a statistical estimate of maximum probable deflection. For the purpose of comparing the behavior of different test sections, however, the mean values of rebounds were used.

Table B-1 in Appendix B lists the mean Benkelman beam rebounds for 1965 to 1969 for 35 of the test sections. Section 23, with a 2-in. crushed-gravel base, failed very early in the experiment and was reconstructed in November 1965 to normal standards and dropped from the experiment. The values listed are for the rebounds measured in the outer wheelpath of the driving lane.

### Seasonal Variations

Figure 3 shows typical rebound histories for the year 1966 for five test sections with equal thicknesses of surfacing, base, and subbase but with five different base materials. In the winter months the base, subbase, and subgrade are frozen and the load response is negligible; thus no rebound values are recorded for these months. In the spring and early summer months the deflections increase rapidly as the thaw sets in and peak when the weakened condition of the untreated bases, subbase, and subgrade combines with the softening of the asphalt binder in the surfacing to give the greatest rebounds. As the summer progresses into fall, the rebounds slowly decrease as the untreated base, sub-

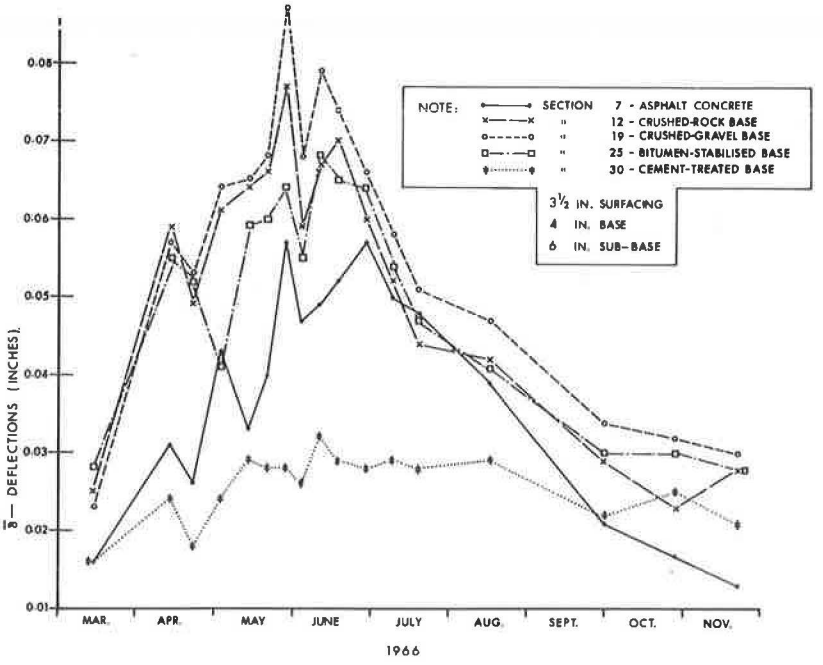


Figure 3. Typical seasonal changes in deflection.

base, and subgrade recover their strength. The spring/fall ratio of the deflections for each type of base material is different, and Figure 3 shows the crushed-gravel and crushed-stone bases to be most susceptible to seasonal changes whereas the cement-treated base is least susceptible.

In its analysis of pavement performance data, the CGRA concluded that "The elastic rebound Benkelman beam deflection value is a significant parameter in predicting the performance of flexible pavement sections" (2). The question arises as to which part of the seasonal deflection curve should be used in predicting the performance of the test sections. Consideration of the form of these seasonal deflection curves indicates that it is convenient and logical to use the spring and early summer peak values because the pavements are then most vulnerable to damage by traffic. Although the intervals between deflection observations are large and it is quite likely that the weakest conditions

TABLE 1

PEAK MEAN BENKELMAN BEAM DEFLECTIONS, $\bar{\delta}$

| Section Number | Pavement Thickness (in.) | | | | 1966 | | 1967 | | 1968 | | 1969 | |
|---|---|---|---|---|---|---|---|---|---|---|---|---|
| | Surfacing | Base | Subbase | Total | Deflection (in.) | Temperature (deg F) | Deflection (in.) | Temperature (deg F) | Deflection (in.) | Temperature (deg F) | Deflection (in.) | Temperature (deg F) |
| **Asphalt-Concrete Base** | | | | | | | | | | | | |
| 1 | 3.5 | 2 | 0 | 5.5 | 0.043 | 84 | 0.057 | 83 | 0.089 | 94 | 0.072 | 62 |
| 2 | 3.5 | 4 | 0 | 7.5 | 0.029 | 95 | 0.041 | 85 | 0.065 | 94 | 0.048 | 62 |
| 5 | 3.5 | 6 | 0 | 9.5 | 0.026 | 92 | 0.031 | 88 | 0.047 | 94 | 0.033 | 85 |
| 3 | 3.5 | 8 | 0 | 11.5 | 0.023 | 79 | 0.023 | 87 | 0.032 | 94 | 0.023 | 70 |
| 6 | 3.5 | 2 | 6 | 11.5 | 0.118 | 92 | 0.069 | 88 | 0.086 | 94 | 0.077 | 85 |
| 7 | 3.5 | 4 | 6 | 13.5 | 0.057 | 95 | 0.050 | 89 | 0.061 | 94 | 0.049 | 85 |
| 8 | 3.5 | 4 | 6 | 13.5 | 0.057 | 92 | 0.050 | 89 | 0.059 | 94 | 0.049 | 85 |
| 4 | 3.5 | 6 | 6 | 15.5 | 0.045 | 95 | 0.041 | 81 | 0.058 | 94 | 0.038 | 62 |
| **Crushed-Rock Base** | | | | | | | | | | | | |
| 13 | 3.5 | 2 | 6 | 11.5 | 0.097 | 90 | 0.090 | 103 | 0.094 | 94 | 0.119 | 45 |
| 12 | 3.5 | 4 | 6 | 13.5 | 0.077 | 90 | 0.059 | 101 | 0.080 | 94 | 0.079 | 62 |
| 9 | 3.5 | 6 | 6 | 15.5 | 0.070 | 90 | 0.063 | 84 | 0.066 | 94 | 0.080 | 62 |
| 10 | 3.5 | 6 | 6 | 15.5 | 0.067 | 90 | 0.058 | 107 | 0.066 | 94 | 0.082 | 62 |
| 14 | 3.5 | 8 | 6 | 17.5 | 0.050 | 90 | 0.055 | 86 | 0.063 | 94 | 0.063 | 55 |
| 15 | 3.5 | 2 | 18 | 23.5 | 0.045 | 82 | 0.042 | 104 | 0.044 | 94 | 0.043 | 62 |
| 11 | 3.5 | 4 | 18 | 25.5 | 0.044 | 90 | 0.034 | 76 | 0.038 | 55 | 0.043 | 62 |
| 36 | 5.5 | 6 | 18 | 29.5 | 0.029 | 95 | 0.027 | 82 | 0.032 | 94 | 0.031 | 62 |
| **Crushed-Gravel Base** | | | | | | | | | | | | |
| 23 | 3.5 | 2 | 6 | 11.5 | — | — | — | — | — | — | — | — |
| 19 | 3.5 | 4 | 6 | 13.5 | 0.087 | 89 | 0.079 | 102 | 0.081 | 94 | 0.090 | 85 |
| 20 | 3.5 | 4 | 6 | 13.5 | 0.084 | 88 | 0.081 | 90 | 0.101 | 94 | 0.105 | 85 |
| 22 | 3.5 | 6 | 6 | 15.5 | 0.062 | 88 | 0.060 | 110 | 0.075 | 94 | 0.084 | 45 |
| 24 | 3.5 | 8 | 6 | 17.5 | 0.053 | 90 | 0.042 | 42 | 0.050 | 94 | 0.056 | 62 |
| 18 | 5.5 | 2 | 6 | 13.5 | 0.091 | 88 | 0.075 | 109 | 0.086 | 94 | 0.071 | 85 |
| 17 | 3.5 | 2 | 18 | 23.5 | 0.048 | 88 | 0.040 | 87 | 0.047 | 94 | 0.044 | 85 |
| 21 | 3.5 | 4 | 18 | 25.5 | 0.038 | 90 | 0.030 | 110 | 0.034 | 94 | 0.035 | 55 |
| 16 | 5.5 | 2 | 18 | 25.5 | 0.043 | 76 | 0.033 | 106 | 0.039 | 94 | 0.032 | 85 |
| 35 | 5.5 | 6 | 18 | 29.5 | 0.029 | 84 | 0.027 | 81 | 0.033 | 94 | 0.030 | 62 |
| **Bituminous-Stabilized Base** | | | | | | | | | | | | |
| 28 | 3.5 | 4 | 0 | 7.5 | 0.113 | 86 | — | — | 0.160 | 94 | 0.177 | 85 |
| 25 | 3.5 | 4 | 6 | 13.5 | 0.068 | 88 | 0.067 | 84 | 0.076 | 94 | 0.083 | 85 |
| 26 | 3.5 | 6 | 6 | 15.5 | 0.059 | 88 | 0.055 | 110 | 0.064 | 94 | 0.070 | 85 |
| 29 | 3.5 | 6 | 6 | 15.5 | 0.055 | 94 | 0.054 | 111 | 0.074 | 94 | 0.076 | 85 |
| 27 | 3.5 | 8 | 6 | 17.5 | 0.040 | 88 | 0.039 | 111 | 0.050 | 94 | 0.057 | 85 |
| **Cement-Treated Base** | | | | | | | | | | | | |
| 32 | 3.5 | 4 | 0 | 7.5 | 0.056 | 99 | 0.071 | 90 | 0.096 | 94 | 0.099 | 70 |
| 30 | 3.5 | 4 | 6 | 13.5 | 0.032 | 94 | 0.039 | 87 | 0.056 | 94 | 0.053 | 85 |
| 31 | 3.5 | 4 | 6 | 13.5 | 0.031 | 94 | 0.035 | 84 | 0.046 | 94 | 0.050 | 85 |
| 33 | 3.5 | 6 | 6 | 15.5 | 0.023 | 79 | 0.029 | 42 | 0.035 | 94 | 0.038 | 85 |
| 34 | 3.5 | 8 | 6 | 7.5 | 0.016 | 112 | 0.019 | 42 | 0.019 | 94 | 0.022 | 62 |

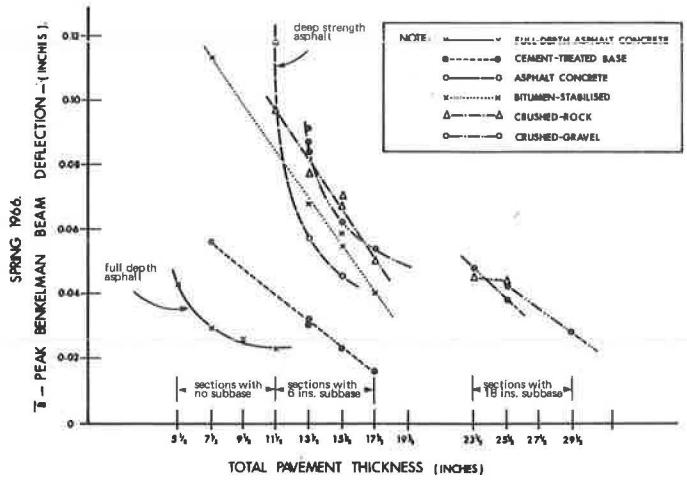


Figure 4. Peak deflections versus total thickness, 1966.

are not tested, the peak values observed are considered to be the most useful for these comparative evaluations.

## Temperature Variation

Ideally, when comparing the load response characteristics of various pavement sections, account should be taken of the effects of temperature on the pavement deflection, and deflections should be compared at some common temperature. No temperature corrections have been made to the deflections in this report. The peak deflections are generally observed at fairly high temperatures, and it is considered that any corrections would have an insignificant effect on the comparative evaluations.

## Thickness-Deflection Relationships

Table 1 gives the peak mean rebounds of the test sections for the years 1966, 1967, 1968, and 1969 and shows that peak rebounds decrease with increased thickness and change from year to year. A plot of peak rebounds (1966) versus total pavement thickness is shown in Figure 4. From this figure it is very apparent that the full-depth asphalt sections cannot be grouped with the deep-strength asphalt, and the sections with 18 in. of subbase cannot be grouped with sections having only 6 in. of subbase. (In a full-depth asphalt section, asphalt mixtures are employed for all courses above the subgrade or improved subgrade.)

To provide a starting point for analysis, it was assumed that sections with equal deflections under the Benkelman beam test load would give equal performance. If a deflection value of 0.050 in. is chosen, the thicknesses of pavement of each base type that would have this deflection can be determined from Figure 4. Because the thickness of surfacing and subbase is reasonably constant, it is possible to express each inch of thickness of each type of base material as an equivalent thickness of crushed gravel.

TABLE 2

GRAVEL EQUIVALENCIES

| Base Type | Equivalence in Inches of Crushed Gravel[a] | | | |
|---|---|---|---|---|
| | 1966 | 1967 | 1968 | 1969 |
| 1 in. of cement-treated base | 3.8 | 3.50 | 2.0 | 1.89 |
| 1 in. of asphalt concrete | 1.79 | 1.75 | 1.14 | 2.12 |
| 1 in. of bituminous-stabilized base | 1.3 | 1.08 | 1.00 | 0.95 |
| 1 in. of crushed rock | 1.06 | 0.75 | 0.73 | 0.90 |
| 1 in. of sand subbase | 0.59 | 0.52 | 0.54 | 0.62 |

[a]For a 0.050-in. deflection.

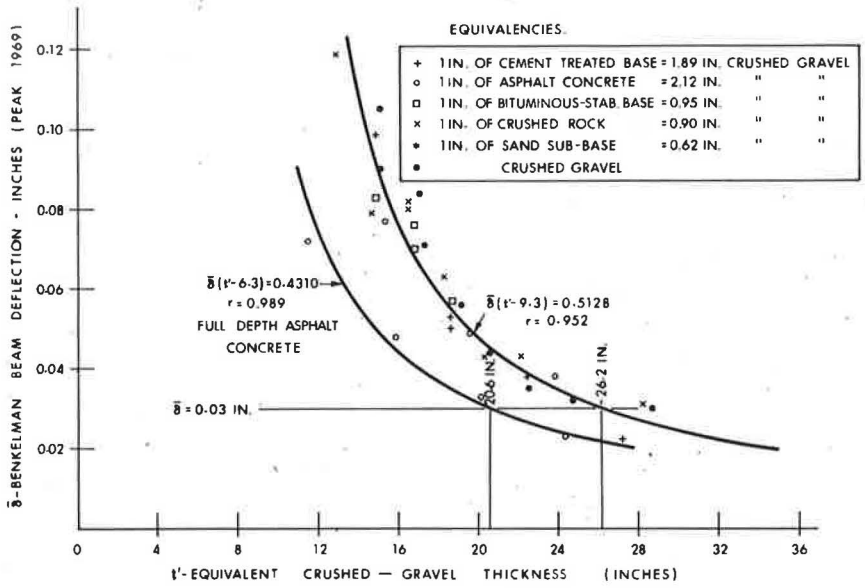


Figure 5. Deflection versus thickness, 1969.

Gravel equivalencies are given in Table 2 for 1966, 1967, 1968, and 1969. For example, at 0.050 in. deflection, an 18-in. thick crushed-gravel base section ($3\frac{1}{2}$ in. of asphalt surfacing, $8\frac{1}{2}$ in. of crushed-gravel base, 6 in. of sand subbase) is equivalent to a $14\frac{1}{4}$-in. asphalt-concrete base section ($3\frac{1}{2}$ in. of asphalt surfacing, $4\frac{3}{4}$ in. of asphalt-concrete base, 6 in. of sand subbase). From this it is taken that $8\frac{1}{2}$ in. of crushed gravel is equivalent to $4\frac{3}{4}$ in. of asphalt concrete, or 1 in. of asphalt concrete is equivalent to 1.79 in. of crushed gravel. These equivalencies can then be used to convert each test section into an equivalent thickness of crushed gravel ($t'$), and if the peak rebounds are then plotted against $t'$ the resulting type of relationship is shown in Figure 5. Table 3 gives the regression equations and correlation coefficients for these relationships for the years 1966, 1967, 1968, and 1969.

It will be noted that full-depth asphalt construction has a rebound/thickness relationship that differs quite significantly from that of other types of construction, although there is a tendency for the two groups of data to come closer to each other as the years progress. It will also be noted that all of the regression lines are of the form

$$\bar{\delta}\,(t' + a) = K \qquad (1)$$

where $\bar{\delta}$ = peak mean deflection,
$t'$ = equivalent thickness of inches of gravel, and
a and K = constants that change from year to year and are different for full-depth asphalt.

In an analysis of the Benkelman beam procedure, Meyerhof (8) calculated that

$$\bar{\delta}t = \frac{0.52W}{E_s \sqrt[3]{n \cdot t}} \qquad (2)$$

TABLE 3

THICKNESS-DEFLECTION RELATIONSHIPS

| Year | Equation $\bar{\delta}(t' + a) = K$ | Correlation Coefficient r |
|---|---|---|
| | Full-Depth Asphalt Concrete | |
| 1966 | $\bar{\delta}(t' + 4.1) = 0.552$ | 0.971 |
| 1967 | $\bar{\delta}(t' - 2.8) = 0.4085$ | 0.9932 |
| 1968 | $\bar{\delta}(t' - 2.92) = 0.3427$ | 0.9807 |
| 1969 | $\bar{\delta}(t' - 6.3) = 0.4310$ | 0.989 |
| | Other Construction | |
| 1966 | $\bar{\delta}(t' - 7.6) = 0.552$ | 0.983 |
| 1967 | $\bar{\delta}(t' - 2.9) = 0.6648$ | 0.9056 |
| 1968 | $\bar{\delta}(t' - 5.63) = 0.4458$ | 0.9240 |
| 1969 | $\bar{\delta}(t' - 9.3) = 0.5128$ | 0.952 |

where

$$n = \frac{E_p}{E_s} = \text{modular ratio of elasticity of pavement to subgrade}$$

Assuming that $E_S$ and n are constants, Meyerhof proposed that

$$\overline{\delta}\, t = C \qquad (3)$$

It was shown by Heukelom and Klomp (9) that this modulus is not constant throughout the granular layer and that the effective modular ratio increases as the thickness of granular layer increases. Seed et al. (10) suggest that this is due to an "aggregate interlocking factor", which varies with the overburden pressure. Because n can no longer be considered a constant but can be considered a function of t, then the form of the regression equation $\overline{\delta}\ (t' + a) = K$ appears consistent with Meyerhof's analysis.

## PAVEMENT PERFORMANCE

### Rutting

The average rut depths in all of the pavement sections continued to increase throughout the period of observation and by the spring of 1969 had in two instances exceeded ½ in. The average rut depths of all of the sections reached at April 1969 is shown in Figure 6.

During the earlier stages of the experiment, all of the test sections developed rutting of at least 0.1 in., and this was considered to be occurring within the asphalt surfacing. Most recent observations show the amount of rutting to be less severe where the base thickness is greater, and Figure 6 shows that the severity of rutting decreases as the thickness of base material increases. It was also observed that (for all base types) the larger the pavement deflection, the greater the severity of rutting. For the unbound granular base materials, where peak deflections are greater than 0.050 in. and rutting has progressed beyond 0.25 in., cracking failure occurs and the severity of cracking increases as the peak deflection and rutting increases. The provision of 5½ in. of surfacing over unbound granular bases, instead of 3½ in., reduced rutting where the total thickness of the section was small but has little effect on the thicker sections.

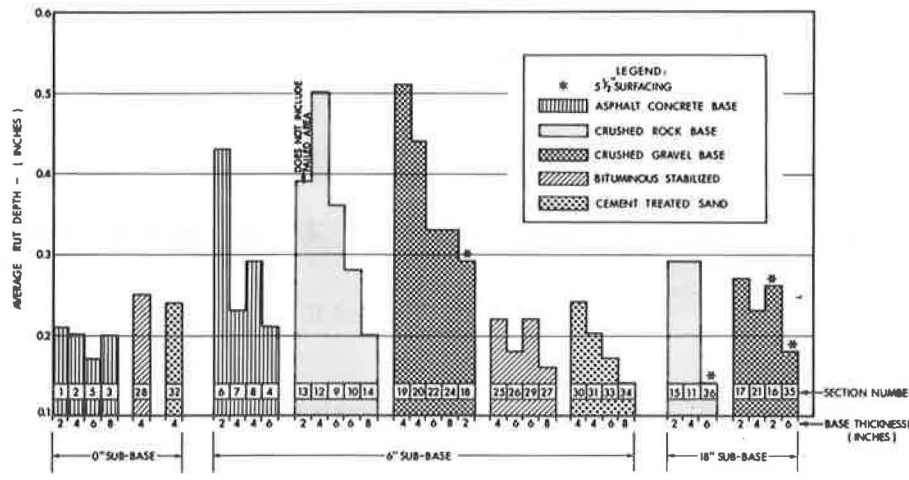


Figure 6. Rut depths, April 1969.

The greater amount of rutting is exhibited in those sections where the base material is unbound granular material, crushed rock, and crushed gravel. The rutting is least on the cement-treated base, and is greater on the bituminous-stabilized sand and the asphalt concrete. The unbound granular bases exhibit the most rutting. Significantly, however, where the asphalt-concrete base was laid directly on the subgrade without a subbase, the amount of rutting was consistently smaller than where a subbase was provided.

If a laterally confined material is subjected to vertical pressure, it compresses vertically at low levels of strain. As the strain increases, the material is compressed vertically and expanded laterally. When released from the load, the material tends to return to its original dimensions, but some unrecoverable strain may remain. The amount of this residual permanent strain depends on the characteristics and physical condition of the material. Under repeated traffic loading, the vertical and lateral residual strains in the pavement layers and in the subgrade accumulate to form a rut. The rut depth is dependent on the strain imposed, material characteristics, seasonal effects, and the number of load repetitions.

The rut depth measurements in this experimental project tend to follow the general behavior pattern described. Where the base thickness is small, larger stress levels are applied to the subbase and larger lateral residual strains result from a given load. Also, because the elastic modulus of the subbase material is usually quite low, at higher stress levels the residual strains are likely to be relatively high. Thus, in sections with small base thicknesses, much of the deformation probably occurs in the subbase. With thicker bases, the high stress levels occur within the base, and much of the rutting is in the base itself. This is evident when performances of the different bases are considered. The unbound granular crushed-rock and crushed-gravel materials have rutted considerably, whereas the bound materials with thicknesses of greater than 4 in. have rutted much less. The difference between bound and unbound material is explained by the difference in elastic moduli. Where the test sections have been stiffened by an increase in subbase thickness from 6 to 18 in., the strain levels in the bases have been considerably reduced and residual strains in the base are less.

The rutting in the full-depth asphalt-concrete sections does not appear to conform to this concept of rutting behavior. Because the elastic modulus of clay materials is quite low, high values of rutting might be expected, but this is not the case. It is possible that the rate of loading may be more important on clay materials. Some laboratory tests of the cyclic creep of the granular materials used in this experiment have been reported (12), and tentative suggestions are made for a testing method that will make it possible to predict rutting.

## Cracking and Patching

The extent of cracking and the amount of maintenance patching undertaken up to June 1969 is shown in Figure 7. None of the full-depth asphalt sections have exhibited any cracking. The deep-strength asphalt sections have little or no cracking, and the thicker bituminous-stabilized bases are relatively free from cracking.

All sections having an 18-in. subbase are either free from cracking or have negligible amounts of cracking. The thin crushed-stone bases have deteriorated considerably, but the 6-in. and thicker base courses have relatively light cracking. The thin crushed-gravel base courses have small areas of patching or areas that will need patching shortly. Cracking still appears in the thin crushed-gravel base even through $5\frac{1}{2}$ in. of surfacing (section 18).

## Frost Penetration and Vertical Movement of the Surface

Frost-penetration measurements were taken during the winters of 1967 and 1968 at sections with 6-in. bases and 6-in. subbases. Figure 8 shows that the greatest frost penetration occurs with the crushed-stone base material and the least with asphalt-concrete base.

Measurement of the vertical movements of the pavement surface caused by frost-heaving was accomplished by means of levels taken at periodic intervals on reference

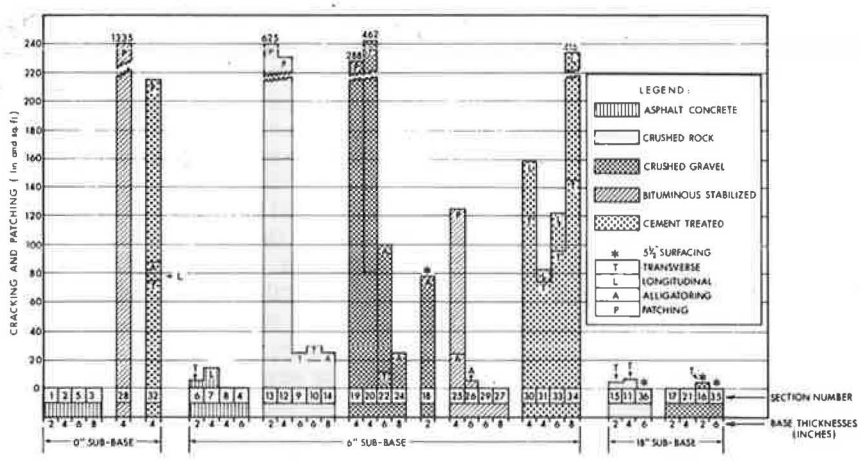


Figure 7. Cracking and patching to June 1969.

pins fixed in the pavement surface. The average value of these levels was plotted for each section, and the difference between the lowest and the highest value was taken as the amount of heave occurring during the period of observation. Frost-heave movements measured in this way are shown in Figure 9.

It will be noted that sections without granular subbase heaved less than sections with a granular subbase, showing that heave has taken place in the subbase material as well as in the clay subgrade. It will also be noted that the base materials themselves contribute to the magnitude of the heaving; e.g., in the asphalt-concrete base it was much less than in the cement-treated base although frost penetration was not much different. Moisture within the granular material could not act as reservoirs for the clay subgrade because prior freezing locks in this moisture, and the thermal gradients tend to move moisture toward the colder areas instead of the opposite. The increase in thickness of subbase from 6 to 18 in. results in slight increases in heaving, which is further evidence that heaving has taken place in the subbase. Thicker surfacings appear to cause slight reductions in the amount of heave of granular bases.

Volume increases resulting from frost heave in a material cause the material to become less dense and consequently weaker and less able to resist traffic stresses. Bound granular materials that increase in volume because of frost heave suffer strength losses. This appears to be the case particularly with the cement-treated sand bases, where pavement deflections have increased consistently over the observation period.

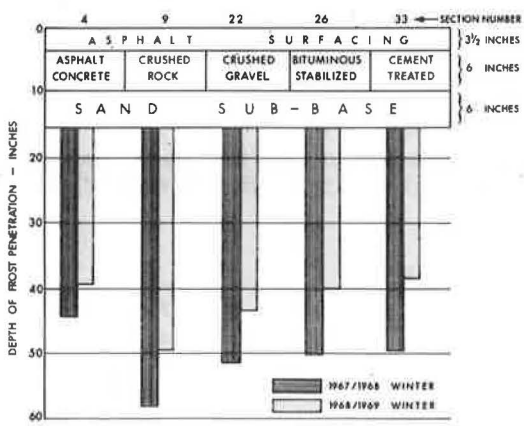


Figure 8. Frost penetration.

## Present Performance Rating

Because conditions are the same for all test sections, a comparison of their PPR values provides an evaluation of their relative performance. The PPR values are derived from surface roughness measurements obtained from profilometer readings. Figure 10 shows the PPR values of the sections determined in July 1969.

Before the test sections were exposed to traffic, their PPR values were generally

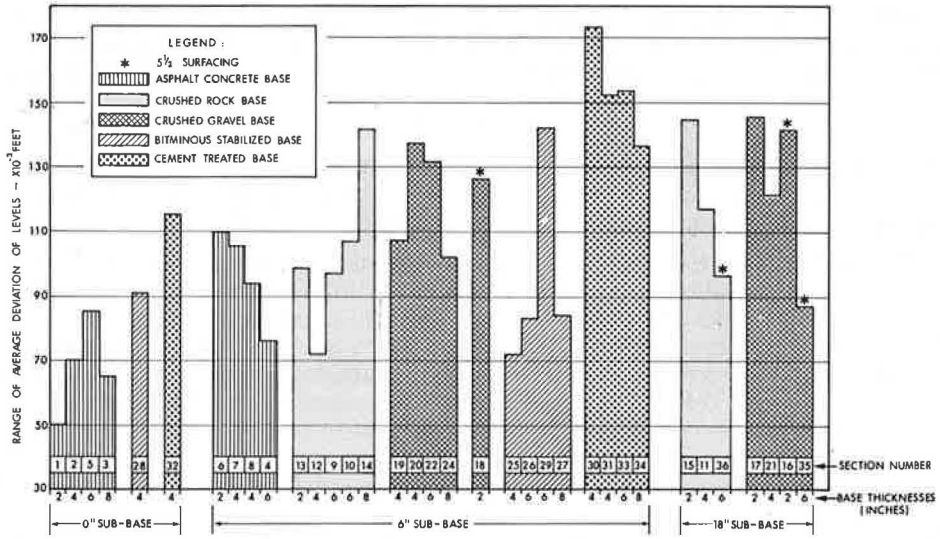


Figure 9. Frost-heave movements.

higher than 8, although two sections exceeded this and eight sections were somewhat lower. By July 1969 only one test section (full-depth asphalt) had retained a PPR value of 7, and all full-depth asphalt sections had PPR values greater than 6. For the test sections with a 6-in. subbase, most of the deep-strength asphalt and the cement-treated base sections, together with one of the bituminous-stabilized base sections, had retained PPR values greater than 6. All of these test sections with the unbound granular base, crushed-stone and crushed-gravel bases, had PPR values less than 6. Thus, the bound bases have performed better than the unbound granular bases.

The crushed-stone and crushed-gravel base sections with 18 in. subbase have higher PPR values than sections with only 6 in. of subbase. The addition of 2 in. of asphalt surfacing in four of these sections has not improved the PPR.

As a result of pavement evaluation studies published by CGRA, it is suggested that when the PPR value is less than 4.5 remedial measures become necessary (2). Two of

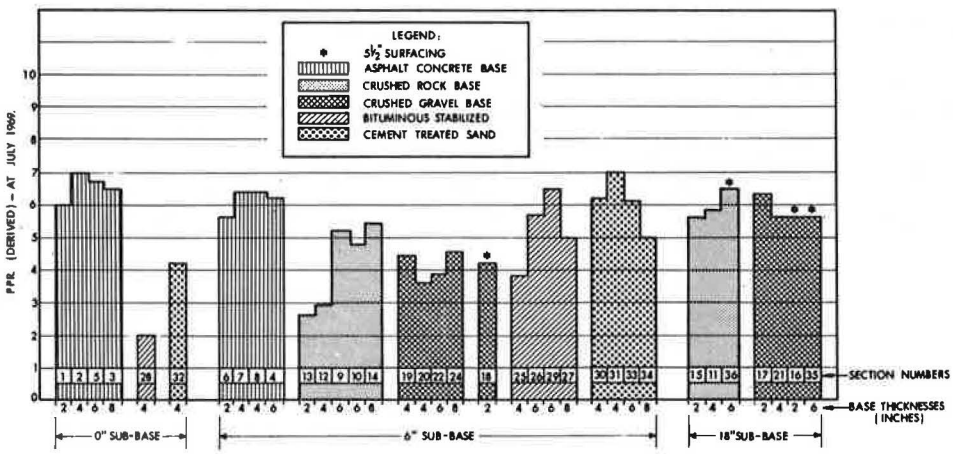


Figure 10. Present performance ratings, July 1969.

the bituminous-stabilized base sections, one cement-treated base section, two crushed-stone base sections, and four crushed-gravel base sections have PPR values less than 4.5 and indeed all of these sections have been patched or have areas of alligatoring.

## CONCLUSIONS

This report summarized the results of 4 years' observation of the experiment. Data collection is continuing and performance results are continually reviewed. Some general conclusions based on these results appear warranted:

1. Seasonal variation in pavement deflection is more pronounced in bases with unbound granular materials than with bases that have either bituminous or portland cement binders. Both the crushed-stone and crushed-gravel bases have rutted more, cracked more, and become rougher than the other types of base. In addition, frost penetration tends to be greatest in these unbound materials, and the associated frost heave also tends to be relatively large. All of these general observations may be combined to conclude that bases that are less susceptible to seasonal variations in strength are more likely to be the better performers.
2. The cement-treated sand bases have generally performed very well under traffic, with rut depths in these sections being small. Deflection tests reveal a progressive loss of strength, however, that may be due to a deficiency of cement. Some shrinkage cracks have opened up to such an extent that the riding quality is affected. At three locations secondary cracking has developed and some pumping has been observed.
3. An increase in subbase thickness from 6 to 18 in. has improved the performance of the unbound granular base materials. A similar increase in performance appears to be obtainable by utilizing bound granular base materials instead of increased thickness.
4. The asphalt concrete bases have performed well. Where the construction is without subbase, the overall performance has been superior. These full-depth asphalt sections deflect less under load than similar thicknesses of asphalt in deep-strength construction, even though these sections have an additional 6 in. of sand subbase. The amount of rutting in the full-depth sections has been relatively small. There have been no signs of cracking and frost penetration, and frost heave is the least evident for all of the base types. The riding quality of these full-depth sections has remained consistently higher than for any other type of construction.
5. The immediate structural response to loading has been used as a basis for determining layer equivalencies for the various base materials. It was shown that these equivalencies changed with time, and are therefore dependent on both traffic and environmental conditions. Equivalencies developed from peak deflections are not the same as those developed from present serviceability indexes (AASHO Road Test), as is readily illustrated by the relative performance of the unbound granular base materials. The deflection-based equivalence of the crushed-stone base is less than for crushed gravel, yet the thicker crushed-stone bases have retained better riding qualities than the crushed-gravel bases. Nevertheless, the equivalencies developed from pavement deflections appear to be valuable guides to future performance.
6. It has been demonstrated that pavement deflection is related to pavement thickness by an equation of the form $\overline{\delta}\ (t' + a) = K$ where $t'$ is in equivalent inches of crushed gravel and the constants a and K change with time. Significantly, the full-depth asphalt sections do not fall on the same curves as for all of the other base types, but are consistently different, with lower thickness requirements for any given deflection.

## REFERENCES

1. Schonfeld, R. Construction of a Full-Scale Road Experiment as Part of a Unit-Price Contract. Proc. Canadian Good Roads Assn., 1966, pp. 406-424.
2. Canadian Good Roads Association. Pavement Evaluation Studies in Canada. Proc. Internat. Conf. on Structural Design of Asphalt Pavements, Ann Arbor, Mich., 1962, pp. 137-218.
3. Scott, W. J. O. Roads and Their Riding Qualities. Jour. Institution of Civil Engineers, Road Engineering Design, Road Paper No. 25, 1948.

4. Sebastyan, G. Y., and Demellweek, J. Airport Pavement Roughness and Aircraft Response Affecting Pavement Design and Construction. Joint Meeting, American Institute of Aeronautics and Astronautics and Canadian Aeronautics and Space Institute, 1965.
5. Chong, G. A Road Rideability Rating Experiment. DHO unpublished report.
6. The AASHO Road Test. HRB Spec. Rept. 61E, 1962.
7. Shook, J. R., and Finn, F. N. Thickness Design Relationships for Asphalt Pavements. Proc. Internat. Conf. on Structural Design of Asphalt Pavements, Ann Arbor, Mich., 1962, pp. 52-83.
8. Meyerhof, G. G. Preliminary Analysis of Benkelman Beam Deflections and Flexible Pavement Design. Proc. Canadian Good Roads Assn., 1962, pp. 390-401.
9. Heukelom, W., and Klomp, A. J. G. Dynamic Testing as a Means of Controlling Pavements During and After Construction. Proc. Internat. Conf. on Structural Design of Asphalt Pavements, Ann Arbor, Mich., 1962, pp. 667-679.
10. Seed, H. B., Mitry, F. G., Monismith, C. L., and Chan, C. K. Prediction of Flexible Pavement Deflections From Laboratory Repeated-Load Tests. NCHRP Rept. 35, 1967.
11. Chong, G., and Phang, W. The PCA Road Meter, Measuring Road Roughness at 50 Miles Per Hour. DHO Rept. IR26, unpublished report, 1968.
12. Holubec, I. Cyclic Creep of Granular Materials. DHO Rept. RR147, 1969.

## *Discussion*

F. P. NICHOLS, JR., National Crushed Stone Association—The Department of Highways, Ontario, is to be complimented for their construction of a well-planned, full-scale field experiment. Its performance over the years will provide some measure of comparison between certain base types and thicknesses. A word of caution is in order, however, against drawing premature and too broad conclusions on the basis of the materials actually used in the test sections and particularly of the inadequate compaction in the crushed dolomite sections.

The granular subbase, referred to as sand but including "about 15 percent passing the No. 200 screen", obviously did not perform the usual purpose for which a subbase is employed. (Actually, an unpublished construction report shows it to have contained about 13 percent material finer than a No. 270 sieve.) This silty sand, especially where it was only 6 in. thick over the "light clay" subgrade, apparently was detrimental to performance, because it was very prone to absorbing moisture from beneath and developing frost lenses and heaving in this climate. This phenomenon has been extensively investigated at the U. S. Army's Terrestrial Sciences Center (formerly known as the Cold Regions Research Lab) at Hanover, New Hampshire. Using methods developed there, the National Crushed Stone Association has conducted research confirming that aggregates containing this much silty fines are likely to heave excessively if subject to freezing where a supply of moisture is available. Even the average of 9 percent minus No. 200 (about 8 percent minus No. 270) in the crushed dolomite material is often conducive to some frost-heaving.

But there is another fault that must be pointed out in connection with the construction of the crushed-rock sections. According to private correspondence from Schonfeld, who was the Special Projects Engineer in charge of construction of this project, the mean compaction value shown in Table A-3 for this material was only 97.7 percent of standard Proctor, AASHO T 99-57 Method D. This is even lower than the percent compaction achieved all too easily on a similar material at the AASHO Road Test. A recently distributed National Crushed Stone Association report (13) includes data on the effectiveness of a modest increase in compaction on the CBR value and resistance to deformation under triaxial loading. Briefly, one set of specimens compacted to 100 percent standard AASHO T 99 density deformed twice as much under given triaxial load

conditions and developed CBR values less than half as high as specimens made from the same graded crushed-stone materials compacted to 100 percent modified AASHO T 180 density.

The same NCSA report includes recommended specifications for crushed aggregate bases that should give far superior performance to that experienced either in the AASHO Road Test or at the Brampton Test. Modern processing and laydown procedures are now available to permit construction of reliable bases of this type at rates of 600 tons per hour and higher with little or no difficulty. Engineers are urged not to overlook the value and economy of crushed aggregate bases in combination with moderate thicknesses of bituminous concrete base. In support of this recommendation, the following conclusion from a 1969 NCSA convention presentation by Linell (14) of the Corps of Engineers is offered:

> If any funds should be available to permit improvement of pavement quality, a better alternative than thickening the surface course would be to increase the combined thickness of pavement and base with additional free-draining non-frost-susceptible base . . . . the concept of using deeper than normal sections of surfacing type materials does not lead us in the right direction.

## References

13. Nichols, F. P., Jr. Appropriate Specifications for Crushed Aggregate Bases. Presented at 28th Annual AASHO Convention, 1969; distributed by National Crushed Stone Association, Washington, D. C.
14. Linell, K. A. Pavement Design for Areas of Deep Frost Penetration. NCSA Convention paper, 1969.

W. A. PHANG, Closure—The points made by Nichols are quite pertinent as qualifying considerations. As in other test roads, the results of the Brampton Test Road experiment are related directly to the particular materials used and the traffic and environmental conditions to which the test sections were exposed.

The "modified sand cushion" material used in the subbases was the same material that formed the basic ingredient of the emulsion-stabilized and cement-treated bases. Because a high fines content appeared desirable for these two base materials, the fines content of the subbase was allowed to exceed the normal specified limits. However, this subbase material is common throughout the experiment, so that comparative behavior of various base materials can still be considered.

Specification requirements of 100 percent of maximum Proctor density for the compaction of a granular crushed-stone bases were not generally attained during the construction of the test sections, although in normal construction there is little difficulty in reaching this degree of compaction. Further compaction of the granular bases may have taken place when traffic was permitted onto the test sections. The effect of this lower initial compaction on the performance of the sections is not readily discernible at this time.

# *Appendix A*

## CHARACTERISTICS OF MATERIALS USED IN THE EXPERIMENT

### TABLE A-1, SUBGRADE, MEDIUM TO LIGHT CLAY

| | MEAN $\bar{x}$ | STANDARD DEVIATION $\sigma$ | NUMBER OF TESTS N |
|---|---|---|---|
| C.B.R. Percent | 2.5 | | |
| Liquid Limit Percent | 29 | 2.2 | 35 |
| Plastic Limit Percent | 15.5 | 1.9 | 35 |
| Plasticity Index Percent | 13.5 | | |
| Field Dry Density (lbs./ft.$^3$) | 124.9 | 5.1 | 756 |
| Proctor Maximum Dry Density (lbs./ft.$^3$) | 123.9 | 1.7 | 180 |
| Compaction Moisture Percent | 9.6 | 0.8 | 756 |
| Optimum Moisture Percent | | | |
| Compaction Percent | 100.9 | 4.2 | 180 |

### TABLE A-2, SUB-BASE, SAND CUSHION

| GRADATION | | |
|---|---|---|
| PASSED | RETAINED | PERCENT |
| 1/2 | 3/8 | 8 |
| 3/8 | 4 | 17.5 |
| 4 | 8 | 25 |
| 8 | 16 | 34 |
| 16 | 30 | 46 |
| 30 | 50 | 62 |
| 50 | 100 | 76 |
| 100 | 200 | 85 |

| | MEAN $\bar{x}$ | STANDARD DEVIATION $\sigma$ | NUMBER OF TESTS N |
|---|---|---|---|
| Field Dry Density (lbs./ft.$^3$) | 137.7 | 2.7 | 609 |
| Proctor Maximum Dry Density (lbs./ft.$^3$) | 133.9 | 1.6 | 36 |
| Compaction Moisture Percent | 4.3 | 1.8 | 609 |
| Compaction Percent | 102.7 | | |

### TABLE A-3, CRUSHED-ROCK BASE AND CRUSHED-GRAVEL BASE

| GRADATION | | | |
|---|---|---|---|
| PASSED | RETAINED | PERCENT CRUSHED-ROCK | PERCENT CRUSHED-GRAVEL |
| | 3/4 | 4 | 1 |
| 3/4 | 1/2 | 18 | 15 |
| 1/2 | 3/8 | 29 | 27 |
| 3/8 | 4 | 49.5 | 46.0 |
| 4 | 8 | 62 | 56 |
| 8 | 16 | 74 | 66 |
| 16 | 30 | 81 | 76 |
| 30 | 50 | 86 | 85 |
| 50 | 100 | 89 | 91 |
| 100 | 200 | 91 | 93 |

| | CRUSHED-ROCK | | | CRUSHED-GRAVEL | | |
|---|---|---|---|---|---|---|
| | MEAN $\bar{x}$ | STANDARD DEVIATION $\sigma$ | NUMBER OF TESTS N | MEAN $\bar{x}$ | STANDARD DEVIATION $\sigma$ | NUMBER OF TESTS N |
| Field Dry Density (lbs./ft.$^3$) | 137.9 | 3.9 | 30 | 138.4 | 3.1 | 86 |
| Proctor Maximum Dry Density (lbs./ft.$^3$) | 141.2 | 0.5 | 30 | 138.6 | 1.1 | 30 |
| Field Compaction Moisture Percent | 4.4 | 1.4 | 30 | 3.8 | 0.9 | 86 |
| Compaction Percent | 97.7 | | | 99.9 | | |

## TABLE A-4, ASPHALTIC CONCRETE BASE

| | AVERAGE $\bar{x}$ | STANDARD DEVIATION $\sigma$ | RANGE | NUMBER OF RESULTS N |
|---|---|---|---|---|
| GRADATION PERCENT RETAINED | | | | |
| 3/4 in. | 2.3 | 1.14 | 0 - 4 | 34 |
| 5/8 in. | 8.6 | 2.50 | 5 - 12 | 34 |
| ½ in. | 16.6 | 2.86 | 10 - 24 | 34 |
| 3/8 in. | 26.9 | 3.38 | 21 - 34 | 34 |
| no. 3 | 36.8 | 3.20 | 30 - 42 | 34 |
| no. 4 | 42.4 | 2.97 | 37.3 - 47.9 | 34 |
| no. 8 | 52.1 | 2.16 | 48 - 56 | 34 |
| no. 16 | 61.5 | 1.79 | 58 - 66 | 34 |
| no. 30 | 75.9 | 1.33 | 73 - 78 | 34 |
| no. 50 | 91.4 | 0.84 | 89 - 93 | 34 |
| no. 100 | 96.6 | 0.70 | 95 - 98 | 34 |
| no. 200 | 97.7 | 0.41 | 96.6 - 98.2 | 34 |
| ASPHALT CONTENT PERCENT | 5.8 | 0.29 | 5.3 - 6.5 | 34 |
| PAVEMENT DENSITY (lbs./ft$^3$) | 143.3 | 2.73 | 139.4 - 145.1 | 15 |
| COMPACTION PERCENT | 96.3 | 1.26 | 94.4 - 98.8 | 15 |
| CALCULATED PAVEMENT VOIDS (PERCENT) | 7.2 | 1.25 | 4.0 - 9.2 | 15 |
| COMPACTION TEMP., °F. | 262 | 21.61 | 220 - 320 | 50 |
| RECOMPACTION: STABILITY (lbs.) | 1,958 | 248.68 | 1,488 - 2,639 | 32 |
| FLOW (0.01 IN.) | 8.9 | 0.90 | 7.4 - 11.0 | 32 |
| VOIDS (PERCENT) | 3.6 | 0.67 | 2.4 - 4.8 | 32 |
| V.M.A. (PERCENT) | 17.5 | 0.73 | 15.6 - 19.1 | 32 |

## TABLE A-5, BITUMINOUS-STABILIZED BASE

| | AVERAGE $\bar{x}$ | STANDARD DEVIATION $\sigma$ | RANGE | NUMBER OF RESULTS N |
|---|---|---|---|---|
| GRADATION PERCENT RETAINED | | | | |
| 3/4 in. | | | | |
| 5/8 in. | | | | |
| ½ in. | 2.9 | 1.70 | 0 - 8 | 80 |
| 3/8 in. | 7.2 | 2.62 | 2 - 14 | 80 |
| no. 3 | 12.8 | 3.23 | 8 - 27 | 80 |
| no. 4 | 17.7 | 3.32 | 12.0 - 32.4 | 80 |
| no. 8 | 27.6 | 3.26 | 21 - 35 | 80 |
| no. 16 | 38.9 | 3.18 | 32 - 51 | 80 |
| no. 30 | 55.4 | 2.52 | 48 - 61 | 80 |
| no. 50 | 77.1 | 1.88 | 73 - 83 | 80 |
| no. 100 | 90.5 | 1.21 | 87 - 94 | 80 |
| no. 200 | 94.8 | 0.71 | 92.9 - 96.5 | 80 |
| SS-1h EMULSION PERCENT CONTENT | 3.2 | 1.18 | 1.3 - 6.4 | 82 |
| NATURAL MOISTURE PERCENT | 4.5 | 0.55 | 2.4 - 5.5 | 82 |
| PAVEMENT DENSITY (lbs./ft.$^3$) | 134.6 | – | 126.4 - 139.2 | 4 |
| RECOMPACTION: * STABILITY (lbs.) | 1,874 | 433 | 1,262 - 2,817 | 14 |
| * IMMERSED STABILITY | 800 | 44.47 | 616 - 1,125 | 14 |
| VOIDS (PERCENT) | 17.1 | 1.42 | 13.9 - 19.4 | |

* *Stability at 100° F.*

## TABLE A-6, CEMENT-TREATED BASE

| SECTION | CEMENT CONTENT (PERCENT) | 7-DAY COMPRESSIVE STRENGTH (p.s.i.) |
|---|---|---|
| 30 | 4.2 | 306 |
| 31 | - | - |
| 32 | 4.3 | 516 |
| 33 | 3.7 | 356 |
| 34 | 3.9 | 362 |
| MEAN OF ALL SECTIONS | 4.02 | 391.0 |
| RANGE OF ALL SECTIONS | 3.1 - 4.7 | 198 - 616 |
| STD. DEV. OF ALL SECTIONS | 0.42 | 111 |
| NO. OF SAMPLES OF ALL SECTIONS | 30 | 25 |

SPECIFIED CEMENT CONTENT - 4 PERCENT (by wt.)

## TABLE A-7, ASPHALT CONCRETE SURFACING, 2 INCH BINDER COURSE

| | AVERAGE $\bar{x}$ | STANDARD DEVIATION $\sigma$ | RANGE | NUMBER OF RESULTS N |
|---|---|---|---|---|
| GRADATION PERCENT RETAINED | | | | |
| 3/4 in. | | | | |
| 5/8 in. | 7.0 | 2.19 | 3 - 12 | 65 |
| ½ in. | 14.2 | 3.0 | 7 - 21 | 65 |
| 3/8 in. | 23.6 | 3.11 | 17 - 35 | 65 |
| no. 3 | 33.9 | 3.07 | 29 - 42 | 65 |
| no. 4 | 41.5 | 2.91 | 36.3 - 50.3 | 65 |
| no. 8 | 52.5 | 2.74 | 47 - 60 | 65 |
| no. 16 | 62.3 | 2.56 | 56 - 71 | 65 |
| no. 30 | 73.2 | 1.92 | 68 - 77 | 65 |
| no. 50 | 85.5 | 1.38 | 82 - 88 | 65 |
| no. 100 | 93.1 | 1.15 | 89 - 95 | 65 |
| no. 200 | 95.2 | 0.92 | 91.5 - 96.2 | 65 |
| ASPHALT CONTENT PERCENT | 6.2 | 0.32 | 5.6 - 6.9 | 65 |
| PAVEMENT DENSITY (lbs./ft.$^3$) | 146.7 | 2.22 | 141.4 - 150.9 | 33 |
| COMPACTION PERCENT | 96.8 | 1.50 | 93.8 - 99.7 | 33 |
| CALCULATED PAVEMENT VOIDS (PERCENT) | 4.9 | 1.45 | 2.1 - 8.3 | 33 |
| COMPACTION TEMP. °F. | 260 | 21.7 | 200 - 310 | 48 |
| RECOMPACTION: STABILITY (lbs.) | 2,444 | 302.4 | 2,067 - 3,067 | 65 |
| FLOW (0.01 in.) | 14.5 | 2.40 | 11.3 - 22.9 | 65 |
| VOIDS (PERCENT) | 1.7 | 0.68 | 0.5 - 3.1 | 65 |
| V.M.A. (PERCENT) | 16.8 | 0.79 | 15.0 - 19.2 | 65 |

# *Appendix B*

## BENKELMAN BEAM RECORDS

Table B-1, Mean Benkelman Beam Deflections ($\bar{\delta}$)
(3½ in. Asphalt Concrete Surfacing, No Sub-Base)

| SECTION NUMBER | 1 | 2 | 5 | 3 | 28 | 32 |
|---|---|---|---|---|---|---|
| | ASPHALT CONCRETE BASE | | | | BIT. STAB. BASE | CEM. TREAT. BASE |
| | 2 in. | 4 in. | 6 in. | 8 in. | 4 in. | 4 in. |
| **1965** | | | | | | |
| SEPT. 23 | 0.016 | 0.014 | 0.013 | 0.010 | 0.072 | 0.015 |
| OCT. 28 | 0.017 | 0.006 | 0.006 | 0.006 | 0.020 | 0.014 |
| **1966** | | | | | | |
| MAR. 14 | 0.027 | 0.012 | 0.013 | 0.006 | 0.034 | 0.016 |
| APR. 13 | 0.034 | 0.018 | 0.015 | 0.010 | 0.072 | 0.035 |
| APR. 22 | 0.033 | 0.019 | 0.013 | 0.010 | 0.067 | 0.037 |
| MAY 2 | 0.040 | 0.026 | 0.020 | 0.013 | 0.053 | 0.036 |
| MAY 13 | 0.028 | 0.016 | 0.014 | 0.009 | 0.076 | 0.044 |
| MAY 20 | 0.039 | 0.022 | 0.017 | 0.014 | 0.080 | 0.044 |
| MAY 27 | 0.042 | 0.025 | 0.026 | 0.019 | 0.093 | 0.039 |
| JUNE 3 | 0.035 | 0.021 | 0.019 | 0.014 | 0.084 | 0.045 |
| JUNE 10 | 0.034 | 0.022 | 0.020 | 0.013 | 0.096 | 0.054 |
| JUNE 17 | 0.033 | 0.026 | 0.021 | 0.023 | 0.095 | 0.051 |
| JUNE 28 | 0.043 | 0.029 | 0.024 | 0.019 | 0.113 | 0.055 |
| JULY 8 | 0.038 | 0.026 | 0.023 | 0.017 | 0.091 | 0.053 |
| JULY 18 | 0.036 | 0.024 | 0.022 | 0.017 | 0.089 | 0.056 |
| AUG. 16 | 0.025 | 0.019 | 0.017 | 0.013 | 0.071 | 0.043 |
| SEPT. 30 | 0.018 | 0.014 | 0.011 | 0.009 | 0.031 | 0.027 |
| OCT. 27 | 0.016 | 0.011 | 0.009 | 0.007 | 0.030 | 0.031 |
| NOV. 21 | 0.014 | 0.009 | 0.007 | 0.006 | 0.034 | 0.028 |
| **1967** | | | | | | |
| APR. 3 | 0.044 | 0.023 | 0.018 | 0.012 | - | 0.040 |
| APR. 18 | 0.027 | 0.017 | 0.015 | 0.011 | - | 0.046 |
| MAY 1 | 0.054 | 0.037 | 0.021 | 0.017 | - | 0.041 |
| MAY 10 | 0.040 | 0.022 | 0.017 | 0.013 | - | - |
| MAY 19 | 0.037 | 0.023 | 0.016 | 0.013 | - | 0.057 |
| MAY 31 | 0.051 | 0.037 | 0.023 | 0.015 | - | 0.064 |
| JUNE 7 | 0.053 | 0.033 | 0.024 | 0.018 | - | 0.056 |
| JUNE 15 | 0.057 | 0.041 | 0.031 | 0.023 | - | 0.060 |
| JULY 12 | 0.055 | 0.036 | 0.029 | 0.021 | - | 0.071 |
| AUG. 18 | 0.048 | 0.033 | 0.021 | 0.023 | 0.078 | 0.063 |
| SEPT. 11 | 0.034 | 0.025 | 0.016 | 0.014 | 0.082 | 0.059 |
| OCT. 20 | 0.021 | 0.015 | 0.011 | 0.008 | 0.040 | 0.037 |
| NOV. 24 | 0.011 | 0.008 | 0.006 | 0.005 | 0.023 | 0.027 |
| **1968** | | | | | | |
| MAR. 25 | 0.022 | 0.016 | 0.008 | 0.009 | 0.048 | 0.031 |
| APR. 3 | 0.036 | 0.023 | 0.017 | 0.011 | 0.065 | 0.048 |
| APR. 9 | 0.058 | 0.037 | 0.026 | 0.018 | 0.061 | 0.047 |
| APR. 18 | 0.055 | 0.035 | 0.025 | 0.020 | 0.089 | 0.061 |
| APR. 25 | 0.033 | 0.021 | 0.017 | 0.015 | 0.081 | 0.057 |
| MAY 1 | 0.043 | 0.030 | 0.020 | 0.016 | 0.087 | 0.049 |
| JUNE 12 | 0.089 | 0.065 | 0.047 | 0.032 | 0.160 | 0.096 |
| JULY 26 | 0.072 | 0.055 | 0.039 | 0.030 | 0.147 | 0.092 |
| AUG. 14 | 0.057 | 0.046 | 0.030 | 0.028 | 0.108 | 0.079 |
| SEPT. 12 | 0.047 | 0.029 | 0.023 | 0.018 | 0.096 | 0.067 |
| NOV. 5 | 0.024 | 0.014 | 0.011 | 0.009 | 0.050 | 0.045 |
| **1969** | | | | | | |
| MAR. 19 | 0.063 | 0.044 | 0.025 | 0.020 | - | - |
| APR. 10 | 0.072 | 0.048 | 0.031 | 0.021 | 0.090 | 0.068 |
| APR. 22 | 0.054 | 0.029 | 0.023 | 0.018 | - | 0.067 |
| APR. 29 | 0.045 | 0.031 | 0.022 | 0.018 | - | 0.079 |
| MAY 6 | 0.052 | 0.038 | 0.034 | 0.018 | 0.104 | 0.069 |
| MAY 16 | 0.033 | 0.020 | 0.020 | 0.014 | 0.107 | 0.079 |
| MAY 22 | 0.056 | 0.047 | 0.028 | 0.023 | 0.112 | 0.099 |
| JUNE 10 | 0.052 | 0.031 | 0.033 | 0.018 | 0.177 | 0.094 |

Table B-1, Mean Benkelman Beam Deflections ($\bar{\delta}$) (Continued)
(3½ in. Asphalt Concrete Surfacing, 6 in. Sand Sub-Base)

| SECTION NUMBER | 6 | 7 | 8 | 4 | 13 | 12 | 9 | 10 | 14 |
|---|---|---|---|---|---|---|---|---|---|
| | ASPHALT CONCRETE BASE | | | | | CRUSHED-ROCK BASE | | | |
| | 2 in. | 4 in. | 4 in. | 6 in. | 2 in. | 4 in. | 6 in. | 6 in. | 8 in. |
| **1965** | | | | | | | | | |
| SEPT. 23 | 0.027 | 0.033 | 0.027 | 0.020 | 0.053 | 0.051 | 0.042 | 0.043 | 0.040 |
| OCT. 28 | 0.021 | 0.012 | 0.002 | 0.010 | 0.025 | 0.025 | 0.023 | 0.024 | 0.022 |
| **1966** | | | | | | | | | |
| MAR. 14 | 0.036 | 0.016 | 0.020 | 0.014 | 0.028 | 0.025 | 0.018 | 0.021 | 0.025 |
| APR. 13 | 0.056 | 0.031 | 0.033 | 0.020 | 0.063 | 0.059 | 0.051 | 0.050 | 0.041 |
| APR. 22 | 0.053 | 0.026 | 0.027 | 0.021 | 0.055 | 0.049 | 0.042 | 0.046 | 0.032 |
| MAY 2 | 0.067 | 0.043 | 0.037 | 0.030 | 0.070 | 0.061 | 0.047 | 0.052 | 0.040 |
| MAY 13 | 0.058 | 0.033 | 0.037 | 0.027 | 0.073 | 0.064 | 0.052 | 0.053 | 0.043 |
| MAY 20 | 0.053 | 0.040 | 0.041 | 0.034 | 0.074 | 0.066 | 0.063 | 0.057 | 0.044 |
| MAY 27 | 0.018 | 0.057 | 0.057 | 0.039 | 0.097 | 0.077 | 0.070 | 0.067 | 0.051 |
| JUNE 3 | 0.077 | 0.047 | 0.043 | 0.031 | 0.071 | 0.059 | 0.059 | 0.052 | 0.045 |
| JUNE 10 | 0.076 | 0.049 | 0.045 | 0.032 | 0.079 | 0.067 | 0.063 | 0.060 | 0.048 |
| JUNE 17 | 0.078 | 0.052 | 0.049 | 0.032 | 0.088 | 0.070 | 0.065 | 0.062 | 0.050 |
| JUNE 28 | 0.084 | 0.057 | 0.053 | 0.045 | 0.074 | 0.060 | 0.055 | 0.053 | 0.044 |
| JULY 8 | 0.073 | 0.050 | 0.046 | 0.041 | 0.062 | 0.052 | 0.048 | 0.046 | 0.038 |
| JULY 18 | 0.063 | 0.048 | 0.043 | 0.039 | 0.052 | 0.044 | 0.043 | 0.040 | 0.035 |
| AUG. 16 | 0.041 | 0.039 | 0.035 | 0.024 | 0.050 | 0.042 | 0.044 | 0.043 | 0.034 |
| SEPT. 30 | 0.023 | 0.021 | 0.021 | 0.016 | 0.036 | 0.029 | 0.033 | 0.032 | 0.027 |
| OCT. 27 | 0.022 | 0.017 | 0.018 | 0.014 | 0.031 | 0.023 | 0.029 | 0.025 | 0.026 |
| NOV. 21 | 0.020 | 0.013 | 0.014 | 0.011 | 0.030 | 0.028 | 0.029 | 0.027 | 0.024 |
| **1967** | | | | | | | | | |
| APR. 3 | 0.047 | 0.033 | 0.034 | 0.022 | 0.048 | 0.043 | 0.036 | 0.040 | 0.035 |
| APR. 18 | 0.037 | 0.025 | 0.026 | 0.017 | 0.050 | 0.047 | 0.044 | 0.043 | 0.039 |
| MAY 1 | 0.050 | 0.039 | 0.036 | 0.031 | 0.057 | 0.045 | 0.047 | 0.046 | 0.041 |
| MAY 10 | 0.046 | 0.031 | 0.032 | 0.024 | 0.046 | - | 0.044 | 0.040 | 0.035 |
| MAY 19 | 0.046 | 0.035 | 0.038 | 0.024 | 0.075 | 0.052 | 0.052 | 0.049 | 0.044 |
| MAY 31 | 0.067 | 0.050 | 0.038 | 0.032 | 0.070 | 0.058 | 0.049 | 0.050 | 0.044 |
| JUNE 7 | 0.058 | 0.050 | 0.050 | 0.033 | 0.074 | 0.056 | 0.052 | 0.052 | 0.050 |
| JUNE 15 | 0.069 | 0.048 | 0.048 | 0.036 | 0.090 | 0.059 | 0.062 | 0.058 | 0.045 |
| JULY 12 | 0.069 | 0.045 | 0.044 | 0.041 | 0.067 | 0.059 | 0.063 | 0.055 | 0.055 |
| AUG. 18 | 0.048 | 0.032 | 0.034 | 0.035 | 0.054 | 0.030 | 0.034 | 0.040 | 0.032 |
| SEPT. 11 | 0.040 | 0.026 | 0.027 | 0.023 | 0.055 | 0.044 | 0.038 | 0.037 | 0.037 |
| OCT. 20 | 0.026 | 0.020 | 0.021 | 0.019 | 0.055 | 0.042 | 0.037 | 0.036 | 0.038 |
| NOV. 24 | 0.019 | 0.013 | 0.010 | 0.010 | 0.026 | 0.025 | 0.025 | 0.025 | 0.024 |
| **1968** | | | | | | | | | |
| MAR. 25 | 0.039 | 0.021 | 0.022 | 0.015 | 0.047 | 0.043 | 0.028 | 0.032 | 0.024 |
| APR. 3 | 0.042 | 0.028 | 0.027 | 0.021 | 0.050 | 0.046 | 0.043 | 0.044 | 0.043 |
| APR. 9 | 0.066 | 0.046 | 0.044 | 0.028 | 0.067 | 0.060 | 0.060 | 0.060 | 0.054 |
| APR. 18 | 0.052 | 0.035 | 0.036 | 0.029 | 0.060 | 0.050 | 0.048 | 0.043 | 0.046 |
| APR. 25 | 0.036 | 0.023 | 0.024 | 0.020 | - | 0.052 | 0.046 | 0.042 | 0.043 |
| MAY 1 | 0.050 | 0.036 | 0.038 | 0.026 | 0.063 | 0.054 | 0.054 | 0.050 | 0.047 |
| JUNE 12 | 0.086 | 0.061 | 0.059 | 0.058 | 0.094 | 0.080 | 0.066 | 0.066 | 0.063 |
| JULY 26 | 0.073 | 0.053 | 0.051 | 0.054 | 0.078 | 0.067 | 0.056 | 0.057 | 0.059 |
| AUG. 14 | 0.054 | 0.036 | 0.042 | 0.043 | 0.065 | 0.062 | 0.047 | 0.045 | 0.051 |
| SEPT. 12 | 0.045 | 0.030 | 0.032 | 0.033 | 0.069 | 0.061 | 0.046 | 0.045 | 0.048 |
| NOV. 5 | 0.029 | 0.019 | 0.018 | 0.018 | 0.046 | 0.043 | 0.033 | 0.035 | 0.040 |
| **1969** | | | | | | | | | |
| MAR. 19 | 0.058 | 0.034 | 0.035 | 0.030 | 0.119 | 0.085 | 0.048 | 0.059 | 0.046 |
| APR. 10 | 0.075 | 0.042 | 0.046 | 0.038 | 0.091 | 0.079 | 0.080 | 0.082 | 0.060 |
| APR. 22 | 0.050 | 0.031 | 0.032 | 0.029 | - | - | 0.064 | 0.057 | 0.063 |
| APR. 29 | 0.036 | 0.023 | 0.034 | 0.026 | 0.072 | 0.060 | 0.061 | 0.061 | 0.050 |
| MAY 6 | 0.066 | 0.046 | 0.047 | 0.038 | 0.086 | 0.069 | 0.063 | 0.062 | 0.058 |
| MAY 16 | 0.045 | 0.023 | 0.024 | 0.023 | 0.062 | 0.046 | 0.046 | 0.047 | 0.043 |
| MAY 22 | 0.056 | 0.035 | 0.036 | 0.032 | 0.075 | 0.064 | 0.058 | 0.056 | 0.089 |
| JUNE 10 | 0.077 | 0.049 | 0.049 | 0.024 | 0.094 | 0.073 | 0.062 | 0.064 | 0.062 |

Table B-1, Mean Benkelman Beam Deflections ($\bar{\delta}$) (Continued)
(3½ in. Asphalt Concrete Surfacing, 6 in. Sand Sub-Base)

| SECTION NUMBER | 19 | 20 | 22 | 24 | 25 | 26 | 29 | 27 |
|---|---|---|---|---|---|---|---|---|
| | CRUSHED-GRAVEL BASE | | | | BITUMINOUS-STABILIZED BASE | | | |
| | 4 in. | 4 in. | 6 in. | 8 in. | 4 in. | 6 in. | 6 in. | 8 in. |
| **1965** | | | | | | | | |
| SEPT. 23 | 0.054 | 0.063 | 0.034 | 0.060 | 0.079 | 0.069 | 0.059 | 0.063 |
| OCT. 28 | 0.023 | 0.025 | 0.030 | 0.029 | 0.025 | 0.021 | 0.020 | 0.020 |
| **1966** | | | | | | | | |
| MAR. 14 | 0.023 | 0.027 | 0.026 | 0.021 | 0.028 | 0.028 | 0.027 | 0.014 |
| APR. 13 | 0.057 | 0.056 | 0.052 | 0.050 | 0.055 | 0.048 | 0.044 | 0.035 |
| APR. 22 | 0.053 | 0.054 | 0.047 | 0.046 | 0.052 | 0.046 | 0.036 | 0.031 |
| MAY 2 | 0.064 | 0.064 | 0.058 | 0.050 | 0.041 | 0.035 | 0.036 | 0.028 |
| MAY 13 | 0.065 | 0.067 | 0.057 | 0.047 | 0.059 | 0.048 | 0.051 | 0.038 |
| MAY 20 | 0.068 | 0.068 | 0.055 | 0.051 | 0.060 | 0.050 | 0.052 | 0.038 |
| MAY 27 | 0.087 | 0.076 | 0.062 | 0.053 | 0.064 | 0.056 | 0.051 | 0.036 |
| JUNE 3 | 0.068 | 0.074 | 0.046 | 0.037 | 0.055 | 0.044 | 0.047 | 0.027 |
| JUNE 10 | 0.079 | 0.084 | 0.062 | 0.049 | 0.068 | 0.059 | 0.055 | 0.040 |
| JUNE 17 | 0.074 | 0.077 | 0.060 | 0.051 | 0.065 | 0.053 | 0.054 | 0.038 |
| JUNE 28 | 0.066 | 0.073 | 0.057 | 0.048 | 0.064 | 0.052 | 0.052 | 0.039 |
| JULY 8 | 0.058 | 0.064 | 0.055 | 0.041 | 0.054 | 0.043 | 0.048 | 0.034 |
| JULY 18 | 0.051 | 0.050 | 0.049 | 0.039 | 0.047 | 0.040 | 0.044 | 0.033 |
| AUG. 16 | 0.047 | 0.057 | 0.047 | 0.034 | 0.041 | 0.036 | 0.036 | 0.026 |
| SEPT. 30 | 0.034 | 0.037 | 0.031 | 0.026 | 0.030 | 0.025 | 0.024 | 0.019 |
| OCT. 27 | 0.032 | 0.036 | 0.034 | 0.028 | 0.030 | 0.026 | 0.026 | 0.019 |
| NOV. 21 | 0.030 | 0.033 | 0.033 | 0.026 | 0.028 | 0.024 | 0.022 | 0.016 |
| **1967** | | | | | | | | |
| APR. 3 | 0.053 | 0.057 | 0.045 | 0.042 | 0.047 | 0.037 | 0.040 | 0.028 |
| APR. 18 | 0.047 | 0.051 | 0.047 | 0.044 | 0.043 | 0.039 | 0.039 | 0.030 |
| MAY 1 | 0.042 | 0.042 | 0.042 | 0.033 | 0.040 | 0.033 | 0.032 | 0.027 |
| MAY 10 | 0.042 | 0.042 | 0.040 | 0.030 | - | - | - | - |
| MAY 19 | 0.062 | 0.066 | 0.054 | 0.038 | 0.057 | 0.050 | 0.049 | 0.036 |
| MAY 31 | 0.063 | 0.061 | 0.057 | 0.040 | 0.067 | 0.050 | 0.050 | 0.036 |
| JUNE 7 | 0.050 | 0.063 | 0.057 | 0.037 | 0.055 | 0.042 | 0.043 | 0.033 |
| JUNE 15 | 0.079 | 0.079 | 0.060 | 0.041 | 0.066 | 0.055 | 0.054 | 0.039 |
| JULY 12 | 0.075 | 0.081 | 0.060 | 0.040 | 0.059 | 0.048 | 0.046 | 0.033 |
| AUG. 18 | 0.041 | 0.048 | 0.037 | 0.025 | 0.035 | 0.024 | 0.039 | 0.019 |
| SEPT. 11 | 0.048 | 0.050 | 0.042 | 0.030 | 0.043 | 0.037 | 0.037 | 0.027 |
| OCT. 20 | 0.041 | 0.042 | 0.040 | 0.028 | 0.030 | 0.026 | 0.028 | 0.016 |
| NOV. 24 | 0.024 | 0.027 | 0.026 | 0.022 | 0.025 | 0.022 | 0.019 | 0.014 |
| **1968** | | | | | | | | |
| MAR. 25 | 0.040 | 0.043 | 0.023 | 0.021 | 0.031 | 0.029 | 0.028 | 0.019 |
| APR. 3 | 0.052 | 0.057 | 0.050 | 0.049 | 0.050 | 0.049 | 0.046 | 0.040 |
| APR. 9 | 0.046 | 0.047 | 0.045 | 0.044 | 0.043 | 0.041 | 0.040 | 0.032 |
| APR. 18 | 0.053 | 0.060 | 0.050 | 0.044 | 0.050 | 0.048 | 0.051 | 0.036 |
| APR. 25 | 0.053 | 0.061 | 0.053 | 0.042 | 0.052 | 0.042 | 0.045 | 0.033 |
| MAY 1 | 0.055 | 0.060 | 0.052 | 0.043 | 0.049 | 0.047 | 0.040 | 0.036 |
| JUNE 12 | 0.081 | 0.101 | 0.075 | 0.050 | 0.076 | 0.062 | 0.074 | 0.050 |
| JULY 26 | 0.066 | 0.090 | 0.068 | 0.041 | 0.069 | 0.056 | 0.061 | 0.042 |
| AUG. 14 | 0.058 | 0.071 | 0.057 | 0.036 | 0.059 | 0.048 | 0.050 | 0.036 |
| SEPT. 12 | 0.056 | 0.067 | 0.053 | 0.035 | 0.049 | 0.045 | 0.048 | 0.029 |
| NOV. 5 | 0.037 | 0.043 | 0.039 | 0.030 | 0.031 | 0.034 | 0.033 | 0.024 |
| **1969** | | | | | | | | |
| MAR. 19 | - | - | - | - | - | - | - | - |
| APR. 10 | 0.074 | 0.076 | 0.078 | 0.056 | 0.064 | 0.052 | 0.060 | 0.041 |
| APR. 22 | 0.066 | 0.063 | 0.060 | 0.056 | 0.058 | 0.052 | 0.053 | 0.039 |
| APR. 29 | 0.076 | 0.091 | 0.084 | 0.048 | 0.058 | 0.060 | 0.060 | 0.040 |
| MAY 6 | 0.086 | 0.095 | 0.078 | 0.053 | 0.066 | 0.058 | 0.053 | 0.039 |
| MAY 16 | 0.046 | 0.052 | 0.052 | 0.053 | 0.069 | 0.060 | 0.071 | 0.044 |
| MAY 22 | 0.067 | 0.076 | 0.068 | 0.051 | 0.063 | 0.055 | 0.052 | 0.042 |
| JUNE 10 | 0.090 | 0.105 | 0.083 | 0.055 | 0.083 | 0.070 | 0.076 | 0.057 |

**Table B-1, Mean Benkelman Beam Deflections ($\bar{\delta}$) (Continued)**
**(3½ in. Asphalt Concrete Surfacing, 6 in. Sand Sub-Base)**

| SECTION NUMBER | 30 | 31 | 33 | 34 | 15 * | 11 * | 17 * | 21 * |
|---|---|---|---|---|---|---|---|---|
| | CEMENT-TREATED BASE | | | | CR.-ROCK BASE | | CR.-GRAVEL BASE | |
| | 4 in. | 4 in. | 6 in. | 8 in. | 2 in. | 4 in. | 2 in. | 4 in. |
| **1965** | | | | | | | | |
| SEPT. 23 | 0.030 | 0.017 | 0.019 | 0.009 | 0.034 | 0.037 | 0.029 | 0.028 |
| OCT. 28 | 0.011 | 0.011 | 0.008 | 0.006 | 0.024 | 0.021 | 0.020 | 0.025 |
| **1966** | | | | | | | | |
| MAR. 14 | 0.016 | 0.016 | 0.011 | 0.010 | 0.024 | 0.016 | 0.023 | 0.022 |
| APR. 13 | 0.024 | 0.023 | 0.023 | 0.012 | 0.041 | 0.041 | 0.042 | 0.035 |
| APR. 22 | 0.018 | 0.025 | 0.020 | 0.015 | 0.036 | 0.033 | 0.031 | 0.031 |
| MAY 2 | 0.024 | 0.023 | 0.018 | 0.012 | 0.043 | 0.037 | 0.041 | 0.036 |
| MAY 13 | 0.029 | 0.027 | 0.023 | 0.014 | 0.044 | 0.040 | 0.039 | 0.035 |
| MAY 20 | 0.028 | 0.026 | 0.020 | 0.015 | 0.044 | 0.040 | 0.044 | 0.036 |
| MAY 27 | 0.028 | 0.024 | 0.012 | 0.002 | 0.044 | 0.044 | 0.048 | 0.038 |
| JUNE 3 | 0.026 | 0.025 | 0.020 | 0.013 | 0.043 | 0.032 | 0.037 | 0.052 |
| JUNE 10 | 0.032 | 0.031 | 0.021 | 0.013 | 0.045 | 0.042 | 0.047 | 0.037 |
| JUNE 17 | 0.029 | 0.026 | 0.021 | 0.015 | 0.043 | 0.039 | 0.041 | 0.034 |
| JUNE 28 | 0.028 | 0.024 | 0.020 | 0.016 | 0.039 | 0.035 | 0.039 | 0.028 |
| JULY 8 | 0.029 | 0.023 | 0.018 | 0.013 | 0.037 | 0.033 | 0.034 | 0.027 |
| JULY 18 | 0.028 | 0.025 | 0.018 | 0.011 | 0.034 | 0.032 | 0.033 | 0.024 |
| AUG. 16 | 0.029 | 0.025 | 0.018 | 0.011 | 0.032 | 0.030 | 0.031 | 0.027 |
| SEPT. 30 | 0.022 | 0.020 | 0.015 | 0.010 | 0.026 | 0.022 | 0.024 | 0.021 |
| OCT. 27 | 0.025 | 0.023 | 0.017 | 0.009 | 0.026 | 0.019 | 0.024 | 0.023 |
| NOV. 21 | 0.021 | 0.020 | 0.015 | 0.011 | 0.023 | 0.022 | 0.023 | 0.022 |
| **1967** | | | | | | | | |
| APR. 3 | 0.034 | 0.034 | 0.029 | 0.019 | 0.032 | 0.028 | 0.037 | 0.034 |
| APR. 18 | 0.033 | 0.033 | 0.025 | 0.018 | 0.028 | 0.028 | 0.031 | 0.031 |
| MAY 1 | 0.031 | 0.029 | 0.023 | 0.016 | 0.036 | 0.031 | 0.034 | 0.027 |
| MAY 10 | - | - | - | - | 0.031 | 0.029 | 0.029 | 0.025 |
| MAY 19 | 0.039 | 0.036 | 0.027 | 0.018 | 0.036 | 0.034 | 0.038 | 0.029 |
| MAY 31 | 0.037 | 0.031 | 0.027 | 0.014 | 0.037 | 0.034 | 0.040 | 0.029 |
| JUNE 7 | 0.035 | 0.033 | 0.022 | 0.015 | 0.038 | 0.031 | 0.038 | 0.028 |
| JUNE 15 | 0.034 | 0.030 | 0.022 | 0.013 | 0.042 | 0.029 | 0.040 | 0.030 |
| JULY 12 | 0.033 | 0.030 | 0.022 | 0.014 | 0.038 | 0.032 | 0.039 | 0.028 |
| AUG. 18 | 0.037 | 0.031 | 0.020 | 0.013 | 0.030 | 0.018 | 0.031 | 0.019 |
| SEPT. 11 | 0.036 | 0.032 | 0.021 | 0.012 | 0.029 | 0.024 | 0.029 | 0.021 |
| OCT. 20 | 0.023 | 0.022 | 0.018 | 0.013 | 0.029 | 0.023 | 0.030 | 0.025 |
| NOV. 24 | 0.022 | 0.022 | 0.015 | 0.011 | 0.021 | 0.015 | 0.020 | 0.018 |
| **1968** | | | | | | | | |
| MAR. 25 | 0.028 | 0.024 | 0.015 | 0.012 | 0.021 | 0.022 | 0.023 | 0.021 |
| APR. 3 | 0.040 | 0.037 | 0.029 | 0.018 | 0.035 | 0.038 | 0.035 | 0.031 |
| APR. 9 | 0.035 | 0.035 | 0.026 | 0.018 | 0.042 | 0.038 | 0.032 | 0.027 |
| APR. 18 | 0.041 | 0.038 | 0.027 | 0.017 | 0.035 | 0.032 | 0.035 | 0.030 |
| APR. 25 | 0.039 | 0.038 | 0.025 | 0.018 | 0.034 | 0.025 | 0.034 | 0.031 |
| MAY 1 | 0.041 | 0.040 | 0.028 | 0.018 | 0.036 | 0.032 | 0.035 | 0.029 |
| JUNE 12 | 0.056 | 0.046 | 0.035 | 0.019 | 0.044 | 0.036 | 0.047 | 0.034 |
| JULY 26 | 0.048 | 0.043 | 0.031 | 0.018 | 0.042 | 0.034 | 0.041 | 0.029 |
| AUG. 14 | 0.046 | 0.040 | 0.027 | 0.017 | 0.037 | 0.031 | 0.037 | 0.028 |
| SEPT. 12 | 0.038 | 0.037 | 0.027 | 0.016 | 0.033 | 0.030 | 0.034 | 0.026 |
| NOV. 5 | 0.032 | 0.030 | 0.022 | 0.016 | 0.028 | 0.023 | 0.027 | 0.021 |
| **1969** | | | | | | | | |
| MAR. 19 | - | - | - | - | 0.032 | 0.030 | - | - |
| APR. 10 | 0.050 | 0.045 | 0.032 | 0.022 | 0.043 | 0.043 | 0.042 | 0.034 |
| APR. 22 | 0.046 | 0.039 | 0.029 | 0.022 | 0.042 | 0.037 | 0.040 | 0.035 |
| APR. 29 | 0.051 | 0.043 | 0.031 | 0.020 | 0.037 | 0.030 | 0.032 | 0.034 |
| MAY 6 | 0.043 | 0.042 | 0.032 | 0.022 | 0.034 | 0.034 | 0.042 | 0.033 |
| MAY 16 | 0.047 | 0.044 | 0.032 | 0.019 | 0.028 | 0.021 | 0.025 | 0.020 |
| MAY 22 | 0.042 | 0.039 | 0.032 | 0.018 | 0.036 | 0.031 | 0.037 | 0.029 |
| JUNE 10 | 0.053 | 0.050 | 0.038 | 0.019 | 0.042 | 0.036 | 0.044 | 0.035 |

* *18 in. Sand Sub-base*

Table B-1, Mean Benkelman Beam Deflections ($\bar{\delta}$) (Continued)
(5½ in. Asphalt Concrete Surfacing, 6 and 18 in. Sand Sub-Base)

| SECTION NUMBER | 18* | 16† | 35† | 38† |
|---|---|---|---|---|
| | CR.-GRAVEL BASE | CR.-GRAVEL BASE | | CR.-ROCK BASE |
| | 2 in. | 2 in. | 6 in. | 6 in. |
| **1965** | | | | |
| SEPT. 23 | 0.087 | 0.027 | 0.021 | 0.026 |
| OCT. 28 | 0.020 | 0.014 | 0.013 | 0.015 |
| **1966** | | | | |
| MAR. 14 | 0.018 | 0.013 | 0.022 | 0.020 |
| APR. 13 | 0.054 | 0.034 | 0.023 | 0.025 |
| APR. 22 | 0.047 | 0.024 | 0.023 | 0.020 |
| MAY 2 | 0.063 | 0.037 | 0.029 | 0.028 |
| MAY 13 | 0.063 | 0.033 | 0.021 | 0.023 |
| MAY 20 | 0.062 | 0.043 | 0.025 | 0.028 |
| MAY 27 | 0.091 | 0.040 | 0.029 | 0.028 |
| JUNE 3 | 0.081 | 0.030 | 0.026 | 0.026 |
| JUNE 10 | 0.082 | 0.040 | 0.018 | 0.028 |
| JUNE 17 | 0.079 | 0.035 | 0.028 | 0.027 |
| JUNE 28 | 0.075 | 0.036 | 0.026 | 0.029 |
| JULY 8 | 0.060 | 0.031 | 0.025 | 0.025 |
| JULY 18 | 0.055 | 0.031 | 0.023 | 0.024 |
| AUG. 16 | 0.044 | 0.028 | 0.016 | 0.017 |
| SEPT. 30 | 0.027 | 0.020 | 0.017 | 0.018 |
| OCT. 27 | 0.026 | 0.020 | 0.016 | 0.016 |
| NOV. 21 | 0.022 | 0.017 | 0.014 | 0.014 |
| **1967** | | | | |
| APR. 3 | 0.039 | - | 0.024 | 0.022 |
| APR. 18 | 0.036 | 0.023 | 0.021 | 0.021 |
| MAY 1 | 0.045 | 0.027 | 0.024 | 0.024 |
| MAY 10 | 0.029 | 0.022 | - | - |
| MAY 19 | 0.038 | 0.029 | 0.023 | 0.027 |
| MAY 31 | 0.068 | 0.030 | 0.024 | 0.025 |
| JUNE 7 | 0.060 | 0.032 | 0.024 | 0.026 |
| JUNE 15 | 0.075 | 0.033 | 0.027 | 0.027 |
| JULY 12 | 0.063 | 0.032 | 0.021 | 0.019 |
| AUG. 18 | 0.041 | 0.025 | 0.022 | 0.024 |
| SEPT. 11 | 0.046 | 0.023 | 0.015 | 0.019 |
| OCT. 20 | 0.037 | 0.022 | 0.014 | 0.018 |
| NOV. 24 | 0.019 | 0.015 | 0.011 | 0.013 |
| **1968** | | | | |
| MAR. 25 | 0.033 | 0.015 | 0.014 | 0.018 |
| APR. 3 | 0.035 | 0.021 | 0.021 | 0.021 |
| APR. 9 | 0.034 | 0.021 | 0.026 | 0.025 |
| APR. 18 | 0.051 | 0.026 | 0.023 | 0.022 |
| APR. 25 | 0.046 | 0.023 | 0.020 | 0.018 |
| MAY 1 | 0.043 | 0.024 | 0.022 | 0.023 |
| JUNE 12 | 0.086 | 0.039 | 0.033 | 0.032 |
| JULY 26 | 0.070 | 0.031 | 0.028 | 0.028 |
| AUG. 14 | 0.057 | 0.031 | 0.027 | 0.026 |
| SEPT. 12 | 0.052 | 0.025 | 0.018 | 0.023 |
| NOV. 5 | 0.030 | 0.018 | 0.013 | 0.016 |
| **1969** | | | | |
| MAR. 19 | - | - | 0.026 | 0.023 |
| APR. 10 | 0.050 | 0.028 | 0.030 | 0.031 |
| APR. 22 | 0.064 | 0.028 | 0.024 | 0.024 |
| APR. 29 | 0.057 | 0.024 | 0.019 | 0.017 |
| MAY 6 | 0.069 | 0.027 | 0.024 | 0.025 |
| MAY 16 | 0.035 | 0.020 | 0.017 | 0.018 |
| MAY 22 | 0.061 | 0.027 | 0.022 | 0.026 |
| JUNE 10 | 0.071 | 0.032 | 0.013 | 0.016 |

* *6 in. Sand Sub-base*
† *18 in. Sand Sub-base*

# Performance Rating for Aggregate-Surfaced Roads

JOHN W. LUND, Oregon Technical Institute; and
LARRY G. HENDRICKSON, U.S. Forest Service, Portland, Oregon

Aggregate-surfaced roads, especially those constructed with volcanic cinders, have performed with variable results. The U.S. Forest Service, in connection with forest development road construction, initiated a study to determine what parameters influenced the performance of cinders when used as a wearing surface. A road-rating system, similar to the AASHO Road Test methods, was developed to determine which were "good roads" and which were "poor roads" based on 0 to 5 numerical rating scale. Forty-seven roads in forests in south-central Oregon were rated and statistically correlated with maintenance, rutting, watering, speed, and traffic volume by means of a multiple linear regression program. The resulting regression equation had a multiple correlation coefficient of 0.812, with rutting and speed being the most significant variables. The results are felt to apply to all types of aggregate-surfaced roads, with the resultant numerical rating referred to as a performance index. The information from this rating system will be used to recommend specifications for untreated surface-course material.

•ONE OF THE MAJOR SOURCES of aggregates for low-class roads in central Oregon and northern California is volcanic cinders (scoria). The use of cinders and the performance of cinder-surfaced roads has been varied, with both good and poor results. The U.S. Forest Service began a study in 1968 to determine the parameters that influence the performance of volcanic cinders when used as a wearing surface for forest development roads.

The approach to this problem suggested an evaluation of the performance of existing untreated cinder roads to determine which were "good roads" and which were "poor roads" based on a numerical rating scale. This in turn was related to the physical properties of the cinders in the roadway and from the borrow pit. A survey of current literature and construction practice was also performed. These relationships, together with other field observations, were used to recommend specifications for selecting borrow material and for constructing quality control techniques. This paper is concerned only with the development of the performance-rating procedure. The details of the entire study are presented in a U.S. Forest Service report (1).

A performance-rating system (serviceability over a period of time) had to be developed because none existed for untreated aggregate roads. Serviceability (developed by the AASHO Road Test) was not felt to be applicable because the condition of an untreated road changes rapidly from day to day. This is especially true if a road is rated immediately before maintenance (its poorest condition) and immediately after maintenance (its best condition). Instead, the performance of the road was considered and related to the maintenance period.

## BACKGROUND INFORMATION

An evaluation of the ability of a pavement or riding surface to perform its intended function has been attempted for many years, mainly in the form of a "good" or "poor" classification. These subjective terms obviously varied from rater to rater. In an

Paper sponsored by Committee on Pavement Condition Evaluation and presented at the 49th Annual Meeting.

effort to solve this problem, several systems using an objective evaluation based on a numerical scale were developed, utilizing such terms as performance rating, serviceability index, condition survey, and sufficiency rating. The end result was to somehow determine the beneficial and detrimental features affecting the performance of an existing road so that the detrimental properties could be avoided in future projects and the beneficial items used or improved on to prevent failures and to upgrade the surface riding quality.

Unfortunately, very little has been done concerning the rating of untreated or gravel surfaces. The necessary requisites of untreated surfaces have been documented (2). They are (a) stability, or the ability to support the superimposed loads without detrimental deformation, (b) ability to resist abrasive action of traffic, (c) ability to shed a large portion of rain because excess moisture may cause loss of stability, (d) capillary properties sufficient to replace moisture lost by surface evaporation, and (e) low cost.

To achieve these requisites, the items that have been proved to be necessary are (a) control of grading (AASHO M 61 specifications), (b) control of Atterberg limits in binder (AASHO, maximum liquid limit = 35, PI = 4 to 9), and (c) maximum Los Angeles abrasion = 40.

Roughness of untreated surfaces has also been studied (3). The circumstances that have been ascertained to be associated with the formation of potholes include (a) volume of traffic; (b) width of road surface (related to item a); (c) type of surface material; (d) condition of crown (steep favorable); and (e) condition of shoulders. Of these factors, the volume of traffic is perhaps the most important. The problem of rating untreated roads then becomes one of deciding which features of the roadway are to be considered in recognition of the fact that the purpose of a highway pavement is to provide a smooth riding surface supplying safety, comfort, and economy to the highway user (4, 5).

The most important feature therefore appears to be riding quality. However, this poses a problem for untreated roads, because the riding qualities vary considerably with maintenance. When the riding quality becomes poor or reaches a certain critical point, then the road is maintained and upgraded to its original condition (this may vary according to available money, men, or equipment). Thus, the evaluation of untreated surfaces varies from good to poor and back to good. The logical means of evaluating riding quality then becomes a function of maintenance frequency and ease of maintenance, with some consideration given to the severity of dusting. In addition, the type of rutting should be included, such as washboard (transverse), erosion or wheel ruts (longitudinal), and potholes or local failures. The depth and spacing of washboards are generally constant and independent of the nature of the material in which they occur (3).

The deterioration or required frequency in maintenance of a road is also dependent on the amount and type of traffic and on speed. The latter appears to be influenced by geometric design; i.e., the straighter the road, the greater the speed and the faster the deterioration. However, sharp curves will cause lateral shoving of material, and steep grades will present problems of sudden speed changes due to shifting as well as traction problems (6).

The consideration of maintenance in serviceability and performance studies has been recognized by Crawford and Anderson (7), who believe that ". . . ride alone is not a criterion of pavement performance. It must be coupled with a knowledge of maintenance activity to be meaningful—any pavement can be made to have a smooth 'ride' if enough money is spent for maintenance activity. However, a smooth riding highway that is being maintained at excessive costs cannot be said to be performing satisfactorily."

In high-type bituminous pavements, maintenance can be correlated with thickness increase resulting from patching and repair. For all types of pavements, maintenance frequency or cost could be measured. Traffic volumes, as indicated previously, affect the maintenance frequency and riding quality of a road. Reports of traffic volume versus wear vary. In 1924 Ladd reported that gravel roads subjected to a volume of not more than 200 to 300 vehicles per day remained practically free from washboard if they were occasionally dragged (3). As soon as the volume reached 400 to 450 vehicles per day, washboards developed very rapidly. Carpenter and Dana found in 1927 that 300 to 400 vehicles per day did not usually cause serious formation of washboards (3). Willis,

Aaron, and Lindberg found in 1942 that washboards may appear when the count is as low as 100 vehicles per day (8). In 1961 Huang speculated that, considering that weights and speeds of vehicles have been considerably increased during the past 30 years, a volume of 50 vehicles per day can probably be regarded at present as the average volume that would initiate washboarding in a fairly well-constructed road even under favorable climatic conditions (3).

Relating the surface wear or maintenance responsibility attributed to various types of traffic has always presented a problem. The U. S. Forest Service, in an attempt to solve this problem, converts various types of traffic to equivalent units for assigning maintenance. Shares are based on the following (9):

1,000 board feet hauled (round trip) = 2 passenger vehicles (one way)
= 1½ passenger vehicles with trailer (one way)
= 2 cubic yards of rock or ore (round trip)

Because one truck load equals approximately 5,000 board feet (net), then one log truck (round trip) is equivalent to 100 passenger vehicles (one way).

Opinions vary as to the validity of these relationships. Some Forest Service personnel would place more emphasis on loaded logging trucks as compared to passenger cars, whereas others feel that high-speed passenger cars, especially in the form of recreational traffic with campers and boat trailers, are more destructive than the relationship indicates.

## DEVELOPMENT OF RATING SYSTEM

It was decided to use a procedure similar to the AASHO Road Test methods (10) for the rating of untreated aggregate roads. The AASHO Road Test serviceability performance-rating system appeared to be reliable and generally accepted by many transportation agencies. However, one major deviation was made in this study; the road was given a performance rating instead of a serviceability rating by the rater. Because the serviceability (rating at a particular time) varies considerably between maintenance periods, performance (a rating over a period of time) is used instead.

The rating of each individual road segment was obtained from three knowledgeable persons on the particular National Forest or Ranger District, such as the district engineering assistant, the road maintenance foreman, or the district ranger. Unfortunately, different personnel were used on each forest and even on each district because only the local people had a good knowledge of how the particular road performed over a period of time. The authors were unable to rate the roads because in most instances they saw the particular road only once or twice, which would not necessarily be the "average" condition of the surface.

The raters were asked to rate the particular road on the basis of the AASHO Road Test 0 to 5 scale (11). They were told to rate the road as to its ability to carry the existing traffic efficiently and conveniently under the average conditions of the road between maintenance periods, comparing the road with a high-quality gravel surface. The individual rating was called the performance rating (PR) and the average of the three values obtained for a particular road was called the performance value (PV).

The use of a performance rating has certain inherent advantages. Because the rating was an average over a period of time, requiring the rater to be a person familiar with the operations of the road over an extended period, it was not necessary for the rater to drive the road at the time the rating was made. In most cases the ratings were made individually in the office. Thus, the individual ratings were convenient for the raters to make and less time-consuming than a serviceability-type rating. If necessary, the required ratings could be obtained by mail. One major disadvantage is that this rating may contain considerable bias.

The more difficult aspect of the rating system was the determining of properties of the roadway surface that could be used to predict the performance value (PV). This prediction, based on measurable surface properties, was necessary to standardize the performance value, inasmuch as the value for a particular road could vary from district

to district because a new group of raters had to be used in each district. The predicted value, called the performance index (PI), could then minimize any bias included in the individual ratings.

Based on earlier discussions, maintenance was felt to be the basic parameter to relate the performance index. In addition, both longitudinal profile and speed were felt to be important. Finally, traffic volume, with considerations for weight, was suspected to affect the items mentioned. All of these quantifiable properties were considered based on experience derived by other investigators, as outlined in an earlier section. The specific items thus evaluated were (a) maintenance frequency, in days; (b) length of time for ruts, washboards, or potholes to develop after maintenance (so that they affect the efficient and safe operation of the vehicles using the road), in days; (c) interval between period of watering during the dry season, in days; (d) maximum safe speed that can be maintained by the majority of vehicles during the average conditions of the road surface, in miles per hour; (e) average number of traffic units (two-way) per day over the road during the period of the rating, in units per day (9); and (f) amount of logging traffic units (two-way) as determined in item e, in percent.

During the course of the study, several other variables were investigated, such as subgrade strength, surface strength, surface thickness, age since construction, and the effect of the roadway cross section and width. However, none of these items appeared to have any measurable relationship to the road rating.

So as not to introduce other unnecessary variables, the raters were asked to consider only a straight, nearly level, and unshaded portion of road when assigning a performance-rating value. It was felt that grades, curves, and tree cover (affecting the moisture content of the road) would affect the rating and thus should be avoided if possible. The properties used in the performance index were obtained from experienced personnel who were familiar with the maintenance and operations of the individual roads in the forests. Again these values were obtained for a straight section as indicated.

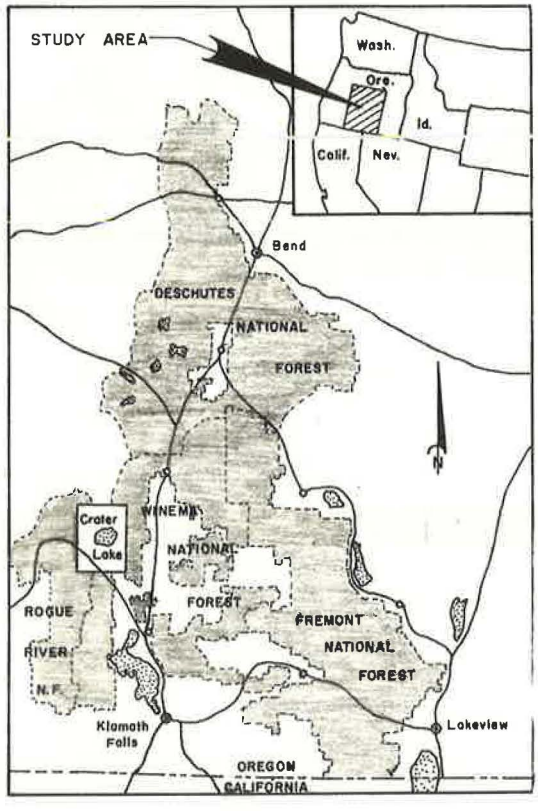


Figure 1. Study location map.

The total of 47 roads selected for study consisted of (a) 5 roads in the eastern portion of the Rogue River National Forest, (b) 9 roads in the western portion of the Fremont National Forest, (c) 9 roads in the southern portion of the Deschutes National Forest, and (d) 24 roads in the Winema National Forest. The general location of the study area is shown in Figure 1. In many cases the road was rated twice, once based on logging traffic during a recent timber sale and a second time based on light passenger-vehicle traffic. Thus, a total of 57 ratings were made. The results of the ratings and the associated properties used in the performance index are given in Table 1.

The average of the ratings (performance value) and the road properties were then analyzed using a multiple regression computer program (BMD-02R). This program weights each property and enters it into a linear equation that best estimates the performance value based on a least squares analysis. The single correlation coefficient between each variable and the performance value is given in Table 2.

TABLE 1

ROAD DESCRIPTION AND RATINGS

| Road Number | | PV | PI | Speed (mph) | Ruts (days) | Maintenance (days) | Water (days) | Traffic Units per Day | Percent Logging Traffic |
|---|---|---|---|---|---|---|---|---|---|
| | | | | Winema National Forest | | | | | |
| 1 | 361 | 2.0 | 2.6 | 25 | 14 | 600 | 300 | 15 | 20 |
| 2 | 3660 | 3.2 | 3.0 | 35 | 30 | 300 | 300 | 25 | 40 |
| 3 | 350 | 2.8 | 2.6 | 25 | 21 | 120 | 300 | 100 | 0 |
| 4 | 3633 | 3.1 | 2.8 | 30 | 30 | 120 | 300 | 50 | 0 |
| 5a | 3700 | 4.6 | 4.2 | 50 | 300 | 300 | 300 | 20 | 0 |
| 5b | 3700 | 4.6 | 3.3 | 50 | 5 | 3 | 2 | 70 | 71 |
| 6 | 350D | 4.8 | 4.5 | 50 | 300 | 7 | 1 | 50 | 90 |
| 7 | 3790 | 3.8 | 4.5 | 50 | 300 | 7 | 1 | 140 | 90 |
| 8 | 358 | 3.7 | 4.5 | 50 | 300 | 7 | 1 | 220 | 90 |
| 9a | 31043(N) | 1.5 | 2.3 | 30 | 14 | 180 | 300 | 20 | 0 |
| 9b | 31043(N) | 1.5 | 2.3 | 30 | 4 | 4 | 2 | 61 | 82 |
| 10a | 31043(S) | 2.7 | 2.3 | 40 | 4 | 180 | 300 | 16 | 62 |
| 10b | 31043(S) | 2.7 | 3.0 | 40 | 10 | 8 | 4 | 61 | 82 |
| 11 | 35010 | 2.5 | 2.9 | 40 | 7 | 7 | 1 | 150 | 67 |
| 12a | 3190 | 2.7 | 3.1 | 45 | 30 | 90 | 300 | 20 | 0 |
| 12b | 3190 | 2.7 | 2.7 | 30 | 14 | 14 | 7 | 77 | 90 |
| 13a | 31049(W) | 1.7 | 1.9 | 35 | 7 | 180 | 300 | 10 | 0 |
| 13b | 31049(W) | 1.7 | 1.5 | 20 | 1 | 7 | 7 | 61 | 82 |
| 14 | 34015 | 2.7 | 2.4 | 45 | 14 | 90 | 300 | 10 | 0 |
| 15 | 31049(E) | 1.5 | 2.5 | 45 | 14 | 180 | 300 | 10 | 0 |
| 16a | 33061 | 3.2 | 3.1 | 50 | 3 | 7 | 1 | 285 | 88 |
| 16b | 33061 | 3.2 | 3.3 | 50 | 6 | 30 | 7 | 120 | 83 |
| 17a | 2731[a] | 4.2 | 3.8 | 45 | 90 | 90 | 300 | 76 | 0 |
| 17b | 2731[a] | 4.2 | 3.5 | 35 | 90 | 90 | 1 | 131 | 38 |
| 18 | 2652C[a] | 4.6 | 4.1 | 50 | 300 | 180 | 300 | 20 | 0 |
| 19 | 286 | 2.0 | 2.1 | 25 | 4 | 90 | 90 | 19 | 0 |
| 20 | 286[b] | 2.2 | 1.6 | 30 | 1 | 0.5 | 300 | 37 | 68 |
| 21a | R283 | 3.5 | 3.8 | 40 | 180 | 90 | 90 | 11 | 68 |
| 21b | R283 | 3.5 | 2.8 | 40 | 5 | 90 | 90 | 30 | 0 |
| 22 | R2971 | 2.3 | 1.7 | 20 | 5 | 180 | 180 | 10 | 0 |
| 23 | 29079 | 2.5 | 1.9 | 25 | 5 | 180 | 180 | 10 | 0 |
| 24 | 30037 | 2.3 | 2.7 | 45 | 2 | 90 | 90 | 72 | 14 |
| | | | | Deschutes National Forest | | | | | |
| 25 | 1821 | 2.3 | 2.8 | 40 | 7 | 100 | 300 | 80 | 10 |
| 26 | 1915 | 4.7 | 4.2 | 45 | 300 | 300 | 300 | 50 | 0 |
| 27 | 1808(W) | 2.7 | 2.8 | 35 | 10 | 100 | 300 | 150 | 30 |
| 28 | 1808(N) | 3.2 | 3.4 | 50 | 10 | 100 | 300 | 200 | 30 |
| 29 | 217 | 2.7 | 3.1 | 45 | 7 | 150 | 300 | 125 | 15 |
| 30 | 2022(W) | 1.8 | 2.1 | 30 | 30 | 150 | 300 | 10 | 30 |
| 31 | 2022(E) | 3.0 | 2.4 | 30 | 5 | 2 | 1 | 340 | 88 |
| 32 | 2016[d] | 2.5 | 3.4 | 45 | 21 | 150 | 300 | 80 | 50 |
| 33 | 2221 | 1.8 | 2.8 | 35 | 10 | 75 | 300 | 350 | 10 |
| | | | | Rogue River National Forest | | | | | |
| 34a | 3520B | 2.2 | 2.5 | 35 | 3 | 60 | 60 | 110 | 90 |
| 34b | 3520B | 2.2 | 2.4 | 35 | 3 | 120 | 120 | 35 | 71 |
| 35 | 344C | 3.5 | 3.3 | 40 | 30 | 120 | 120 | 40 | 0 |
| 36 | 3520M | 3.7 | 3.1 | 40 | 14 | 80 | 80 | 40 | 0 |
| 37 | 3317 | 2.7 | 3.2 | 40 | 28 | 240 | 240 | 25 | 0 |
| 38a | 3520 | 3.2 | 3.1 | 40 | 14 | 80 | 80 | 25 | 0 |
| 38b | 3520 | 3.2 | 2.9 | 40 | 7 | 60 | 60 | 35 | 34 |
| | | | | Fremont National Forest | | | | | |
| 39 | 30038(N) | 3.7 | 3.7 | 40 | 100 | 70 | 70 | 34 | 90 |
| 40 | 30038(C)[c] | 4.7 | 3.9 | 45 | 100 | 70 | 70 | 34 | 90 |
| 41 | 30038(S) | 3.0 | 2.9 | 40 | 7 | 70 | 70 | 34 | 90 |
| 42 | 3312 | 3.0 | 2.9 | 40 | 7 | 7 | 7 | 131 | 90 |
| 43 | 3610 | 2.7 | 3.1 | 35 | 42 | 240 | 240 | 31 | 90 |
| 44 | 335 | 4.0 | 3.1 | 40 | 42 | 240 | 240 | 10 | 90 |
| 45 | 379(S) | 4.3 | 4.1 | 40 | 300 | 80 | 80 | 116 | 90 |
| 46 | 379(N) | 3.5 | 2.9 | 40 | 300 | 1 | 1 | 116 | 90 |
| 47 | 3609 | 3.0 | 2.8 | 50 | 30 | 120 | 120 | 80 | 90 |

Note: All roads are cinder-surfaced except as follows:

[a]Gravel road (crushed basalt);
[b]Pumice road;
[c]Clay binder added to cinders;
[d]Pit-run glacial outwash (basalt).

Many variations and combinations of variables were investigated, including the common logarithm of the variables, the square of the variables, and combinations of two variables multiplied together or divided by each other. The results of the best equation, with the highest multiple correlation coefficient (MCC), were as follows:

$$PI = 0.704 + 0.041S + 0.702 \log_{10} R - 0.040W/U + 0.022M/U$$

where

PI = performance index,
S = speed in mph,
R = rut development in days,
W = watering interval in days,
U = traffic units, and
M = maintenance interval in days.

The MCC for the equation is 0.812. However, ruts and speed alone contribute 0.768 to the coefficient, with the remaining variables increasing the correlation of the equation by only 4.4 percent. The steps in forming the equation and the influence of each variable is as follows:

$PI = 1.871 + 0.916 \log_{10} R$, MCC = 0.685 (Step 1)

$PI = 0.491 + 0.043S + 0.699 \log_{10} R$, MC = 0.768 (Step 2)

$PI = 0.846 + 0.037S + 0.733 \log_{10} R - 0.025W/U$, MCC = 0.805 (Step 3)

$PI = 0.704 + 0.041S + 0.702 \log_{10} R - 0.040W/U + 0.022M/U$, MCC = 0.812 (Step 4)

As indicated in Table 2, the most important variable is the formation of ruts.

Using the best equation as given previously, the PI of each road can be calculated. This value is then an estimation of the PV with the bias of individual raters removed. A comparison between these two values is given in Table 1. Review of these data shows that the regression analysis tends to eliminate the extreme ratings.

Figures 2, 3, 4, and 5 show typical examples of the various ranges in road rating based on the PI.

## COMMENTS ON ROAD-RATING RESULTS

The significant variables used in the final equation to predict the PV were generally those expected, such as speed and rutting. These variables were expected to be significant, based on the experiences of other writers. The fact that the variables of maintenance, traffic units, watering, and percent of logging traffic were not significant was somewhat unusual and unexpected. The reasons for these departures from the expected are as follows:

1. With an increase in traffic volume (logging operations in most cases), more emphasis was placed on maintaining a smooth surface. As a result, the road performance actually improved with use through additional compaction, blading, and watering. Under low traffic volumes, the road was often maintained only once a year after spring thaw. Thus, maintenance frequency and traffic volume were more functions of use rather than of road performance.

TABLE 2

PROPERTIES OF INDIVIDUAL VARIABLES

| Variable | Mean | Standard Deviation | Correlation With PV |
|---|---|---|---|
| Performance value | 3.0 | 0.9 | 1.000 |
| Ruts | 62.0 | 102.0 | 0.647 |
| Water | 158.1 | 127.4 | -0.226 |
| Maintenance | 110.6 | 104.7 | -0.066 |
| Speed | 38.8 | 8.2 | 0.604 |
| Units | 75.2 | 77.9 | 0.024 |
| Percent logging traffic | 42.2 | 38.9 | 0.142 |
| $\text{Log}_{10}$(ruts) | 1.26 | 0.68 | 0.685 |
| Water/units | 6.83 | 8.93 | -0.294 |
| Maintenance/units | 5.19 | 7.65 | -0.207 |
| $(\text{Speed})^2$ | 1,575.9 | 611.4 | 0.612 |
| $\text{Log}_{10}$(units) | 1.64 | 0.40 | 0.229 |

Figure 2. Road R971 (Little Yamsay) Northest of Chiloquin, Oregon (PV = 2.3, PI = 1.7).

Figure 3. Intersection between road 1821 (China Hat, background; PV = 2.3, PI = 2.8) and road 1915 (Lockit Butte, PV = 4.7, PI = 4.2) East of Bend, Oregon.

Figure 4. Road 33061 (East-West) West of Chiloquin, Oregon (PV = 3.2, PI = 3.3).

Figure 5. Road 379 (Fishhole) South of Bly, Oregon (PV = 4.3, PI = 4.1).

2. The effect of logging traffic and recreational traffic in road performance is actually not well defined; the use of traffic units is only an estimation.

3. The small correlation between traffic volume and performance value (CC = 0.024) indicates that the volume of traffic using a forest-access road is independent of its condition, because there is often no alternate road.

The use of the multiple correlation coefficient indicated that 34 percent of the variations in PV was unexplained. This is more than likely due to the variation in raters from forest to forest and is the reason for using the PI rather than the PV.

## CONCLUSIONS AND APPLICATIONS

Even though the system was developed using cinder-surfaced roads, several crushed aggregate and volcanic pumice roads were also rated (Table 1). Thus, the study is felt to be applicable to all types of aggregate-surfaced roads. With one or two exceptions, the calculated performance index (PI) for each road was felt to be reasonable by Forest Service personnel (i.e., the poorer roads in the forests received low PI values and the better roads the higher values). Once the road-rating system using the PI was established, typical examples of roads within each rating group were selected and the surface material was sampled. The purpose in sampling the roads was to determine physical properties that could be identified with roads of high performance (PI) and those associated with low performance or, more specifically, the correlation

between performance and physical properties. A field-sampling and laboratory-testing program was initiated for 30 different roads. A significant correlation was found between performance and physical properties. The results revealed that several modifications were desirable to standard specifications for road-surfacing aggregate to better fit the properties of cinder aggregates. These modifications are presently being considered for use by the U.S. Forest Service. The details of this study are presented in two reports found elsewhere (1, 12).

In addition to the cinder-sampling program, the results of this study are currently being considered for use in a surfacing-loss study and in evaluating thickness design techniques for Forest Service aggregate-surfaced roads. A similar rating system may be developed for a dust-control program.

## SUMMARY

The results of the study indicate that a performance-rating system can be applied to aggregate-surfaced roads. Because of the variability of the surface riding characteristics of untreated roads, the rating must be referenced to a period of time, the maintanance interval being the most logical one to use. A rating system based on a 0 to 5 numerical scale was used and was correlated with maintenance, rutting, watering, speed, and traffic volume. Speed and rutting frequency were found to be the most significant parameters. Traffic volume was not found to be a significant factor; however, perhaps some means other than the U.S. Forest Service unit system should be investigated.

The advantage of this rating system is that no elaborate equipment is required to rate the road, because only maintenance and traffic data are needed. This is in keeping with the level of service and cost of construction for this low class of road. Expensive and sophisticated measuring equipment is only justified for high-type roads.

## REFERENCES

1. Lund, J.W., and Hendrickson, L.G. Road Performance and Construction Specifications Using Volcanic Cinders. U.S. Forest Service, Pacific Northwest Region, Portland, Oregon.
2. Willis, E.A. Design Requirements for Graded Mixtures Suitable for Road Surfaces and Base Courses. HRB Proc., Part II, Vol. 18, 1938, pp. 206-208.
3. Huang, E.Y. A Study of Occurrence of Potholes and Washboards on Soil-Aggregat Roads. HRB Bull. 282, 1961, pp. 135-159.
4. Hutchinson, B.G. Principles of Subjective Rating Scale Construction. Highway Research Record 46, 1964, pp. 60-70.
5. Housel, W.S. Evaluation of Pavement Performance Related to Design, Construction, Maintenance and Operation. Highway Research Record 46, 1964, pp. 135-153.
6. Sterns L.J., and Mooring, R. Volcanic Cinders as Road Building Material in Region 5. U.S. Forest Service narrative reports for intra-agency use, Aug. 22, 1968.
7. Crawford, R.A., and Anderson, D.W. Pedological Soil-Highway Distress Study, Hand County, South Dakota. South Dakota Dept. of Highways Physical Research Section, Pierre, 1967.
8. Willis, E.A., Aaron, H., and Lindberg, R.C. Volcanic Cinders Suitable for Use in Base Course Construction. Public Roads, Vol. 23, No. 6, Oct.-Nov.-Dec. 1942, pp. 125-136.
9. U.S. Forest Service Manual. Title 5600—Engineering, 5617.5—Conversion Factors, April 1966.
10. Carey, W.N., Jr., and Irick, P.E. The Pavement Serviceability-Performance Concept. HRB Bull. 250, 1960, pp. 40-58.
11. The AASHO Road Test. HRB Spec. Rept. 61E, 1962.
12. Hendrickson, L.G., and Lund, J.W. Construction Specifications for Volcanic Cinders Used as Road-Surfacing Aggregate. Highway Research Record 307, 1970, pp. 11-20.